NATIONAL TRANSPORTATION SAFETY BOARD

Office of Research and Engineering
Washington, D.C. 20594

September 17, 2021

Aircraft Performance & Simulation Study

by John O'Callaghan

Location: Chamberlain, South Dakota
Date: November 30, 2019
Time: 12:33 Central Standard Time (CST)
Aircraft: Pilatus Aircraft Ltd. PC-12/47E, registration N56KJ
NTSB#: CEN20FA022

TABLE OF CONTENTS

NATIONAL TRANSPORTATION SAFETY BOARD

Office of Research and Engineering
Washington, D.C. 20594

September 17, 2021

Aircraft Performance & Simulation Study

by John O'Callaghan

A. ACCIDENT

Location: Chamberlain, South Dakota
Date: November 30, 2019
Time: 12:33 Central Standard Time (CST)[1]
Aircraft: Pilatus Aircraft Ltd. PC-12/47E, registration N56KJ
NTSB#: CEN20FA022

B. GROUP

Not Applicable

C. HISTORY OF FLIGHT

On November 30, 2019, at 12:33 CST, a Pilatus PC-12/47E airplane, N56KJ, was destroyed during an impact with terrain near the Chamberlain Municipal Airport (K9V9) in Chamberlain, South Dakota. The pilot and 8 passengers were fatally injured, and three passengers were seriously injured. The airplane was registered to Conrad & Bischoff, Inc. and operated by the pilot as a Title 14 Code of Federal Regulations (CFR) Part 91 personal flight. Instrument meteorological conditions prevailed, and the flight was operated on an instrument flight rules flight plan. The flight originated from K9V9 shortly before the accident and was destined for Idaho Falls Regional Airport (KIDA), Idaho Falls, Idaho.

This *Aircraft Performance & Simulation Study* presents the results of using recorded flight data from the airplane's Flight Data Recorder (FDR), video evidence, the crash site location, recorded weather data, and simulation results to determine the position, orientation, and other relevant performance parameters of the airplane during the accident flight. An engineering "desktop" simulation of the flight yields a set of control and throttle inputs that make the simulation approximately match the airplane trajectory and performance recorded on the FDR. Tests conducted in a Level D full-flight training simulator provide insight into the effects of improper loading of the airplane and of different takeoff rotation techniques on the workload involved with capturing and maintaining a target pitch attitude during takeoff and initial climb.

Weather information, witness videos, and the FDR data describe the following sequence of events concerning the weather preceding and at the time of the accident, the pilot's pre-flight

[1] Local time at Chamberlain on the day of the accident was Central Standard Time (CST). CST = UTC - 6 hours. Times in this *Study* are in CST unless otherwise noted.

activities, and the airplane's taxi to runway 31, takeoff, initial climb, and descent back to the ground:

According to the NTSB *Meteorology Factual Report* for this accident (Reference 1),

> The [Automated Weather Observing System (AWOS)] observations from K9V9 surrounding the accident time indicated LIFR [low-IFR] to IFR[2] conditions with light to moderate snow with a north to northeast wind between 5 and 10 knots. The 5 minute AWOS data from K9V9 was retrieved and they indicated that 1/2 mile visibility occurred as early as 12:25 CST with moderate snow reported as early as 12:30 CST …. Snowfall information from the Community Collaborative Rain, Hail, and Snow Network (CoCoRaHS) was retrieved for the area surrounding the accident site …. The CoCoRaHS points closest to the accident site indicated that 2.1 and 2.0 inches of snowfall had been observed in the 24 hours prior to 07:30 CST and 07:00 CST, respectively. Unknown precipitation and drizzle had also been reported at K9V9 in the 24 hours prior to the accident time in both the METARs and 5 minute AWOS data ….

The K9V9 AWOS observations for times surrounding the accident are presented in Table 1.

Parameter / Report	K9V9 METAR 11:55 CST	K9V9 METAR 12:15 CST	K9V9 METAR 12:35 CST	K9V9 METAR 12:55 CST
Sky condition	500 ft. overcast	500 ft. overcast	500 ft. overcast	500 ft. overcast
Visibility	0.75 statute miles	0.75 statute miles	0.5 statute miles	0.5 statute miles
Winds	020° @ 7 kt.	020° @ 7 kt.	020° @ 6 kt.	010° @ 7 kt.
Temperature / Dew Point	1°C / 1°C	1°C / 1°C	1°C / 1°C	1°C / 1°C
Altimeter setting	29.30 "Hg	29.30 "Hg	29.30 "Hg	29.29 "Hg
Precipitation	Light snow	Light snow	Moderate snow	Moderate snow

Table 1. AWOS observations at K9V9 at the times surrounding the accident.

An individual at K9V9 took pictures and videos of the accident airplane on the ramp prior to its departure, during its taxi to the runway, and during its takeoff roll and liftoff. The pictures and videos were provided to the NTSB, as described in the NTSB *Image/Video Study* for this accident (Reference 2). Selected images from Reference 2 are duplicated here as Figures 1-3.

Figure 1, a photograph taken at 11:02:49, shows "a person … using a tool to deice the left wing" (Reference 2). There is "visible moisture" (that appears to be snow) falling in the photo. Figure 2 compares the vertical tail portion of the airplane shown in Figure 1 with a similar photo taken at 12:21:40 and with a photo of an exemplar PC-12. Reference 2 notes that, compared to the "clean" exemplar photo, the 11:02:49 photo

> … shows accumulated precipitation build-up above the leading edge of the horizontal stab. It also shows accumulated precipitation had built up on the vertical stab and icicles were present on the horizontal stab bullet fairing.

---

[2] The Federal Aviation Administration (FAA) Aeronautical Information Manual (AIM) section 7-1-7, in accordance with the National Weather Service (NWS), defines the following general flight categories:

- Low Instrument Flight Rules (LIFR*) – ceiling below 500 ft above ground level (agl) and/or visibility less than 1 statute mile.
- Instrument Flight Rules (IFR) – ceiling between 500 to below 1,000 feet agl and/or visibility 1 to less than 3 miles.
- Marginal Visual Flight Rules (MVFR**) – ceiling from 1,000 to 3,000 ft agl and/or visibility 3 to 5 miles.
- Visual Flight Rules (VFR) – ceiling greater 3,000 ft agl and visibility greater than 5 miles.

* By definition, IFR is a ceiling less than 1,000 ft agl and/or visibility less than 3 miles while LIFR is a sub-category of IFR.

**By definition, VFR is a ceiling greater than or equal to 3,000 ft agl and visibility greater than 5 miles while MVFR is a sub-category of VFR.

Similarly, the 12:21:40 photo

> shows accumulated precipitation forward of the horizontal stab's leading edge. The comparison shows accumulated precipitation build-up above the leading edge of the horizontal stab. It also shows accumulated precipitation build-up on the vertical stab and icicles were present on the horizontal stab bullet fairing.

As noted in Reference 2, in the 12:21:40 photo "there is additional accumulated precipitation" and "there is more visible moisture … falling" than in the 11:02:49 photo.

The top part of Figure 3 is a frame from a video of N56KJ taken while the airplane was taxiing for takeoff, zoomed-in to highlight the horizontal tail area. The bottom part of Figure 3 is a photograph of the same area from an exemplar PC-12. Per Reference 2,

> The exemplar photo at the bottom of figure 7 shows the free area above the horizontal stab in relation to the amount of vertical stabilizer fairing, the horizontal stabilizer fairing and the seam-line between the two fairings that is visible. In the photo of the accident aircraft at the top of figure [3], accumulated precipitation is visible on the top surface of the horizontal stab. The accumulated precipitation obscures some of the free area seen on the exemplar photo when related to surface area visible on the vertical stabilizer fairing, the horizontal stabilizer fairing and the seam-line between the two fairings.

Based on the photographic and video evidence presented in Reference 2, N56KJ departed with accumulated precipitation on the horizontal and vertical stabilizers. According to the Pilatus PC-12 Airplane Flight Manual (AFM) (Reference 3), Section 10, "Safety and Operational Tips," "Removal of Snow, Ice, and Frost from the Aircraft,"

> Flight crews are responsible for ensuring the aircraft is free of ice, snow or any contaminants.
>
> … Approved de-icing/anti-icing fluids must be used during the de-icing/anti-icing procedure.
>
> The aircraft must be clear of all deposits of snow, ice and frost adhering to the lifting and control surfaces immediately prior to take-off. The clean aircraft concept is essential for safe flight operations. The pilot in command of the aircraft has the ultimate responsibility to determine if the aircraft is clean and in a condition for safe flight.
>
> Manual methods of de-icing provide a capability in clear weather to clean the aircraft to allow a safe take-off and flight. De-icing/anti-icing fluids can be used to quickly remove frost and to assist in melting and removal of snow. In inclement cold weather conditions, the only alternative may be limited to placing the aircraft in a hangar to perform the cleaning process. …

While the effects of the accumulated precipitation on the airplane's aerodynamics and weight could not be quantified, *qualitatively* it is certain that these accumulations would increase the airplane's gross weight and could only hamper, and not improve, the airplane's aerodynamic performance and handling qualities.

The witness video shows N56KJ taxiing to runway 31 and departing (see Figures 4a-4d). The airplane climbs into a low overcast and appears to enter a left turn before being hidden by the clouds.

The FDR data indicates that N56KJ started taxiing towards the runway (ground speed increased above zero) at 12:29:47. FDR data and wreckage evidence documented in Reference 4 indicates that the airplane's configuration during the taxi and takeoff was as shown in Table 2:

Flaps	15° (confirmed by wreckage evidence per Reference 4)
Horizontal stabilizer setting	+0.67° nose up from neutral position, slightly more nose-down than the "green diamond" setting on the pitch trim indicator (confirmed by wreckage evidence per Reference 4)
Engine inertial separator door	OPEN
De-ice boots power switch	ON
Windshield heat	ON
Pitot heat	System 1: OFF[3] System 2: ON
Static port & AOA heat	ON
Propeller heat	ON

Table 2. N56KJ configuration at takeoff as determined by FDR data and wreckage evidence documented in Reference 4. Weight and center of gravity calculations are provided in Table 5 in Section D-I.

The propeller heat ON and inertial separator door OPEN settings indicate that the airplane was in "PUSHER ICE MODE" during the takeoff. As described in the AFM,

> When the propeller de-ice is selected to ON and the inertial separator selected to OPEN, the stall protection system, stick pusher/shaker system is re-datumed to provide both shake and push functions at lower angles of attack and higher speeds. This is to protect against the natural stall through the effects of residual ice on the protected surfaces of the airfoil leading edges. When the system is in the re-datum mode, the aircrew are alerted by illumination of the green ICE PROTECTION caption PUSHER ICE MODE. Failure of the system in ice mode will result in the caption being extinguished and the amber CAS caption Pusher will be illuminated and an aural gong will sound.
> …
> When operating in STICK PUSHER ICE MODE the stick pusher computer automatically reduces the shaker and pusher settings as measured by the angle of attack vanes, by 8°. With operational pneumatic de-ice boots, this results in an increase of the stall speed at the maximum takeoff weight of 12 kts with flaps set to 0° and 9 kts with flaps set to 15°.

In addition, the AFM indicates that when the PUSHER ICE MODE is active, some operational airspeeds must be modified, as shown in Table 3:

Speed	**PUSHER ICE MODE OFF**	**PUSHER ICE MODE ON**
Takeoff rotation speed	82 KIAS flaps 15 76 KIAS flaps 30	92 KIAS flaps 15
Speed at 50 ft.	(Flaps to 0 above 100 KIAS)	113 KIAS flaps 15
Best rate of climb @ sea level, flaps up	130 KIAS	135 KIAS recommended
Flaps 15 approach speed	99 KIAS	105 KIAS
Balked landing (Go-Around)	98 KIAS flaps 15, gear down 89 KIAS flaps 30, gear down 85 KIAS flaps 40, gear down	105 KIAS, flaps 15, gear down (Max flap 15° with residual ice)
Stall speed (pusher activation) at maximum takeoff weight	95 KIAS flaps 0 78 KIAS flaps 15	107 KIAS flaps 0 87 KIAS flaps 15

Table 3. Effect of PUSHER ICE MODE on operational airspeeds (data compiled from the PC-12/47E AFM).

Significantly, the AFM notes that when the PUSHER ICE MODE is on, the rotation speed must be increased by 10 knots, from 82 to 92 KIAS, at flaps 15 and the maximum takeoff weight.

[3] In response to an NTSB query, Pilatus noted that "generally, if the pitot tube is not heated, and icing conditions are present, then this could result in any of the classic pitot-blocked scenarios (stagnating airspeed indication, etc.). However, in the case of the PC-12 accident in Chamberlain, there is evidence that pitot 1 heat off (intentionally or as a result of a system fault) had no effect on the air data or other systems of the aircraft." Evidence of this is that "The airspeed sensed by the left and right pitot as recorded by the [FDR] show excellent correlation once the aircraft started to move at around 12:32:00." (See Reference 5, item 3.1-1.)

During the taxi and before the start of the takeoff roll, the pitch angle (θ) recorded on the FDR varied between 1.8° and 4.4°, averaging about 2.8°. According to Pilatus,[4]

> Looking at the video recordings of the ground rolls, it just looks from experience that the aircraft is squatting low and "dragging its tail" when moving.
>
> More technically, with the heavy loading and aft c.g. position, the main landing gear shock struts will be compressed much more than the nose landing gear strut, so the tail sinks down. This would be even more pronounced at low cold-soaked ambient temperatures which would cause a reduced N2 pressure in the shock absorbers.
>
> In addition, when we produced the exemplar photographs of the PC-12 tail (as submitted to NTSB … on 10 June 2020), we couldn't recreate the viewpoint of a person standing on the ground, even after loading 200 kg of sandbags into the rear of the fuselage. Instead, the photographer had to stand on a ladder. This further corroborates that the accident aircraft was sitting on the ground tail-low (nose-high).
>
> With an average empty weight of 2995 kg and [center of gravity] at 32% [of mean aerodynamic chord], the average pitch angle [on the ground] is 1°, with measured values between 0.4° and 1.3°. When loaded and the [center of gravity] further aft, higher pitch angles can be expected.

Consequently, the relatively high θ during the taxi to the runway is consistent with the heavy weight and aft center of gravity (CG) computed by the NTSB Investigator in Charge (IIC) for the accident flight (see Table 5 in Section D-I).

The FDR data indicates that N56KJ started its takeoff roll at about 12:32:00, when the engine torque and ground speed started to increase. θ during the takeoff roll steadily decreased from about 2.8° to about 1°, until the airplane rotated for takeoff. At 12:32:26.7, θ increased through 1.6° during the takeoff rotation. At this time, the indicated airspeed was about 89 KIAS, 3 knots short of the 92 KIAS specified by in Table 3 for rotation at flaps 15 and maximum takeoff weight with the PUSHER ICE MODE on. Since the pull on the column to initiate the rotation must have occurred slightly before the time the pitch angle increased through 1.6°, the initial pull likely occurred closer to 88 KIAS, or 4 knots below the 92 KIAS target. As will be discussed below, this early rotation could have contributed to the triggering of the stick shaker almost immediately upon liftoff.

During the rotation, θ increased at a rate of about 7 °/s, reaching about 12° at 12:32:28.5, where it lingered for about half a second before continuing to increase (see Figure 12). θ reached 15° at 12:32:30.8 and 15.8° at 12:32:32.5 before decreasing steadily to 9.8° at 12:32:37. However, thereafter θ started a series of oscillations that increased in amplitude and absolute value (reaching a peak of 21° at 12:32:49.6) before starting a sudden drop at 12:32:52.3, decreasing from 19° to -24° at the end of the data at 12:32:59.8.

The FDR "weight on wheels" (WOW) discrete transitioned from "on ground" to "in air" at 12:32:28, when θ was increasing through 9.8°. The stick shaker activated for the first time at 12:32:29.3 (as θ increasing through 12.2°, just after the WOW discrete transitioned), and activated 5 more times before the end of the data. The stick pusher activated for the first time at 12:32:43.3, and activated 4 more times before the end of the data. The angle of attack (α) at the times of the stick shaker and pusher activations will be discussed below in Section D-IV.

The roll angle (ϕ) was between 0° and 2° throughout the takeoff roll, until 12:32:27.5 (about a second after the start of the rotation), when it decreased to about -10° at 12:32:29.5. ϕ

[4] See Reference 5, item 3.6-1.

subsequently oscillated between -10° and 5° before starting a progressive roll to the left, reaching -63° at 12:32:54.2, and -55° at the end of the data at 12:32:59.8 (see Figure 13).

As discussed in Section D-IV, the FDR altitude data suffers from measurement errors resulting from the large α and ϕ angles achieved during the flight. The calculation of the airplane's altitude based on the integration of accelerometer data and estimated corrections to the recorded radar altitude indicate that N56KJ achieved a maximum altitude of 2,062 ft. above mean sea level (MSL) (about 380 ft. above ground level (AGL)) at about 12:32:54 before entering a steep descent, impacting the ground at about 12:33:01 (see Figure 9). The total elapsed time from the WOW "in air" indication to the end of the FDR data is 33 seconds.

The motions and performance of N56KJ during the accident flight will be described in more detail in the subsequent sections of this *Study.* The *Study* describes the various data sources used, the correction of measurement errors inherent in the FDR data, and the computation of additional performance parameters using the corrected data. In addition, the *Study* describes efforts to match the accident takeoff (and the preceding takeoff from KIDA) with a desktop engineering simulator, to 1) compare the airplane's performance with expected performance as defined by the simulator, and 2) to compute a set of flight control inputs that result in an approximate match of the airplane's motions. Insights obtained from simulator tests conducted in a Level D flight training simulator flown at the accident weight and CG are also discussed.

The Level D simulator tests indicate that the takeoff rotation technique, particularly the abruptness and magnitude of the initial column movement and consequent initial pitch rates, when coupled with an airplane loaded beyond its gross weight and aft CG limits, can have a significant effect on the workload involved with maintaining a target pitch attitude. The accident pilot's takeoff rotation technique is compared with another pilot's technique for several takeoffs recorded in the FDR data, and shown to be more abrupt than the other pilot's technique.

D. DETAILS OF THE INVESTIGATION

I. The Pilatus PC-12/47E airplane & N56KJ weight and balance

The Pilatus PC-12 is a single engine turboprop, low-wing, pressurized passenger and cargo aircraft manufactured by Pilatus Aircraft of Stans, Switzerland. The first flight of the PC-12 was in 1991. The PC-12/47E was certified in 2008 and has upgraded avionics and a Pratt & Whitney Canada PT6A-67P engine that produces 1,200 shaft horsepower (SHP). N56KJ is airframe serial #1431, manufactured in 2013 (per the date of the airworthiness application and certificate). Figure 5 shows a 3-view image of the PC-12/47E, taken from Reference 3. Table 4 provides the reference dimensions of the airplane used to non-dimensionalize the aerodynamic coefficients used in the PC-12 simulator model described in Section D-V.

Item	Value
Reference dimensions (used in simulation model):	
Wing area	25.81 m^2 (277.8 $ft.^2$)
Wing span	16.08 m (52.76 ft.)
Mean Aerodynamic Chord (MAC)	1.71 m (5.61 ft.)

Table 4. Reference dimensions of the PC-12/47E.

The IIC performed a weight and balance computation for the accident flight as shown in Table 5. The weight and CG envelope of the airplane (from the AFM) is presented in Figure 6, with the estimated weight and CG of the accident flight plotted over the envelope. Of note:

- There were more people on the airplane than available seats. Passengers 9 and 10 are assumed to be seated in the aisle of the passenger cabin. The CG calculations are performed two ways: 1) assuming these passengers are seated in the forward part of the aisle (moment arm values in white cells), and 2) assuming these passengers are seated in the aft part of the aisle (moment arm values in gray cells). Two different moment arms for the baggage are also assumed, covering a range of possibilities, so that the computed CG covers a range from the most forward combination of passengers and baggage (at 244.26 inches) to the most aft combination (at 245.76 inches).

- The computed takeoff weight of 10,557 lb. is 107 lb. above the envelope's maximum gross weight of 10,450 lb.,

- The most forward computed CG (244.26 in.) is 3.99 inches aft of the aft CG limit (240.27 in.)

- The most aft computed CG (245.76 in.) is 5.49 inches aft of the aft CG limit (240.27 in.)

- The aft CG is consistent with the observation by Pilatus that when taking the exemplar photograph shown in Figure 3, "we couldn't recreate the viewpoint of a person standing on the ground, even after loading 200 kg of sandbags into the rear of the fuselage. Instead, the photographer had to stand on a ladder. This further corroborates that the accident aircraft was sitting on the ground tail-low (nose-high)."

- The effects of accumulated precipitation (snow) on the weight and CG of the airplane are unknown, and are not accounted for in Table 5. However, the airplane main gear tires contact the ground at station 247.7, so the CG could not have been more aft than that or the airplane would have tilted back on its tail while stationary, which did not occur.

The AFM states the following in Section 6, "Weight and Balance," "General:"

> To achieve the performance designed for the aircraft it must be flown with approved weight and center of gravity limits.
>
> **It is the responsibility of the pilot in command to make sure that the aircraft does not exceed the maximum weight limits and is loaded within the center of gravity range before takeoff.** [Emphasis in original]

PC-12/47E LOADING FORM -- N56KJ (s/n 1431)			INTERIOR CODE: EX-6-STD-2S			
Item	**Weight (lbs)**	**Arm (in)**	**Moment/1000 (in-lbs)**		**Arm (in)**	**Moment/1000 (in-lbs)**
Basic Empty Weight	**6682**		**1567.60**			
Pilot	178	160.27	28.53			
Rt Seat Pax	180	160.27	28.85			
Fwd Baggage	46	169.3	7.79			
Pax 1	169	234.09	39.56			
Pax 2	150	234.09	35.11			
Pax 3	221	276.12	61.02			
Pax 4	198	276.12	54.67			
Pax 5 (s)	175	308.12	53.92			
Pax 6 (s)	175	308.12	53.92			
Pax 7 (s)	175	341.00	59.68			
Pax 8	183	341.00	62.40			
Pax 9 (aisle)	91	234.09	21.30		341.00	31.03
Pax 10 (aisle)	60	276.12	16.57		308.12	18.49
Rear Baggage	414	361.00	149.45		371.00	153.59
Zero Fuel Weight / CG	**9097**	**246.28**	**2240.38**		**248.01**	**2256.17**
Fuel	1500	Note 10	347.66			
Ramp Weight / CG	10597		2588.03			
Grnd Ops Fuel	40					
Fuel at Takeoff	1460	Note 10	338.28			
Takeoff Weight / CG	**10557**	**244.26**	**2578.66**		**245.76**	**2594.45**
% MAC		**0.4786**			**0.5008**	

Notes:

1 -- (s) denotes survivor (weights estimated)

2 -- (aisle) denotes pax likely not seated

3 -- fatality weights provided by funeral home and incremented 5 lbs. for winter gear

4 -- pax seating positions based on survivor stmts when possible

5 -- grnd ops fuel is estimated

6 -- fuel loading based on CFI stmt of conversation with pilot

7 -- baggage weighed at accident site

8 -- fwd baggage location estimated (placed at aft end of center console)

9 -- Moment calculations in gray cells correspond to most aft combination of aisle passengers and baggage.

10 -- Fuel moment determined from table in Figure 6-16 of AFM.

Table 5. Weight and balance calculations for N56KJ provided by the IIC.

II. Crash site & wreckage

N56KJ departed from K9V9 runway 31, which is 4,300 ft. long and 75 ft. wide, with a threshold elevation of 1,678 ft. and a true heading of 321°. For additional details about KNIP and its runway, see Appendix A.

Investigators measured the GPS coordinates of the main wreckage site as

Latitude: 43° 45' 56.12" N = 0.2677 nm (1,627 ft.) North of the K9V9 runway 31 threshold
Longitude: 99° 20' 13.78" W = 0.9127 nm (5,546 ft.) West of the K9V9 runway 31 threshold
Elevation: 1,706 ft. (from *Google Earth*)

Reference 4 describes the on-site measurement of N56KJ's control surface trim and flap actuator strokes and extensions to determine the values of these items at the time of impact:

- The aileron trim was slightly right-wing-down, but well within green take-off range.
- The rudder trim was in the green take-off range.
- The pitch trim was in the green take-off range, slightly more nose-down than the diamond.
- The flaps were at 15° with no indication of a flap twist or asymmetry.

According to the preliminary report for this accident,[5]

> A witness located about 1/2-mile northwest of the airport reported hearing the airplane takeoff. It was cloudy and snowing at the time. He was not able to see the airplane but noted that it entered a left [turn] based on the sound. He heard the airplane for about 4 or 5 seconds and the engine seemed to be "running good" until the sound stopped.
>
> The property owner discovered the accident site about 13:57. The site was located approximately 3/4 mile west of the airport in a dormant corn field [see Figure 7]. The debris path was approximately 85 ft long and was oriented on a 179° heading. The engine was separated from the firewall. The left wing was separated from the fuselage at the root. The engine and left wing were both located in the debris path. The main wreckage consisted of the fuselage, right wing and empennage.

The airplane's flight path and wreckage location are plotted in Figure 8. The "simulation" lines in this and other Figures are discussed below in Section D-V.

III. Recorded flight data

FDR and CVR data description

The *Flight Data Recorder Specialist's Factual Report* for this accident (Reference 6) notes that "N56KJ was manufactured in 2013 and was not required to be equipped with an FDR, however, the aircraft was equipped with an L3Harris Lightweight Data Recorder (LDR)." The FDR report describes the LDR as

> a small and lightweight recorder unit providing crash protected recording of audio, image (if equipped), and flight data on small general aviation helicopters and fixed-wing aircraft typically aircraft carrying up to six passengers.

Per this description, flight data and cockpit audio data are recorded on the same device – the LDR – as opposed to being recorded on a separate Flight Data Recorder (FDR) for flight data

[5] See https://data.ntsb.gov/carol-repgen/api/Aviation/ReportMain/GenerateNewestReport/100636/pdf.

and a Cockpit Voice Recorder (CVR) for cockpit audio. For convenience, however, in this *Study* the data function of the LDR is referred to as the "FDR" and the audio function is referred to as the "CVR," even though both functions are contained in the same device.

The LDR was recovered from the wreckage and sent to the NTSB Recorders Laboratory in Washington, DC for readout. Descriptions of the FDR and CVR readout processes can be found in References 6 and 7, respectively. The FDR readout results in tabulated and plotted values of the recorded flight parameters versus time. The CVR readout results in a transcript of the CVR events, a partial list of which is shown in Table 6. The paraphrased version of the selected CVR events listed in Table 6 are also presented along with other information in various Figures throughout this *Study*. For the complete transcript and CVR report, see Reference 7.

CVR time (CST)	Selected CVR items full transcript text	Paraphrased text on plots
12:31:59	CAM: [sound similar to RPM increase]	Start of takeoff roll
12:32:29	SW/SPS: stall stall stall. [automated voice]	Start of stall warnings
12:32:49	HOT-1: oh no.	Pilot comment
12:33:01	CAM: [sound of thud]	Thud sounds
12:33:03	END OF RECORDING	End of recording

Table 6. Full CVR transcript text corresponding to paraphrased text on plots in this *Study*. Sound sources are indicated as: CAM = Cockpit Area Microphone; HOT-1 = pilot audio panel voice or sound source; SW/SPS = Stall Warning / Stick Pusher System.

Correlation of FDR, CVR, and local CST times

The FDR and CVR record their information with respect to time. As described in Reference 6,

> Timing of the FDR data is measured in subframe reference number (SRN), where each SRN equals one elapsed second[6] ….
>
> …
>
> Correlation of the FDR data from SRN to the event local time, CST, was established by using the recorded Coordinated Universal Time (UTC) GPS hours, UTC GPS Minutes, and UTC GPS Seconds and then applying an additional -6.0 hours offset to change UTC to CST.
>
> Accordingly, the time offset for the event flight data from SRN to local CST is the following: CST = SRN + 44080. Therefore, for the rest of this report, all times are referenced as CST, not SRN.

The FDR and CVR specialists provided the times of FDR data and of CVR events to the Aircraft Performance specialist in CST, which is used in this *Study*.

Several of the plots in this *Study* portray selected CVR content. For example, plots of data vs. time include CVR content overlaid on vertical lines that intersect the x axis of the plot at the times that the content was recorded. The content portrayed on the plots is not the verbatim CVR transcript text, but rather a paraphrase or shorthand code for this text. The full CVR transcript text associated with each paraphrase or code is shown in Table 6.

[6] Although the SRN increments every second, parameters on the FDR can be sampled at more than once per second. For example, normal load factor is sampled 8 times per second.

IV. Performance calculations based on FDR data

Overview

The FDR records many, but not all, performance parameters of interest. Many additional parameters can be derived from the FDR parameters. This section describes the calculations used to derive additional performance parameters from the corrected data. The airplane weight used in these calculations is 10,557 lb. (see Table 5). The derivation of the equations and calculation methods used in this *Study* is detailed in Appendix A of Reference 8.

For this *Study*, additional performance parameters derived from the FDR data include:

- True airspeed and altitude.
- Kinematically consistent positions and velocities from accelerometer integration.
- Angle of attack (α) based on FDR vane angle measurements and inertial speeds.
- Radio altimeter height "corrected" for large roll angles.

The results of these corrections and derivations, from a ground speed of about 60 knots on the takeoff roll through the end of the FDR data, are presented in Figures 8 – 14.

True airspeed calculation

True airspeed equals Mach number multiplied by the speed of sound; the speed of sound is a function of the static temperature. Static temperature is obtained from total temperature and Mach number.

Mach number can be computed from calibrated airspeed and static pressure. "Calculated airspeed" (approximately equal to calibrated airspeed) and total temperature are recorded directly by the FDR, and the static pressure can be determined from the pressure altitude recorded by the FDR (which is based on the standard sea-level pressure of 29.92 "Hg).

Figure 11 shows the results of the true airspeed calculation, compared with the indicated (calibrated) airspeed recorded by the FDR. For the accident flight conditions, the true airspeed is about 2 knots higher than the calibrated airspeed.

Pressure-based true altitude and density altitude calculations

The altitude recorded by the FDR is pressure altitude; i.e., it is the altitude in the standard atmosphere corresponding to the pressure sensed at the airplane's static pressure ports. The altitude in the actual atmosphere corresponding to the local static pressure generally does not equal the pressure altitude, and it is insufficient to simply adjust the pressure altitude for the local sea level pressure because, in general, the lapse rate of pressure with altitude does not match the lapse rate in the standard atmosphere.

To estimate the actual altitude of N56KJ, the recorded pressure altitude is first adjusted to account for a 29.30" Hg altimeter setting (see Table 1). During the takeoff, the change in altitude corresponding to a change in static pressure is calculated by solving the hydrostatic equation continuously (the hydrostatic equation describes the pressure increment across a differential element of air required to balance the weight of the element). With static pressure and the static

temperature values from the speed calculations, the density and weight of the air elements can be calculated.

The result of this calculation is shown in Figure 9 as the magenta line labeled "Altitude from FDR pressure altitude & hydrostatic equation." The FDR pressure altitude is about 580 ft. above the magenta line.

The indicated altitude is the altitude shown on the airplane's altimeters. It is the pressure altitude corrected for the non-standard altimeter setting only (29.30 "Hg), and is shown in Figure 9 as the green line. Note that the indicated altitude (green line) deviates slightly from the hydrostatic-derived altitude (magenta line) as altitude increases; this deviation results from the non-standard lapse rate of pressure with altitude.

Note also that the barometric-based altitudes in Figure 9 (the indicated altitude and hydrostatic equation altitude) contain erratic oscillations near the end of the data, starting around time 12:32:52. These oscillations might be the result of erroneous static pressure readings at the static ports, caused by disrupted airflow around the fuselage at large α, and by the large, oscillatory pitch rates present at the time. As will be discussed further below, the airplane likely exceeded the flaps 15 stall α (between 12.9° and 13.9°) a little after 12:32:52.

The density altitude is the altitude in the standard atmosphere corresponding to the actual air density at each point in the flight. Because of the colder-than-standard day, the density altitude during the accident flight was about 520 ft. lower than the true MSL altitude.

True altitude based on radio altimeter and terrain elevation data

The dashed brown line in Figure 9 labeled "FDR radio altitude + terrain elevation" is the altitude that results from adding the height of the airplane above the ground (measured by the radio altimeter) to the elevation of the terrain underneath the airplane. The terrain elevation is determined by using the FDR latitude and longitude data to define the airplane's track over the ground, and then by obtaining the terrain elevation underneath the airplane's track from Shuttle Radar Topography Mission (SRTM) elevation data provided by the United States Geological Survey (USGS). The USGS provides SRTM digital elevation data with a resolution of 1 arc-second (about 100 ft.) for the United States and 3 arc-seconds (300 ft.) for global coverage.[7] The resolution of the terrain data used in this *Study* is 1 arc-second.

Note that the "FDR radio altitude + terrain elevation" altitude is well-behaved during the takeoff and initial climb, but increases to a sharp peak of 2,356 ft. at 12:32:54 before dropping sharply again. This behavior is not reflected in the barometric-based altitude and is unrealistic, as will be shown below by comparing the radio altitude with the altitude obtained by integrating the load factor data recorded on the FDR. It is possible that the "spike" in radio altitude is the result of growing errors affecting the radio altimeter as the airplane's left roll angle increases past -30° at 12:32:49. The NTSB asked Pilatus whether the radio altimeter was affected by large pitch and roll angles, and whether the radio altimeter compensated for large angles. Pilatus responded as follows: [8]

[7] See http://viewer.nationalmap.gov/viewer/.
[8] See Reference 5, item 3.4-1.

> Pilatus received the following information from Honeywell Aerospace [the manufacturer of the radio altimeter] on 8 June 2021:
>
> "The KRA 405B [radio altimeter] uses a frequency counter design – it is not a true leading edge tracker. Frequency counters will tend toward a weighted average of the overall return signal (weighted by their relative amplitudes in the receiver), similar to a centroid tracker. As a result, it can be prone to slant range overshoots with steep bank angles, especially over low reflectivity or diffuse terrain (forest, desert, etc.).
>
> The KRA 405B is designed and verified to TSO-C87. The [Minimum Operational Performance Specifications] requirements within TSO-C87 state that the accuracy requirements (±3 ft/3% up to 500 ft and ±5% above 500 ft for the precision equipment output, and ±5 ft/5% up to 500 ft and ±7% above 500 ft for the display/indicator) must be met at roll angles up to ±20°. In addition, the altimeter must maintain lock at roll angles up to ±30°, but between 20° and 30° roll the accuracy requirement is only ±20%.
>
> And there is no pitch or roll attitude data processing."

Based on this information, it appears that the radio altimeter can lose "lock" beyond roll angles of 30°, and is not guaranteed to meet any accuracy requirements beyond this roll angle.

Assuming that, at any orientation (attitude) of the airplane, the radio altimeter is measuring the distance from the altimeter to the ground along a line parallel to the vertical axis of the airplane (the body z axis in Figure 19), the distance from the altimeter to the ground parallel to the gravity vector (i.e., the altimeter's altitude) is given by

$$h_{corr} = h_{rec} \cos\theta cos\phi \qquad [1]$$

Where h_{rec} is the recorded radio altitude, θ is the pitch angle, ϕ is the roll angle, and h_{corr} is the corrected radio altitude.

h_{corr} is plotted in Figure 9 as the brown line labeled "'Corrected' FDR radio altitude + terrain elevation" (in which the terrain elevation under the airplane has been added to the result of Equation [1]). The correction removes the spike in radio altitude at 12:32:54, and also lowers the highest radio-based MSL altitude below the highest barometric-based altitude.

There is no guarantee that either the barometric-based altitude or the "corrected" radio-based altitude are entirely kinematically consistent with the load factor data recorded on the FDR. In addition, while the FDR ground speed parameter is relatively accurate, it might not be entirely kinematically consistent with the FDR load factor data or the FDR Flight Management System (FMS) position data.[9] "Kinematically consistent" means that the mathematical relationships between acceleration (measured by load factor parameters), speed (measured by the ground speed and heading parameters), and position (measured by the FMS position parameters) hold in the three dimensions of the airplane's motion. In practice, the FDR parameters as recorded are only approximately kinematically consistent, as a result of inherent measurement errors and uncertainties.

Considering these errors and uncertainties, a better, kinematically consistent solution for the airplane's altitude, position, and speed throughout the approach and landing can be obtained by integrating the load factor data recorded on the FDR. This calculation is described below.

[9] Per Reference 3, Global Navigation Satellite System (GNSS) sensors are included in the FMS position solution.

Accelerometer data corrections and integration

The red line in Figure 9 labeled “Altitude from accelerometer integration” is the altitude that results from integrating[10] the FDR load factor data twice to derive aircraft position. It can be a better estimate of the actual path of the airplane since it does not suffer from the static pressure sensing errors inherent in the FDR pressure-based altitude data or the radio altimeter errors associated with large roll angles.

An accurate estimate of the flight path of the airplane during relatively short intervals (about 30 to 60 seconds) can be obtained by integrating the accelerations recorded at the CG of the airplane. In general, the accelerometers are not located exactly on the CG, and so the accelerations at the CG must be computed by adjusting the FDR-recorded load factors for the effects of angular rates and accelerations. In the present case, the accelerometers are sufficiently close to the CG that this correction is negligible.

However, accelerometers generally contain small offsets, or “biases,” that produce large errors in speed and position if not removed prior to integration.[11] In addition, the initial values of speed, rate of climb, and track angle are required during the integration process (these are essentially the “constants of integration” when integrating acceleration to get speeds). The constants of integration and the values of the accelerometer biases can be estimated by selecting them such that the aircraft position that results from the integration agrees with known “target” positions determined from another source.

The accelerometer biases are not necessarily constant over an entire flight, but can drift over time. It is for this reason that integrating the accelerometers works best over relatively short intervals, during which the accelerometer biases are approximately constant. In the present case, the elapsed time from a ground speed of 34 knots on the takeoff roll to the end of the data at the crash site is only 49 seconds. This interval is sufficiently short that satisfactory results can be obtained using a single integration. For this segment, the “target” positions for the accelerometer integration are defined by the FDR data points shown in Figure 10, and by the brown “‘Corrected’ FDR radio altitude…” line in Figure 9.

The constants of integration (the initial ground speed, track angle, and rate of climb) are chosen to minimize the root-mean-square difference between the integrated path and the target path throughout the entire segment. The beginning and end times, constants of integration, and accelerometer biases used are shown in Table 7. The constants of integration are expressed as increments, or biases, on the initial ground speed, track, and rate of climb that would be computed using the target trajectory.

Start time (EDT)	End time (EDT)	Speed bias, knots	Track bias, degrees	Rate of climb bias, ft/min	n_x bias, G’s	n_y bias, G’s	*nlf* bias, G’s
12:32:10.0	12:32:59.9	-8	0.62	15	0.015075	-0.004275	0.008886

Table 7. Constants of integration and accelerometer biases for the accelerometer integration.

[10] In the following discussion, “integrating” the load factor data refers to mathematical integration with respect to time, per the theorems of Calculus.

[11] For details about the equations to be integrated and the bias correction technique described in this *Study*, see Appendix A of Reference 8.

Accelerometer integration results

The airplane position and altitude resulting from the final integrated trajectory is shown in Figures 8-11 as the lines with the "Accelerometer integration" label. The ground speed and rate of climb resulting from the integrated trajectory are plotted in Figure 11.

The corrected load factors are compared to the load factors recorded by the FDR in Figure 14.

Figures 8 and 10 indicate that the north and east positions obtained from the accelerometer integration agree well with the FMS positions recorded on the FDR. Figure 9 indicates that the altitude obtained from the accelerometer integration matches the target altitude (the brown "'Corrected' FDR radio altitude …") well during the takeoff roll, rotation, and initial climb, though it deviates from the target by about 50 ft. at the end of the data. The FDR data ends at 12:33:00, one second before the "thud sounds" recorded on the CVR at 12:33:01, which indicate ground impact. However, an extrapolation of the red integrated altitude line intersects the terrain at about 12:33:00.3, in relatively good agreement with the CVR evidence,[12] and indicates that the corrected radio altitude used as the target for the integration is reasonable. The altitudes based on the barometric pressure altitude are clearly too high at the end of the data, considering that ground impact occurs at about 12:33:01.

Inertial flight path angle (γ), angle of attack (α), and sideslip angle (β) calculations

The flight path angle is defined by

$$\gamma = \sin^{-1}\left(\frac{\dot{h}}{V}\right) \qquad [2]$$

where γ is the flight path angle, $\dot{h}$ is the rate of climb, and V is speed. Using true airspeed gives γ relative to the airmass, and using ground speed gives γ relative to the Earth. If $\dot{h}$ and V from the pressure-based altitude and true airspeed calculations described above are used in Equation [2], the resulting γ is very noisy (i.e., it contains unrealistic "spikes" and oscillations). A better (smoother) calculation of γ results from using $\dot{h}$ and V from integrated accelerometer data. The γ relative to the Earth using $\dot{h}$ and ground speed from the accelerometer integration is shown as the red line in the bottom plot of Figure 12. The $\dot{h}$ used in this calculation is shown as the red line in the bottom plot of Figure 11.

The flight path defined by the accelerometer integration can also be used to estimate the airplane's α and β angles, by considering the components of airspeed along the airplane's body axes. Airspeed, ground speed, and wind are related as follows:

$$\vec{V} = \vec{V}_G - \vec{V}_W \qquad [3]$$

where $\vec{V}$ is the airspeed vector, $\vec{V}_G$ is the ground speed vector and $\vec{V}_W$ is the wind vector. The components of $\vec{V}_G$ in body axes result from the integration of the accelerometer data described above.

[12] The CVR times are provided to the nearest whole second.

In this accident, since the airborne portion of the flight only lasted 33 seconds, the wind vector $\vec{V}_W$ can be assumed to be approximately equal to the wind recorded at K9V9 around the time of the accident. Per Table 1, the AWOS winds were from 20° at 6-7 knots. Simulations of the accident flight (described below) result in a better match of the airplane's trajectory when a wind from 020° at 8 knots is used, and so this wind is used in the calculations described here.

The wind speed and direction can be transformed into wind components in the body-axis system using the FDR Euler angles (pitch, roll, and heading). Once the body-axis components of $\vec{V}_G$ and $\vec{V}_W$ are defined, Equation [3] can be solved to obtain the $\{u, v, w\}$ components of $\vec{V}$ in the body-axis system. The components of the airspeed $\vec{V}$ in body axes, as indicated by Figure 19, are related to α and β as follows:

$$u = V\cos(\beta)\cos(\alpha) \quad [4a]$$
$$v = V\sin(\beta) \quad [4b]$$
$$w = V\cos(\beta)\sin(\alpha) \quad [4c]$$
$$V = \left|\vec{V}\right| = \sqrt{u^2 + v^2 + w^2} \quad [4d]$$

From which α and β can be computed:

$$\alpha = \tan^{-1}\left(\frac{w}{u}\right) \quad [5]$$

$$\beta = \sin^{-1}\left(\frac{v}{V}\right) \quad [6]$$

The total airspeed velocity V computed from the airplane's $\{u, v, w\}$ components is plotted in the top plot of Figure 11 as the brown line labeled "True airspeed from integrated ground speed and assumed wind." The "inertial" α and β computed using Equations [5] and [6] are plotted as the red lines in the middle plots of Figures 12 and 13, respectively. The inertial α is also compared to the α computed from the angle of attack vane data recorded on the FDR in Figure 20, as described below.

α from FDR vane measurements compared to stall warning thresholds

The vane angle of attack signal used to activate the stick shaker, stick pusher, and aural stall warning as α increases and nears the stall is recorded on the FDR, and is plotted as the blue line in Figure 20. Per Reference 5, at flaps 15 the body axis α (illustrated in Figure 19) is related to the vane angle of attack (α_v) as follows:

$$\alpha = (0.0014){\alpha_v}^2 + (0.2091)\alpha_v - 0.04° \quad [7]$$

The relationship is different for other flap settings. The body α computed using Equation [7] is plotted in Figure 20 as the black line. The body inertial α, computed using Equation [5], is plotted in Figure 20 as the red line. The dashed green line in Figure 20 is the inertial α delayed in time by 0.56 seconds (i.e., shifted to the right by 0.56 seconds); this shift makes the phase of the inertial α match the vane-based α better, and might indicate that the recorded vane α lags the actual α slightly.

Figure 20 also plots the stick shaker (orange shading) and stick pusher (red shading) discretes recorded on the FDR. The devices are active when their associated discretes equal 1. The α_v

thresholds at which the stick shaker and stick pusher nominally activate with the "PUSHER ICE MODE" on are also shown in Figure 20 as the dashed orange and red lines crossing the plot horizontally at 27° and 35°, respectively. Reference 5 notes that these α_v values are *effectively* 8° lower than they would be if the "PUSHER ICE MODE" were off:

> When in Ice Mode, [the Stick Pusher Computer] adds 8° to the [α_v] values; this has the same effect as decreasing the (vane) angle thresholds for activation by 8°. In other words, functionally the system does not lower the Stall Warning and Stick Pusher thresholds, but shifts (increases) the calculated [α_v] values (which are also the values recorded by the [F]DR).

For simplicity and clarity, instead of increasing α_v by 8° in Figure 20, the α_v threshold values for stick shaker and stick pusher activation have been lowered by 8° to account for the "PUSHER ICE MODE" being on. The Figure shows that as expected, the stick shaker and stick pusher activated at the times α_v crossed the respective activation thresholds, except at the initial exceedance of the pusher threshold at 12:32:28.4. This too is expected; the AFM (p. 7-21-1) states that "the stick pusher is inhibited for 5 seconds after lift-off. The shaker and the stall warning are operative immediately after lift-off." The FDR WOW discrete indicates that the airplane lifted off at about 12:32:28; consequently, the stick pusher would have been inhibited until about 12:32:33. Per Figure 20, by 12:32:33 α_v had decreased below the stick pusher threshold, and so no pusher activation would have occurred.

V. "Desktop" and piloted simulation studies

Introduction

As mentioned above, both an engineering "desktop" simulation (a computer program run without pilot interaction) and a piloted simulation (conducted in a Level D training simulator[13]) were used to estimate additional aircraft performance parameters not recorded on the FDR, and to evaluate the effects of the airplane's loading on the pilot workload during takeoff and initial climb.

The desktop simulation was used to approximately match the accident takeoff (and the preceding takeoff from KIDA) in order to:

1. Compare N56KJ's performance with expected performance as defined by the simulator; and

2. Compute a set of flight control inputs that result in an approximate match of the airplane's motions (the flight control inputs and control surface positions are not recorded on the FDR).

The desktop simulation model predicts a rate of climb and maximum altitude higher than that recorded on the FDR when forced to match the Euler angles recorded on the FDR. To help determine whether the difference between the simulator and real airplane performance is more likely the result of snow and ice contamination on N56KJ (see Figures 2 & 3) or of inaccuracies in the simulator model, a similar simulator match of N56KJ's previous takeoff (on the flight from KIDA to K9V9, when the airplane was not contaminated with snow) was performed. The simulator climbs faster and higher than the real airplane on this takeoff as well, indicating that the difference in performance is more likely a result of inaccuracies in the simulator model than of ice and snow on the airplane. Consequently, the simulator model was adjusted to produce a better match of the takeoff from KIDA, and then the adjusted model was used to match the

[13] Simulator qualification levels (such as "Level D") are described below.

accident takeoff. The adjusted model matches the accident takeoff much better than the original model. While the results of the adjusted model do not match the FDR data perfectly, they are close enough that it is not possible to discern any performance degradation due to snow and ice on the airframe from these results, or to distinguish such effects from remaining inaccuracies in the model.

The piloted simulator tests indicate that the takeoff rotation technique, particularly the abruptness and magnitude of the initial column movement and consequent initial pitch rates, when coupled with an airplane loaded beyond its gross weight and aft CG limits, can have a significant effect on the workload involved with maintaining a target pitch attitude.

The desktop and piloted simulator tests are described in more detail below.

Desktop simulations

Desktop simulator matches of the accident flight were performed in attempts to generate a flight trajectory that is consistent with the FDR data, crash site location, and the expected performance capabilities of the airplane. The simulations also yield a set of control and throttle inputs that are consistent with the simulated trajectory (though it should be noted that other inputs, which produce similar but slightly different trajectories, could also be generally consistent with the recorded data).

The following information sources define the “target” trajectory and the airplane model used in the simulation, and provide criteria by which to measure the quality of the simulation match:

FDR data: For the simulation to “match” the FDR data, the position, speed, and attitude of the simulated airplane should agree well with corresponding data recorded on the FDR. The simulation altitude should also match the best estimate of altitude obtained from the FDR (the “FDR accelerometer integration” altitude in Figure 9).

Crash site data: The simulation and actual crash sites should coincide.

Wind data: A wind from 020° (true) at 8 knots is used in the simulation. This wind is consistent with the AWOS reports shown in Table 1, though the wind speed is increased from 7 to 8 knots to produce a better match of the recorded flight path.

Simulation model: The model should be representative of the Pilatus PC-12 aerodynamics and engine thrust capabilities. Airplane aerodynamics and engine simulator models provided by Pilatus were used for this *Study*. These models were developed by Pilatus for SIMCOM (a flight simulator manufacturer), and are largely complete, except for the flight control system. For this system, Pilatus provided system description reports (including control gearing ratios and aerodynamic surface hinge moments) from which a flight control system model could be constructed. As described in Reference 9, the resulting model yielded reasonable control forces in the pitch and yaw axes, but did not yield reasonable control forces in the roll axis. For the roll control forces, a simpler, linearized model provided to the NTSB for a previous PC-12 accident investigation was used, and this model did yield reasonable roll control forces. The simulation also incorporates a landing gear model developed by the NTSB using gear geometry and properties data provided by Pilatus.

The fidelity of an airplane simulator model (that is, how accurately it represents the behavior and performance of the real airplane) can be characterized by the simulator "qualification levels" defined in 14 CFR Part 60. Appendix A to Part 60 defines the "qualification performance standards" (QPS) for "Airplane Full Flight Simulators" (FFSs) and Appendix B defines the QPS for "Airplane Flight Training Devices" (FTDs). FFSs include visual and motion systems, and are supported by aerodynamic and system models that must meet objective measures of fidelity in all phases of flight, including takeoff and landing. FTDs do not require visual or motion systems, and meet less stringent measures of fidelity applicable across fewer phases of flight. There are also different qualification levels within the FFS and FTD categories, with higher levels reflecting more demanding requirements. The highest FFS level, used for training transport-category airplane pilots, is Level D. The SIMCOM PC-12 model was developed to support a Level 6 FTD, not a Level D FFS. Of note for the context of this investigation, Level 6 FTDs do not require a "proof of match" (demonstration of fidelity) of takeoff maneuvers, in which the control forces and control surface movements, Euler angles, and flight path of the simulated airplane are shown to duplicate those of the real airplane in identical conditions. As stated by SIMCOM[14] in response to an NTSB request for proof-of-match data for a takeoff maneuver,

> … SIMCOM's engineering department [confirms] that because this is a level 6 device there is no "proof of match data" responsive to your request. In addition, there is not a SIMCOM "engineering model" per se. Rather, the SIMCOM device was developed utilizing a generic (i.e. non-aircraft specific) predictive model provided by a third party vendor, which SIMCOM then adjusted against Pilatus provided aircraft performance data (from sources such as the POH) to achieve the necessary accuracy to obtain level 6 qualification.

Consequently, the modifications to the SIMCOM model required to make the simulation better match the takeoff from KIDA (described below) are more easily justified than they would be if the model were qualified to Level D FFS standards.

The simulation matches were performed in two ways:

1. By forcing a match of the FDR pitch, roll, and heading angles, and letting the simulation compute the resulting flight trajectory with engine power set to match FDR data; and

2. By using a "math pilot" to generate control inputs to approximately match the pitch, roll, and heading angles recorded on the FDR, with engine power set to match FDR data.

In the first strategy, the match of the FDR Euler angles is perfect; in the second, it is only approximate. The first strategy eliminates any differences between the simulated and FDR flight trajectory associated with not matching the Euler angles perfectly.

For both strategies, the weight and CG are set to 10,557 lb. and 245.76 inches aft of datum, per Table 5. The configuration of the airplane (flaps and gear positions) are driven by the gear and flap handle discretes recorded by the FDR. The simulation throttle is set to takeoff power, and the resulting shaft horsepower is multiplied by a factor varying between 1.033 and 1.04 to approximately match the power computed from the torque and propeller RPM (NP) values recorded on the FDR (see Figure 18).

The simulation results using the first strategy are depicted in the Figures of this *Study* as the lines labeled "Simulation: drive Euler angles." The results using the second strategy are depicted as the lines labeled "Simulation: drive flight controls."

[14] Email from SIMCOM to the NTSB dated April 9, 2021.

The line labeled “Simulation: drive Euler angles (unmodified model)” in Figures 9 and 11 shows that driving the original (unmodified) simulation model with the FDR Euler angles results in a rate of climb and maximum altitude notably higher than those computed from the accelerometer integration. Reasons for this might include inaccuracies in the simulator model itself, and / or a degradation in N56KJ’s aerodynamic performance (specifically, decreased lift and increased drag) due to snow and ice accumulation on the airframe.[15]

To evaluate the fidelity of the simulation model without the uncertainties introduced by the snow and ice, simulator matches of the takeoff from KIDA were performed, using the same two strategies introduced above. The loading of the airplane on the takeoff from KIDA is assumed to be similar to that of the accident flight. The results of these simulations are shown in Figures 21-31. Note in Figures 22 and 24 that the unmodified simulation model climbs faster and higher than the actual airplane for the takeoff from KIDA as well, when the airplane was free of snow and ice accumulations. Hence, the differences in climb performance between the simulator and the actual airplane observed during the takeoff from KIDA and the accident takeoff are likely primarily due to inaccuracies in the simulator model. For both takeoffs, a better match of the FDR data is obtained by effectively reducing the incidence angle of the wing in the simulator model.

Specifically, the simulator model was modified so as to reduce the angle of attack used to compute the aerodynamic properties of the airplane:

$$\alpha_m = \alpha + \alpha_c \qquad [8]$$

Where α_m is the angle of attack used in the model to compute the aerodynamic properties, α is the true angle of attack, and α_c is an angle of attack “correction” dependent on the flap angle:

$$\alpha_c = -0.4° \text{ (flaps up)} \qquad [9a]$$
$$\alpha_c = -1.7° \text{ (flaps 15)} \qquad [9b]$$

Values of α_c for flap angles between 0° and 15° are determined by linear interpolation. As shown in Figures 9, 11, 22, and 24, the modified simulation matches the FDR climb performance better than the unmodified simulation. Moreover, the differences between the modified simulation results and the FDR data during the accident takeoff are similar to those during the KIDA takeoff, and so the simulator matches do not reveal any significant degradation in performance due to the snow and ice accumulations shown in Figures 2 & 3.

Figure 20 shows that on the accident flight, the FDR vane angle first enters the stall region at about 12:32:50, and penetrates deeply into the stall region after about 12:32:52. Consequently, after these times separated flow over portions of the wings is likely, and the fidelity of the aerodynamic model will degrade. The divergence between the airplane and FDR flight paths shown in Figures 8 and 9 is consistent with this premise. However, up to the stall, the agreement between the (modified) simulation model and the FDR data is relatively good. Consequently, using the simulation to infer other, unrecorded information about the flight up to the stall is reasonable; of particular interest are the flight control inputs, forces, and control surface

[15] Additional weight resulting from snow and ice on the airplane was also considered, but tests with the simulator indicated that a rational amount of added snow weight, by itself, could not explain the observed differences in performance.

positions. These parameters, determined by using the math pilot to drive the flight controls, are plotted in Figures 15-17 for the accident takeoff, and in Figures 29-31 for the KIDA takeoff.

For the accident flight, Figure 15 indicates that the motions of the airplane until about 12:32:55.5 (after which α is well into the stall region) can be commanded with flight control inputs well within the authority limits of the controls. At 12:32:55.5 the math pilot briefly commands more wheel and aileron than is available, which is invalid. However, this exceedance is brief, and occurs in a regime (stall) where the simulator model is questionable. As discussed above, the simulation results are mostly relevant until about 12:32:52, while α is below the stall region.

It should be noted that as the airplane rolled left from 0° to -32° between 12:32:45 and 12:32:50, the simulation wheel remains within about 30° of neutral, and so there was plenty of wheel authority available to keep the wings level if desired. A little after 12:32:50, as α first entered the stall region, the roll increased to -38°, and after 12:32:52.5, when α penetrated deeply into the stall region, the roll increased rapidly to -63°. Hence, asymmetric wing stall might have contributed to the increase in roll angle beyond -32° after 12:32:50.

Figure 16 indicates that the simulation math pilot required an abrupt, 40 lb. pull on the column at 12:32:27 to match the takeoff rotation pitch angle profile. Figure 12 shows that the pitch angle increased from about 1° to 11.8° in about 1.9 seconds (at a peak rate of about 8.5°/sec). These pitch rate and takeoff pitch angle values are similar to those achieved by the accident pilot on previous takeoffs, and are higher than the values achieved during takeoffs performed by a different pilot. Figure 32 compares the pitch angles achieved during 11 different takeoffs recorded on the FDR; the black lines correspond to the takeoffs performed by the accident pilot, and the blue lines correspond to the takeoffs performed by the second pilot. The red line is the target takeoff pitch angle (9°) commanded by the Flight Director (FD), if turned on.

On the flight from KIDA to K9V9, the airplane was likely loaded similarly to the accident flight (heavy weight and extreme aft CG), and that takeoff exhibits a 36 lb. pull at rotation, an average pitch rate of 4.3°/sec, pitch angles above the 9° FD target, and pitch oscillations that might be the result of decreased stability and light column forces (as discussed in the *Piloted Simulations* section below). The accident pilot's takeoffs on the flights from KIDA to KHSH and back also employ an initial pitch rate similar to that on the accident takeoff, and pitch angles higher than the 9° FD target, though the initial rotation pitch angles on these takeoffs (where the pitch pauses for a second or two before increasing further) are between 7° and 9°. (The accident takeoff rotation overshot the FD target, reaching 11.8° and pausing for less than a second before increasing further, eventually reaching 15.8°.)

In contrast, the takeoffs performed by the second pilot employ much lower pitch rates (less than 3°/s) and a lower initial pitch angle (about 5°) before slowly increasing towards the 9° FD target pitch angle. Figure 32 indicates that the second pilot and the accident pilot used different takeoff rotation techniques. The piloted simulations discussed below suggest that the higher initial rotation pitch rates and angles apparently favored by the accident pilot, combined with the extreme aft CG, heavy weight, and an early rotation on the accident takeoff, contributed to the airplane's high α immediately after rotation, the triggering of the stick shaker and stick pusher, and the pilot's pitch control difficulties.

Piloted simulations

In addition to the desktop simulations described above, the NTSB conducted pilot-in-the-loop simulations in a PC-12 Level D Full Flight Simulator (FFS) operated by FlightSafety International. The simulation test plan and run log for these tests are contained in Appendix B.

As stated in the test plan,

> The objective of this piloted simulator test is to evaluate the effect of the center of gravity (CG) position of the airplane on its longitudinal handling qualities. Specifically, several takeoffs will be performed, starting with the CG in a mid-position and moving the CG further aft during each successive takeoff, ending at the accident CG. For each takeoff, a record will be kept of both the subjective pilot assessment of the workload required to maintain a predetermined climb airspeed and associated pitch attitude while performing other normal tasks, and of objective measures of the pitch attitudes, rates of climb, and speeds achieved, and of the flight control inputs required. If time allows, measures of stick force per knot and per G will also be taken.
>
> This evaluation may help investigators understand the reasons for the pitch oscillations recorded on the accident airplane's LDR during the accident takeoff and the previous takeoff (for which the airplane was likely loaded in a similar manner to the accident flight). This information may also help evaluate the accident pilot's workload and susceptibility to spatial disorientation during the accident takeoff.

It was not possible to retain recorded electronic data from the simulator (that would have provided a record similar to an FDR recording), so instead the "objective measures of pitch attitudes …" etc. mentioned in the test plan were obtained by taking video recordings of the instrument panel during each run.

The simulator was used to test the effect of CG position on the airplane's longitudinal stability (measured as column force per knot in steady trims and column force per G in constant-speed steep turns). In the trim tests, the airplane was trimmed in steady level flight at 120 knots, and then the column was moved to achieve airspeeds above and below 120 knots (without changing thrust). The column force required to maintain each of the different speeds was noted. In the steep turn tests, the airplane was trimmed in steady level flight at 120 knots, and then rolled to progressively steeper bank angles, while the column was used to maintain 120 knots without changing thrust. The column force required to maintain 120 knots at each bank angle was noted.

The results of the FFS stability tests are compared to the results of similar tests performed with the desktop simulation in Figures 33 and 34. The desktop tests were performed in two ways: by keeping power constant and maintaining speed by varying the flight path angle (as was done in the FFS), and by maintaining level flight (zero flight path angle) while adjusting power at each airspeed or bank angle to maintain speed. Figures 33 and 34 present the results of both methods.

As expected, the airplane is less stable at the accident CG of 245.76 inches than at a mid-CG of 236 inches: at the aft CG, it takes a smaller increment in column force to maintain an airspeed increment from the trim speed or to maintain 120 knots at a given bank angle. The airplane is also less stable (has lower column forces) at high α (low airspeed and steeper bank angles) than at low α (high airspeed and shallower bank angles). Nonetheless, the airplane still has positive stability (negative column force per knot and positive column force per G) in the α and CG ranges tested, even at a CG of 245.76 inches, which is behind the aft CG limit.

The FFS results in Figures 33 and 34 show a lower stability than the desktop simulation, though they show similar trends (lower stability at aft CG and high α). One likely reason the FFS column forces are lighter than in the desktop simulation is that the FFS incorporates a more sophisticated model of the control system, including the effects of friction and hysteresis, which are not incorporated in the desktop model.[16]

The decreased stability at aft CG was apparent to the participants in the FFS takeoff tests. At a CG of 245.76 inches, the workload to keep the airplane tracking down the runway with the rudder pedals was higher than at a mid-CG, as was the concentration and effort required to keep the airplane from over-rotating into the stall region, and to keep the pitch angle stable near the 9° FD takeoff target. Once a pilot over-rotated the airplane into the stick shaker or stick pusher α region, he was much more likely to develop a pitch oscillation that would exit and re-enter the stall warning region (similar to the pitch behavior on the accident flight).

As noted above, with the PUSHER ICE MODE active, the α vane values that trigger the stall protection systems are effectively lowered by 8°, which in turn increases the airspeeds below which these systems will be active. Consequently, the additional 10 knots that the AFM indicates should be added to the rotation speed with the PUSHER ICE MODE active becomes important, as it provides the required margin from stall warning upon rotation. If rotation is initiated early (at a speed lower than prescribed), then the margin to the stall warning is reduced. In the accident, the nominal rotation speed with the PUSHER ICE MODE active was 92 knots; as noted above, the FDR data (and Figure 16) indicates that the pull on the column to initiate the rotation likely occurred closer to 88 KIAS, or 4 knots below the 92 KIAS target.

The FFS participants found the takeoff much easier to control using a rotation technique like that used by the second pilot in Figure 32, involving lower pitch rates and angles than the technique used by the accident pilot during the accident and previous takeoffs. In the alternative technique, the airplane is allowed to gently fly off the runway, without using a relatively abrupt and heavy pull on the column, which (at the accident CG) can easily lead to over-rotation.

E. CONCLUSIONS

This *Aircraft Performance & Simulation Study* presents the results of using recorded flight data from the airplane's Flight Data Recorder (FDR), video evidence, the crash site location, recorded weather data, and simulation results to determine the position, orientation, and other relevant performance parameters of the airplane during the accident flight. An engineering "desktop" simulation of the flight yields a set of control and throttle inputs that make the simulation approximately match the airplane trajectory and performance recorded on the FDR. Tests conducted in a Level D full-flight training simulator provide insight into the effects of improper loading of the airplane and of different takeoff rotation techniques on the workload involved with capturing and maintaining a target pitch attitude during takeoff and initial climb.

The sequence of events during the accident, from the pilot's efforts to remove snow and ice from the airplane before taxi, to the takeoff and subsequent impact with terrain, are described in Section C (History of Flight). As detailed there, the pilot made several operational errors:

[16] Information about the PC-12 flight control system provided by Pilatus included friction data, but this information was not built into the NTSB's implementation of the simulator model. The column friction force is about 10 lb.

- Contrary to guidance in the AFM, the pilot attempted to remove snow and ice from the airplane outdoors while frozen precipitation was falling, and he did not completely remove snow and ice accumulations from the vertical and horizontal stabilizers.
- There were more people on the airplane than available seats.
- The airplane was loaded 107 lb. above the maximum gross weight.
- The airplane was loaded between 3.99 and 5.49 inches aft of the aft CG limit, significantly lessening the longitudinal stability of the airplane.
- The pilot initiated the takeoff rotation at about 88 knots, 4 knots slower than the prescribed rotation speed with the ICE PUSHER MODE active, decreasing the margin to the stall warning at rotation.

Adjustments to the desktop simulation model had to be made to match the rate of climb and altitude achieved during the takeoff from KIDA on the flight to K9V9 (the flight preceding the accident flight). The modified model matches the previous takeoff and the accident takeoff relatively well. The simulation of the accident takeoff did not reveal any obvious performance degradation resulting from the residual snow and ice on the airframe depicted in Figures 2 and 3, though the effects of these accumulations on the airplane CG and airflow over the horizontal stabilizer (which could affect the elevator hinge moments and column forces) are unknown.

The piloted simulations conducted in the Level D FFS suggest that the pilot's rotation technique, which involved a relatively abrupt and heavy pull on the column, when combined with the extreme aft CG, heavy weight, and early rotation on the accident takeoff, contributed to the airplane's high α immediately after rotation, the triggering of the stick shaker and stick pusher, and the pilot's pitch control difficulties. The resulting pitch oscillations eventually resulted in a deep penetration into the stall region and subsequent loss of control.

The FFS participants found the takeoff much easier to control using a rotation technique like that used by a different pilot during previous flights of N56KJ, involving lower pitch rates and angles than the technique used by the accident pilot during the accident and previous takeoffs. In the alternative technique, the airplane is allowed to gently fly off the runway, without using a relatively abrupt and heavy pull on the column, which (at the accident CG) can easily lead to over-rotation.

_____

John O'Callaghan
National Resource Specialist – Aircraft Performance
Office of Research and Engineering

F. REFERENCES

1. National Transportation Safety Board, Office of Aviation Safety, *Factual Report: Meteorology, Pilatus PC-12, N56KJ, Chamberlain, South Dakota, November 30, 2019, NTSB Accident Number CEN20FA022.* (Washington, D.C. February 28, 2020). Available at: https://data.ntsb.gov/Docket/Document/docBLOB?ID=40482633&FileExtension=.PDF&FileName=Weather%20Factual-Master.PDF

2. National Transportation Safety Board, Office of Research and Engineering, *Image/Video Study, Pilatus PC-12, N56KJ, Chamberlain, South Dakota, November 30, 2019, NTSB Accident Number CEN20FA022*. (Washington, D.C., July 17, 2020). (Contact NTSB at pubinq@ntsb.gov.)

3. Pilatus Aircraft Ltd, *Pilot's Operating Handbook and EASA Approved Airplane Flight Manual, PC-12/47E Series MSN 545, 1001 and UP,* Pilatus Report # 02277 revision 19, dated October 16, 2018.

4. Pilatus Technical Memo TM-12-006580, Issue 2, *PC-12 MSN 1431 Trims and Flaps Position Measurement*, February 2, 2020.

5. Pilatus Aircraft Ltd., *NTSB Query Response Document (NTSB CEN20FA022), version 09,* provided in email correspondence on August 3, 2021.

6. National Transportation Safety Board, Office of Research and Engineering, *Flight Data Recorder Specialist's Factual Report, Pilatus PC-12, N56KJ, Chamberlain, South Dakota, November 30, 2019, NTSB Accident Number CEN20FA022*. (Washington, D.C., July 28, 2020). (Contact NTSB at pubinq@ntsb.gov.)

7. National Transportation Safety Board, Office of Research and Engineering, *Cockpit Voice Recorder Specialist's Factual Report, Pilatus PC-12, N56KJ, Chamberlain, South Dakota, November 30, 2019, NTSB Accident Number CEN20FA022*. (Contact NTSB at pubinq@ntsb.gov.)

8. National Transportation Safety Board, Office of Research and Engineering, *Group Chairman's Aircraft Performance Study, American Airlines Flight 587, Airbus A300B4-605R, Belle Harbor, New York, November 12, 2001, NTSB Accident Number DCA02MA001*, Docket Item 188 (Washington, DC: NTSB, October 10, 2002). (Contact NTSB at pubinq@ntsb.gov).

9. National Transportation Safety Board, Office of Research and Engineering, *Aircraft Performance Radar and Simulation Study, Pilatus PC-12, N933DC, Amarillo, Texas, April 28, 2017, NTSB Accident Number CEN17FA168* (Washington, DC: NTSB, December 6, 2017). Available at: https://data.ntsb.gov/Docket/Document/docBLOB?ID=40461657&FileExtension=.PDF&FileName=Aircraft%20Performance%20Radar%20and%20Simulation%20Study-Master.PDF

G. GLOSSARY

Acronyms

AFM	Airplane Flight Manual
AGL	Above ground level
AWOS	Automated Weather Observing System
CFR	Code of Federal Regulations
CG	Center of Gravity
CST	Central Standard Time
CVR	Cockpit Voice Recorder
FAA	Federal Aviation Administration
FD	Flight Director
FDR	Flight Data Recorder
FFS	Full Flight Simulator
FMS	Flight Management System
FTD	Flight Training Device
GNSS	Global Navigation Satellite System
GPS	Global Positioning System
K9V9	Chamberlain Municipal Airport, Chamberlain, South Dakota
KIDA	Idaho Falls Regional Airport, Idaho Falls, Idaho
LDR	Light Data Recorder
MAC	Mean Aerodynamic Chord
METAR	Meteorological Terminal Air Report
NP	Propeller RPM
NTSB	National Transportation Safety Board
RPM	Revolutions per minute
SRN	Subframe Reference Number
SRTM	Shuttle Radar Topography Mission
UTC	Coordinated Universal Time

English symbols

h	Altitude
h_{corr}	Corrected radio altitude
h_{rec}	Recorded radio altitude
$\dot{h}$	Rate of climb
u	Component of airspeed along body x-axis
v	Component of airspeed along body y-axis
V	Airspeed
$\vec{V}$	Airspeed vector
V_G	Ground speed
$\vec{V}_G$	Ground speed vector
$\vec{V}_W$	Wind speed vector
w	Component of airspeed along body z-axis

Greek symbols

α	Angle of attack
α_m	Modified α used to determine aerodynamic properties in simulator model
α_c	Angle of attack correction for simulator model
β	Sideslip angle
γ	Flight path angle
θ	Pitch angle
ϕ	Roll angle

FIGURES

Figure 1. Photograph of N56KJ taken at 11:02:49 CST (from Reference 2).

Figure 2. Comparisons of N56KJ's vertical tail area before takeoff on the accident flight with an exemplar airplane (from Reference 2).

Figure 3. Comparison of N56KJ's horizontal tail area before takeoff on the accident flight with an exemplar airplane (from Reference 2).

(a) (b)

(c) (d)

Figure 4. Video frames showing (a) taxi towards runway; (b) start of takeoff roll; (c) approximate liftoff point; and (d) N56KJ turning left and climbing into low overcast.

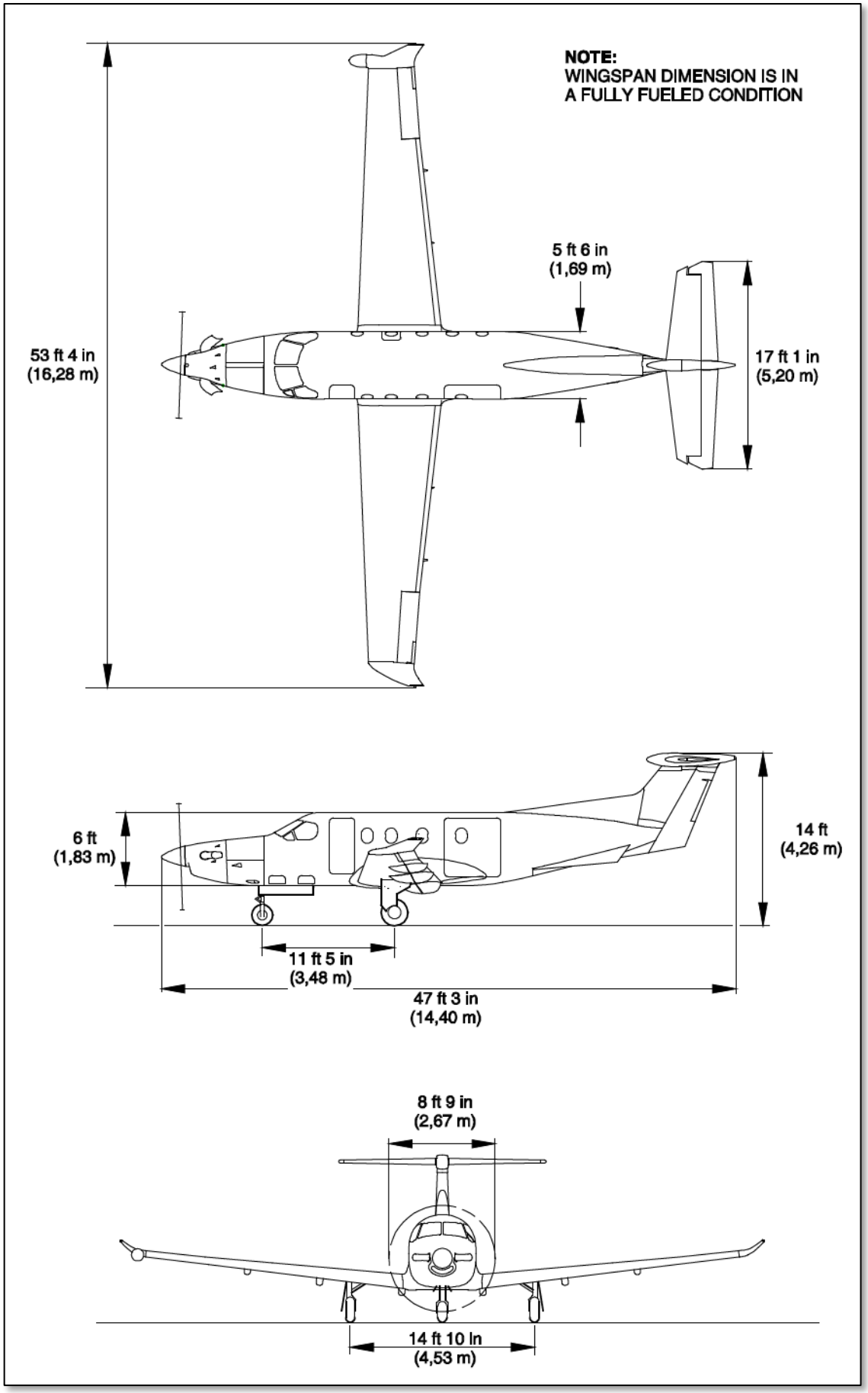

Figure 5. Pilatus PC-12/47E three-view drawing with dimensions, from Reference 3.

Pilatus PC-12/47E C.G. Envelope

Constructed from Figure 6-18 of AFM

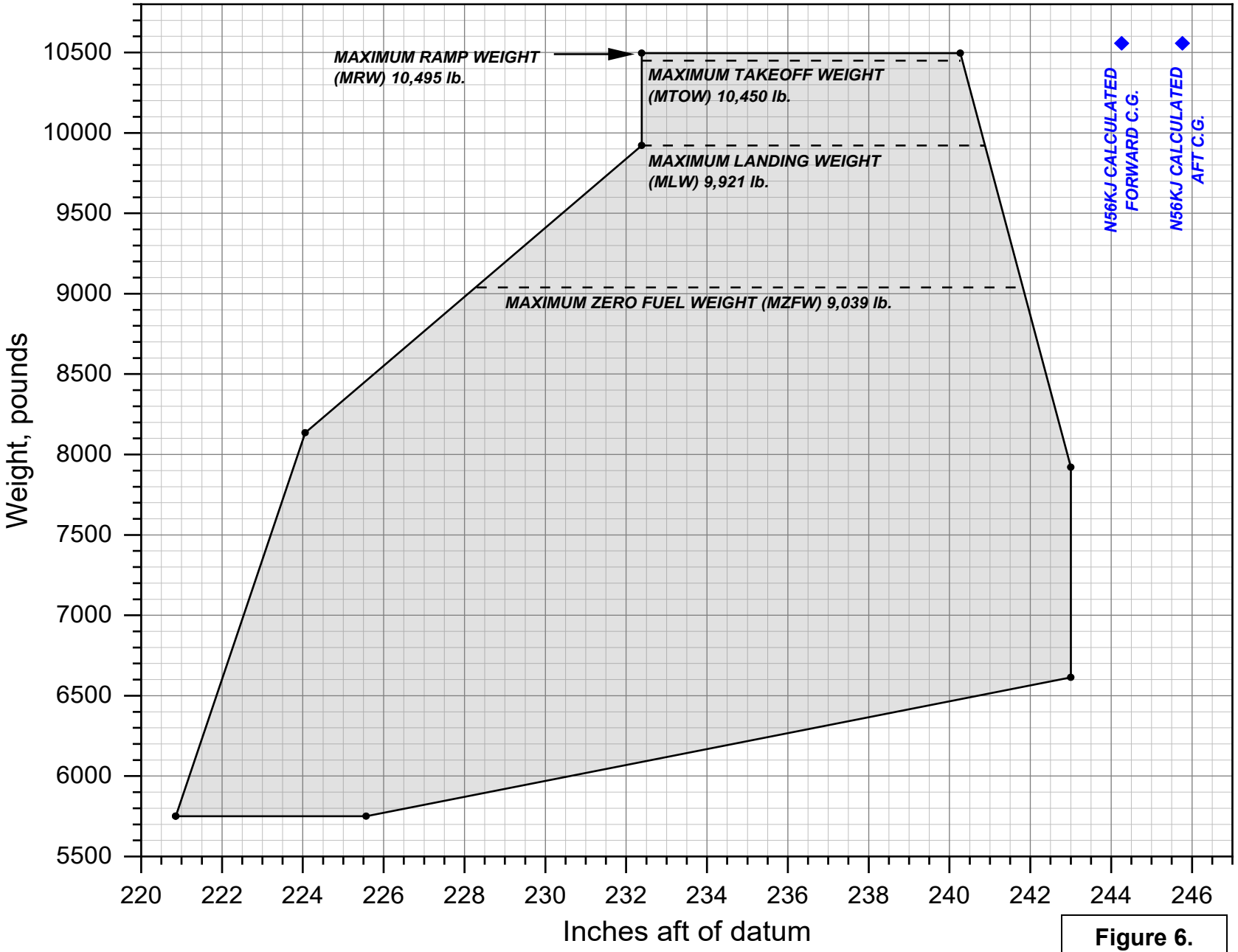

Figure 6.

Figure 7. Photograph of the wreckage of N56KJ in a dormant corn field.

CEN20FA022: Pilatus PC-12/47E, N56KJ, Chamberlain, SD, 11/20/2019

Accident takeoff simulator match: plan view of flight path

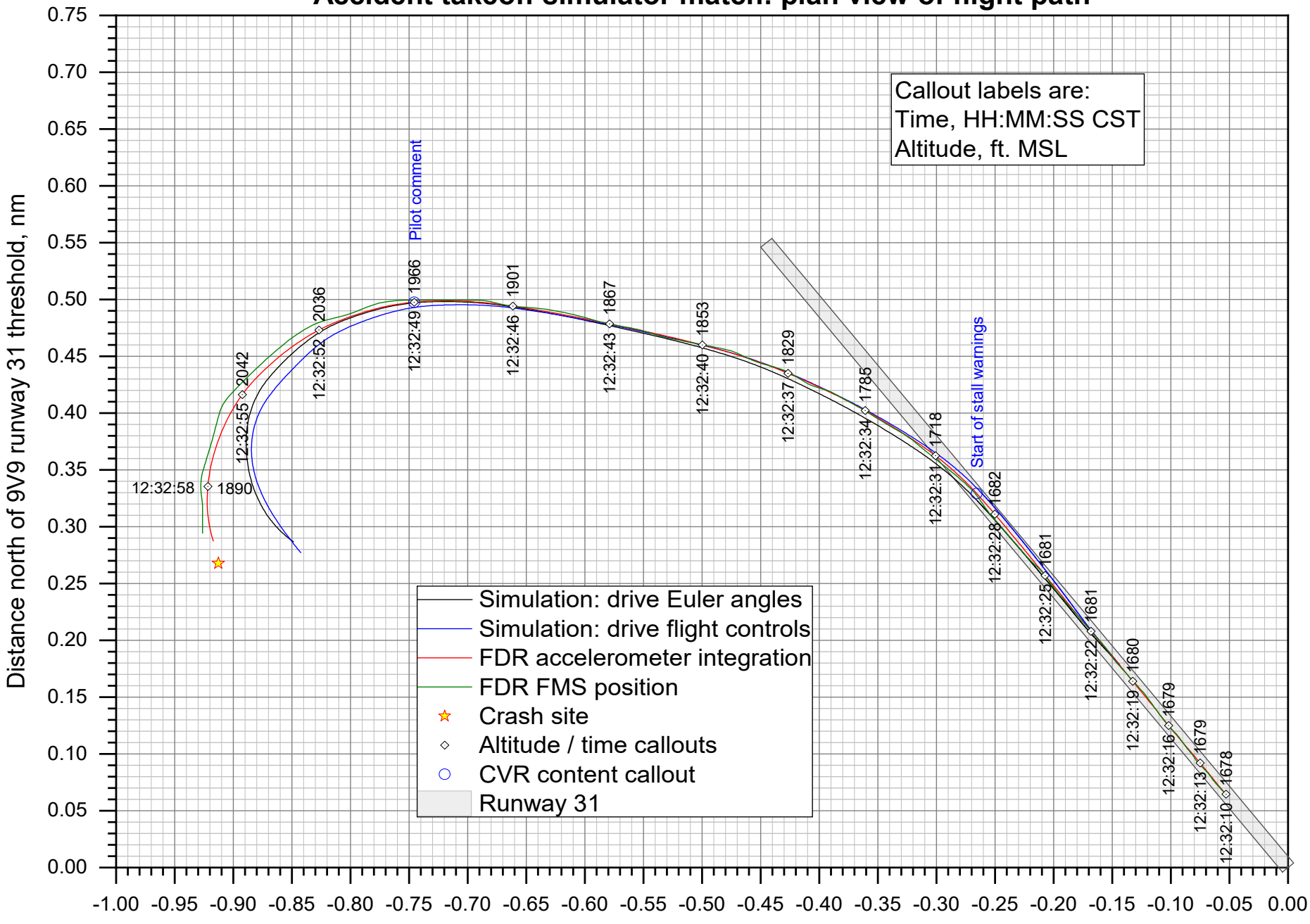

Figure 8a.

CEN20FA022: Pilatus PC-12/47E, N56KJ, Chamberlain, SD, 11/20/2019

Accident takeoff simulator match: plan view of flight path

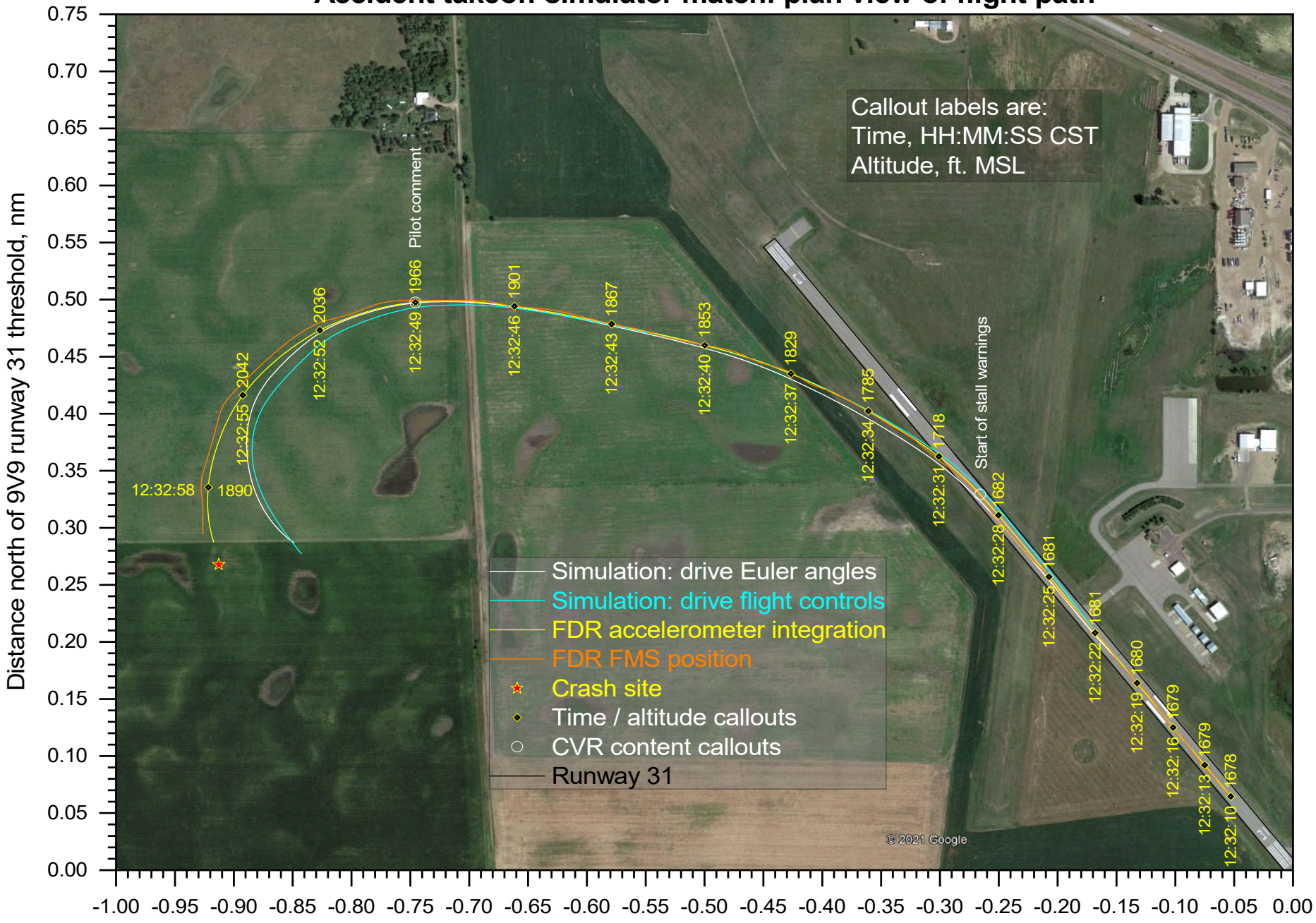

Figure 8b.

CEN20FA022: Pilatus PC-12/47E, N56KJ, Chamberlain, SD, 11/20/2019

Accident takeoff simulator match: altitude

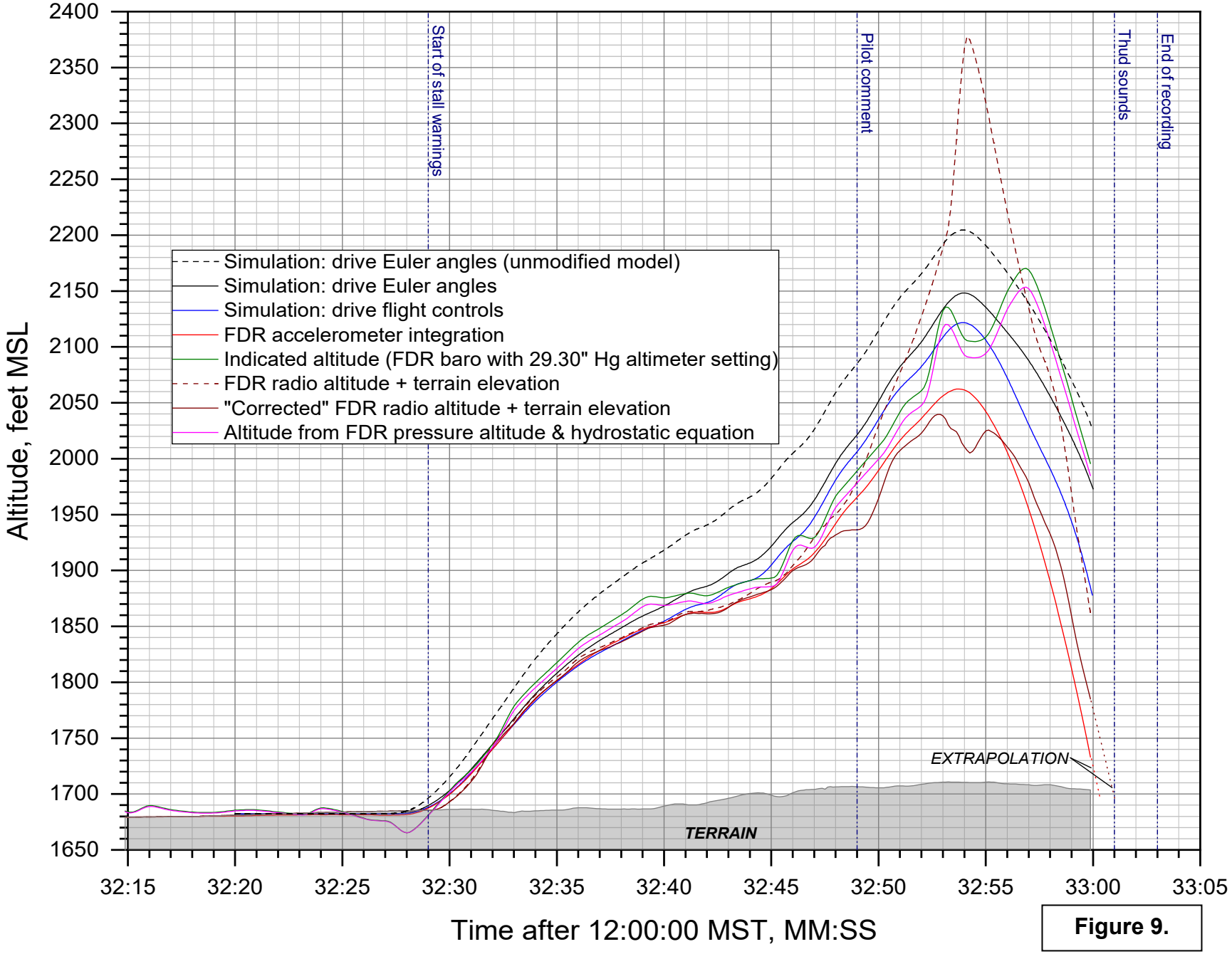

Figure 9.

CEN20FA022: Pilatus PC-12/47E, N56KJ, Chamberlain, SD, 11/20/2019

Accident takeoff simulator match: north and east coordinates vs. time

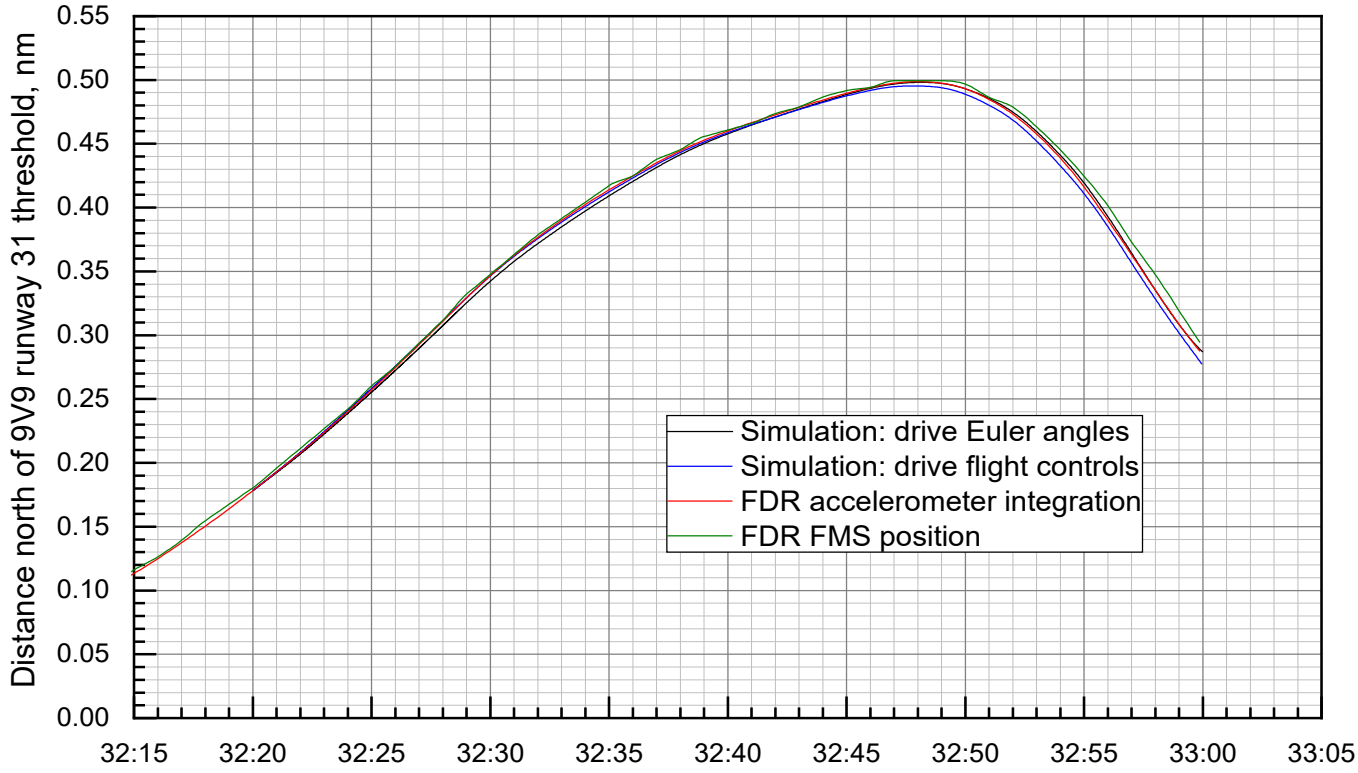

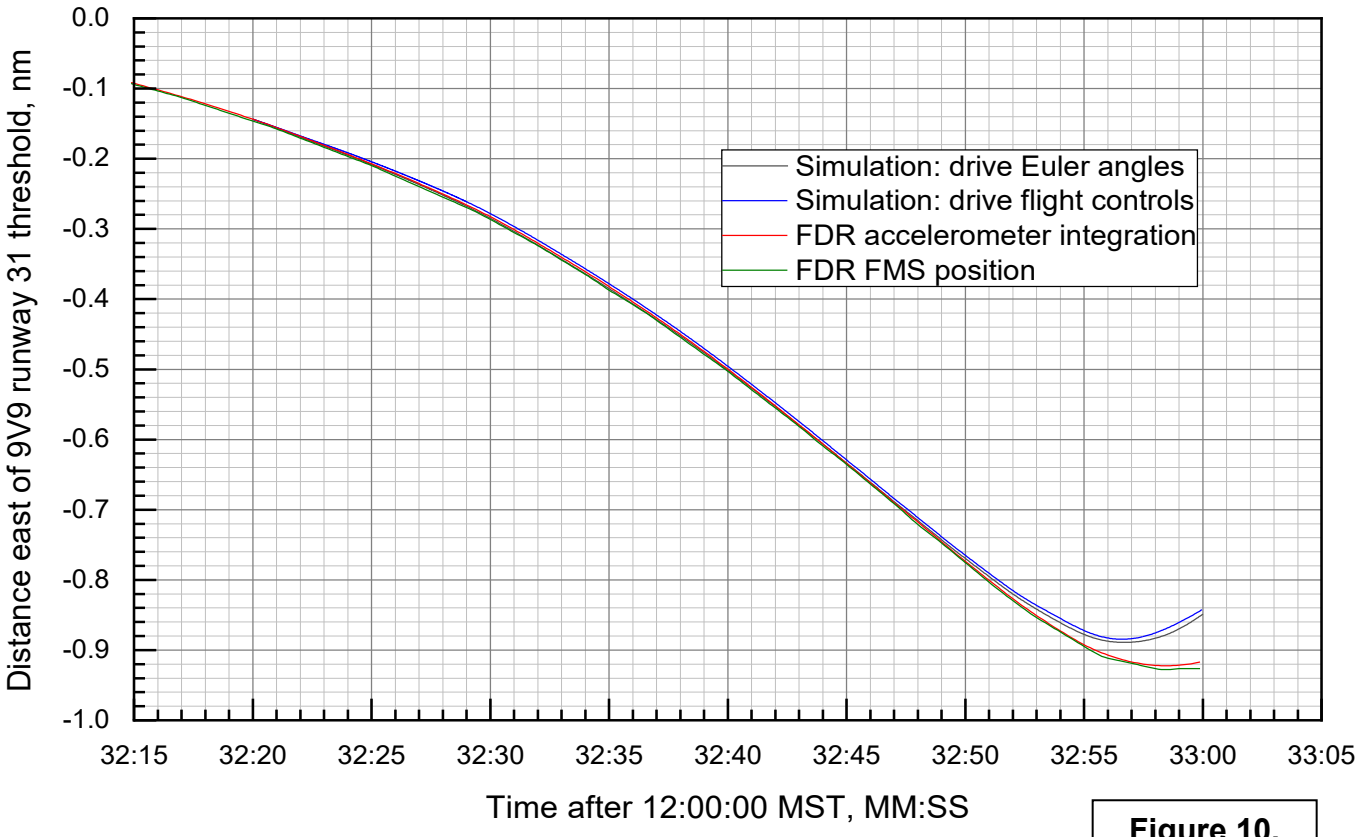

Figure 10.

CEN20FA022: Pilatus PC-12/47E, N56KJ, Chamberlain, SD, 11/20/2019

Accident takeoff simulator match: speeds vs. time

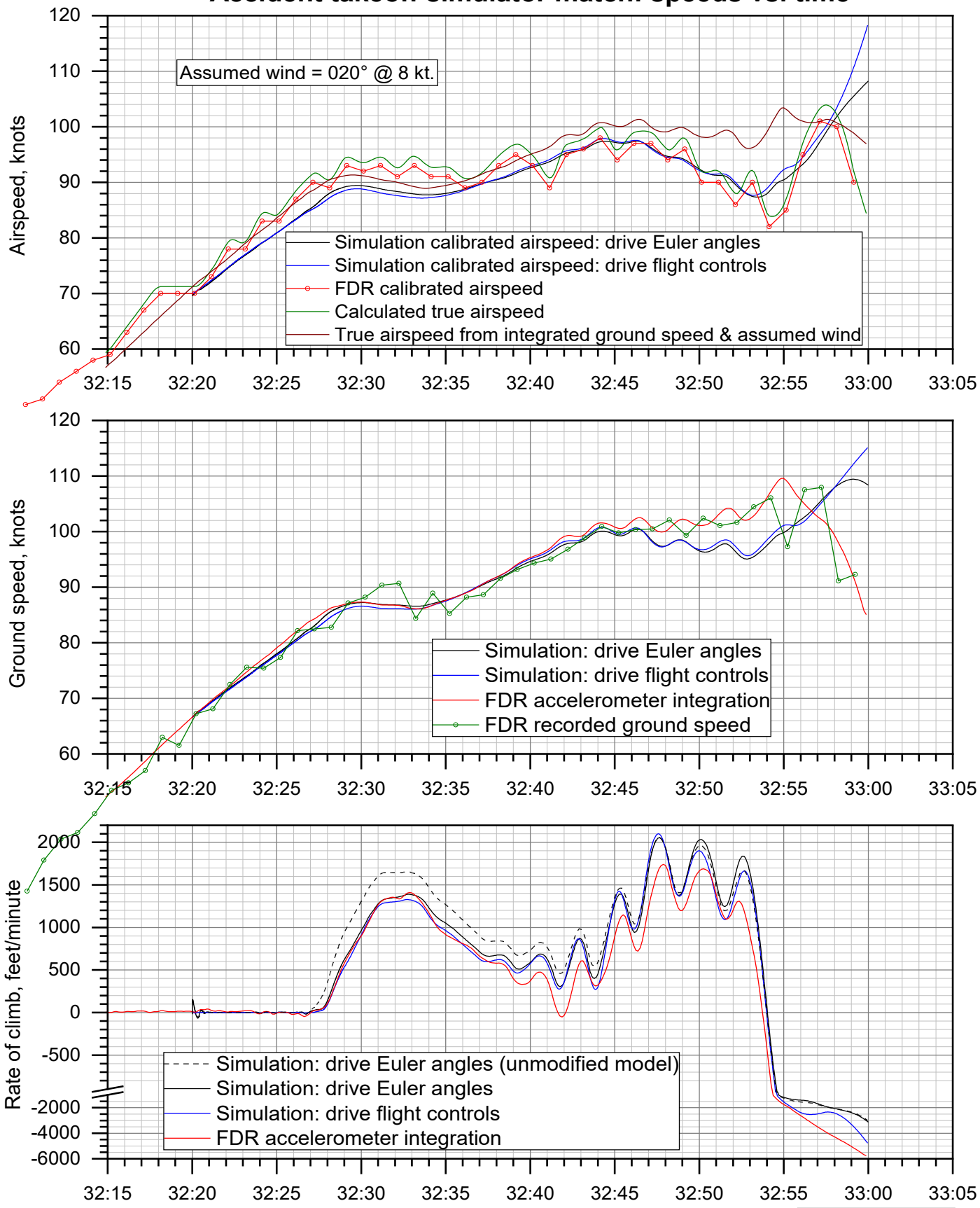

Figure 11.

CEN20FA022: Pilatus PC-12/47E, N56KJ, Chamberlain, SD, 11/20/2019

Accident simulator match: longitudinal flight angles vs. time

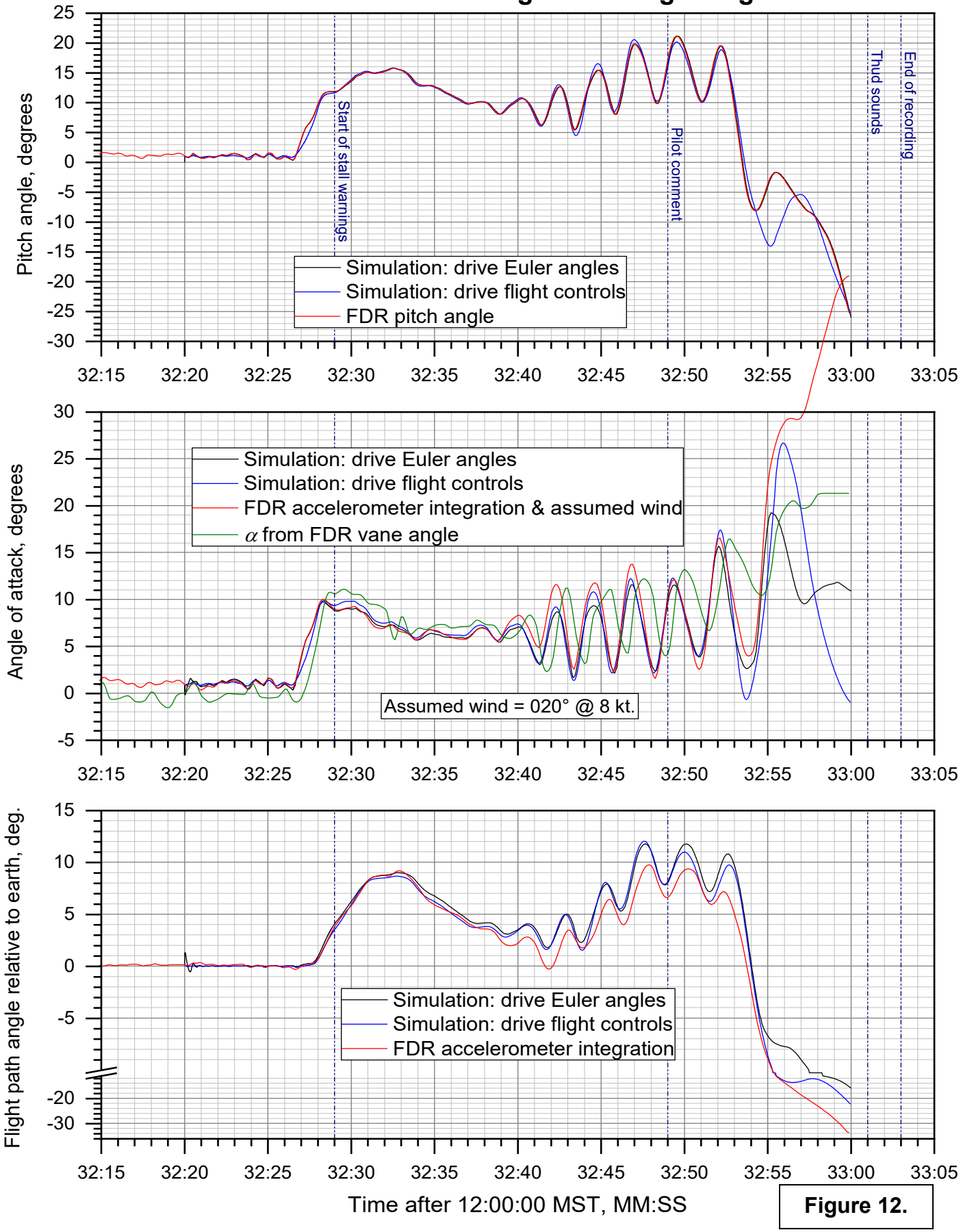

Figure 12.

CEN20FA022: Pilatus PC-12/47E, N56KJ, Chamberlain, SD, 11/20/2019

Accident takeoff simulator match: lateral flight angles vs. time

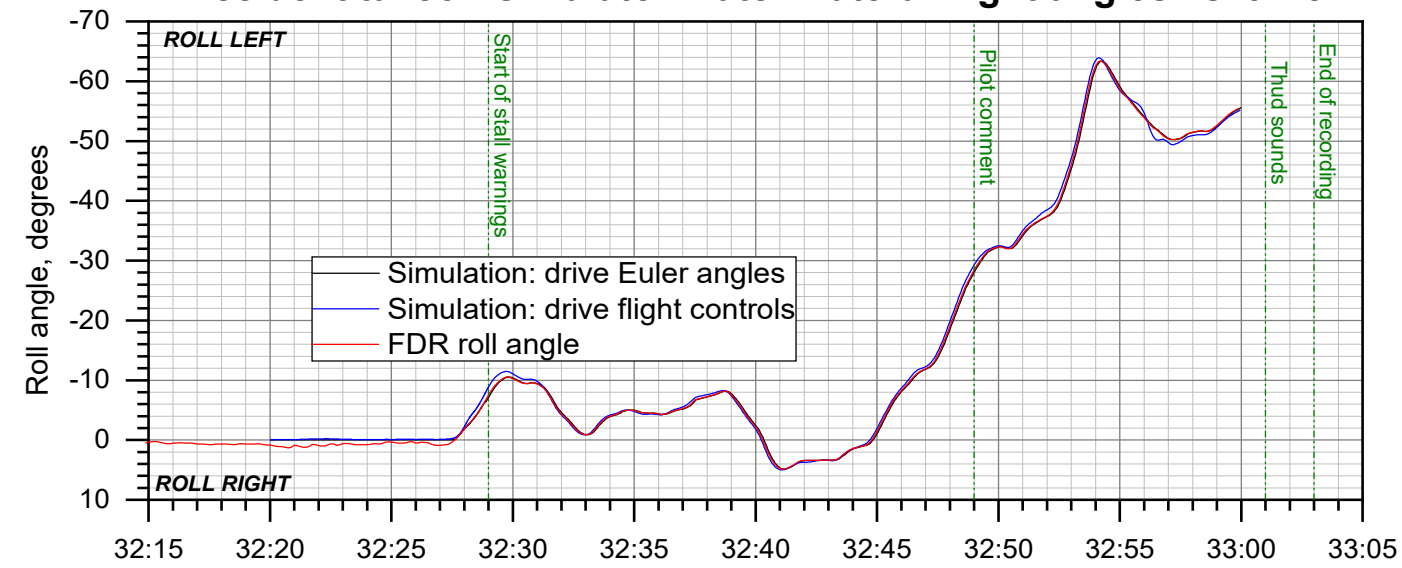

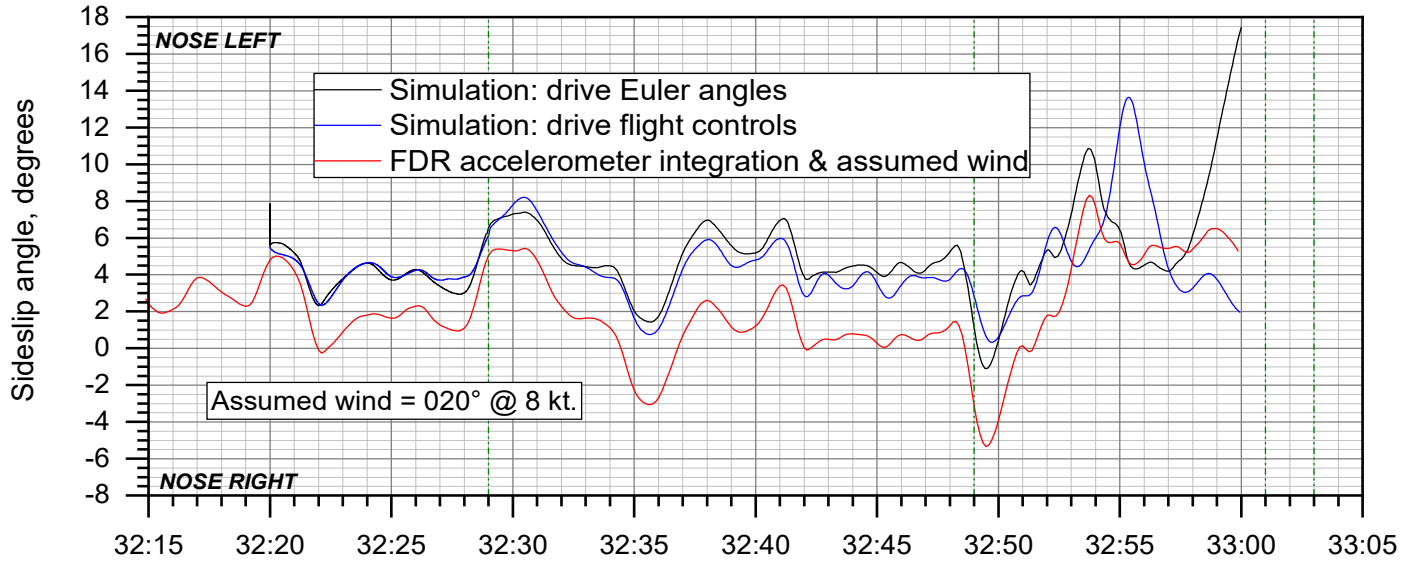

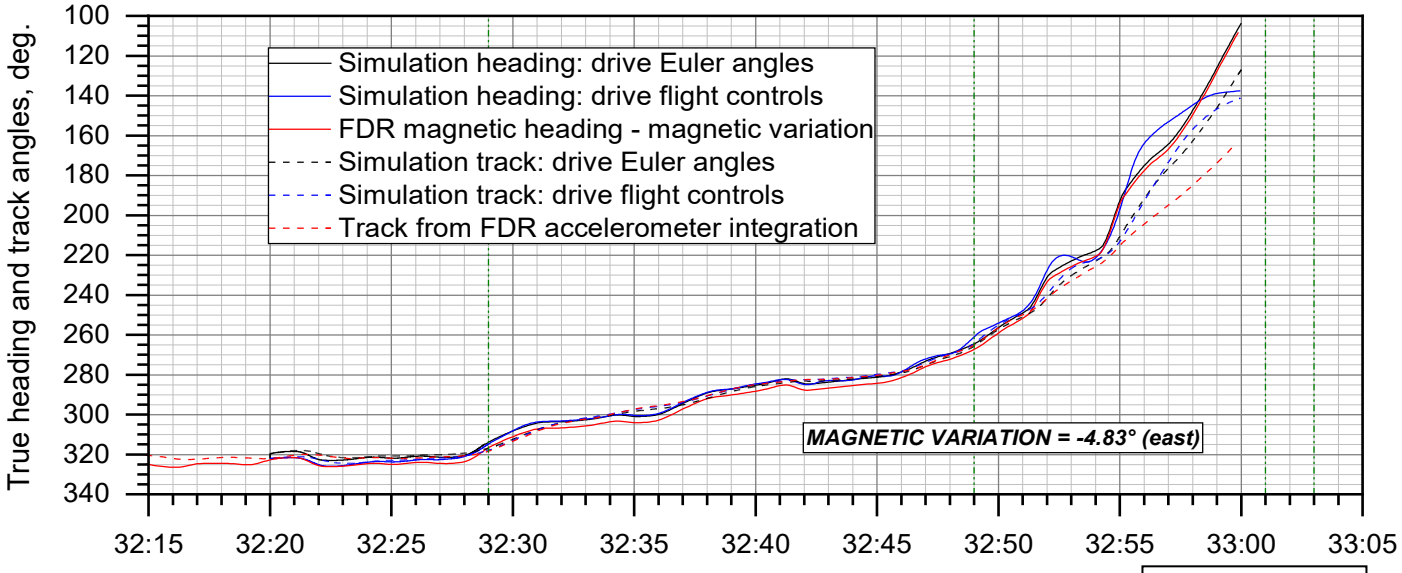

Figure 13.

CEN20FA022: Pilatus PC-12/47E, N56KJ, Chamberlain, SD, 11/20/2019

Accident takeoff simulator match: load factors vs. time

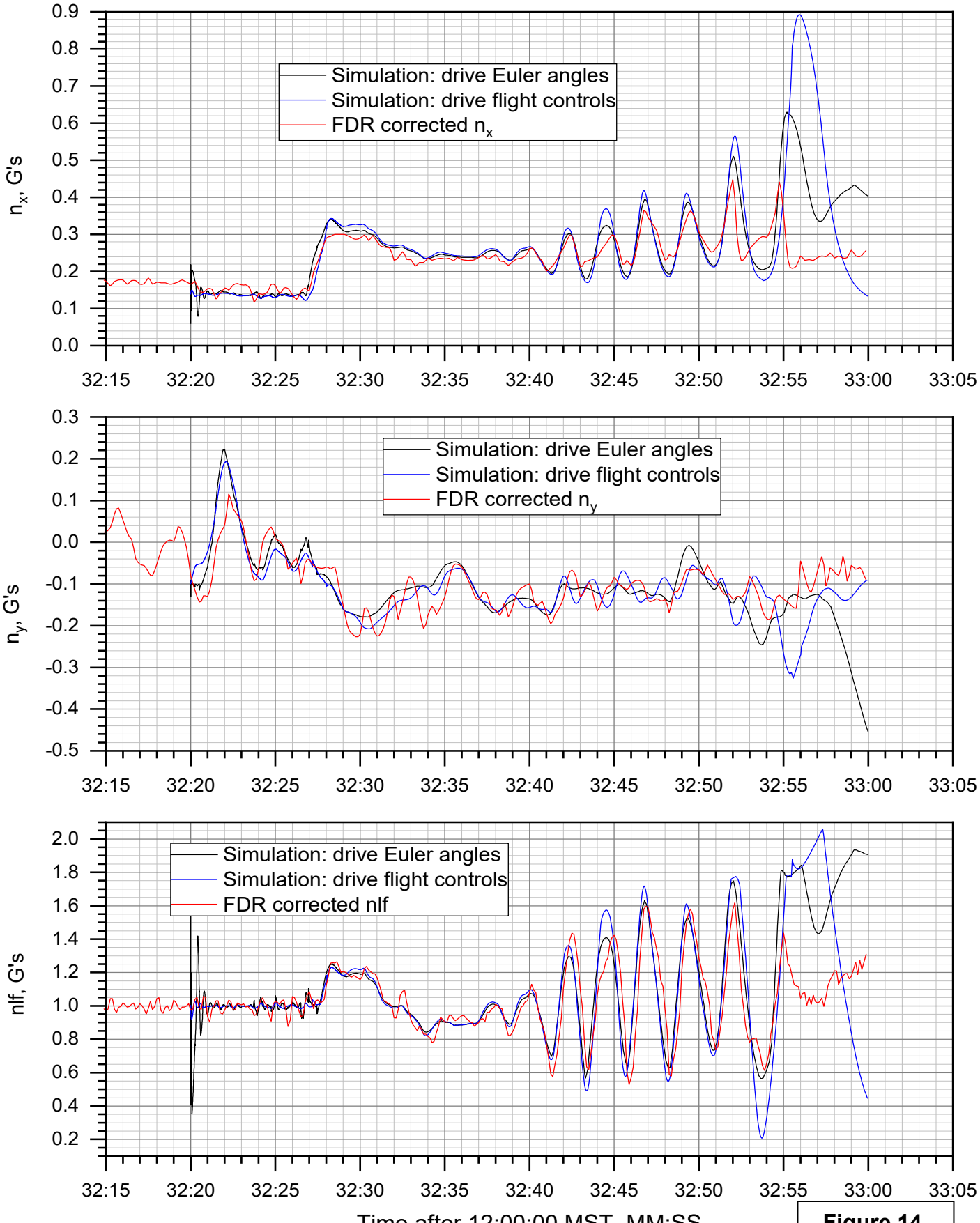

Figure 14.

CEN20FA022: Pilatus PC-12/47E, N56KJ, Chamberlain, SD, 11/20/2019

Accident takeoff simulator match: flight controls vs. time

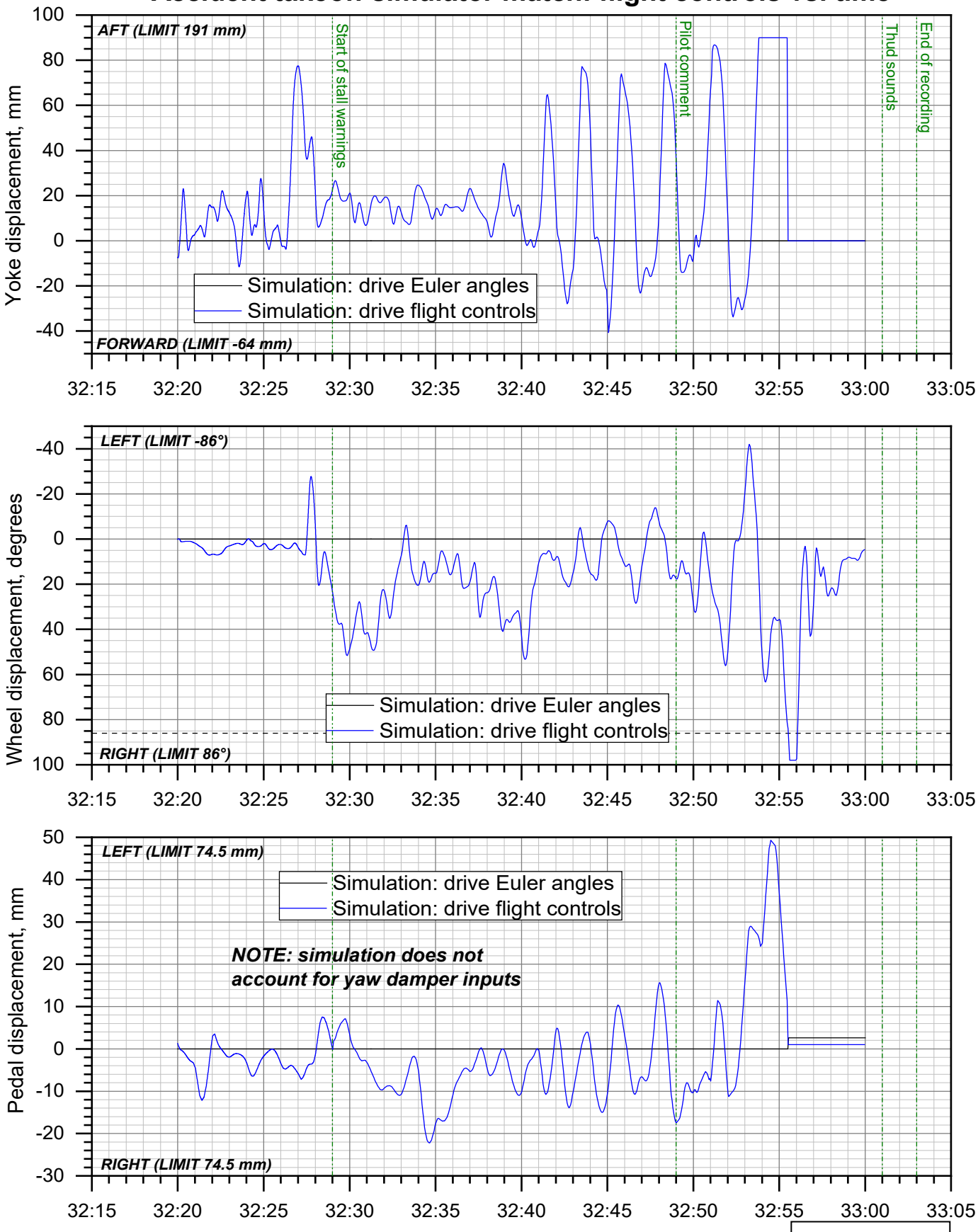

Figure 15.

CEN20FA022: Pilatus PC-12/47E, N56KJ, Chamberlain, SD, 11/20/2019

Accident takeoff simulator match: control forces vs. time

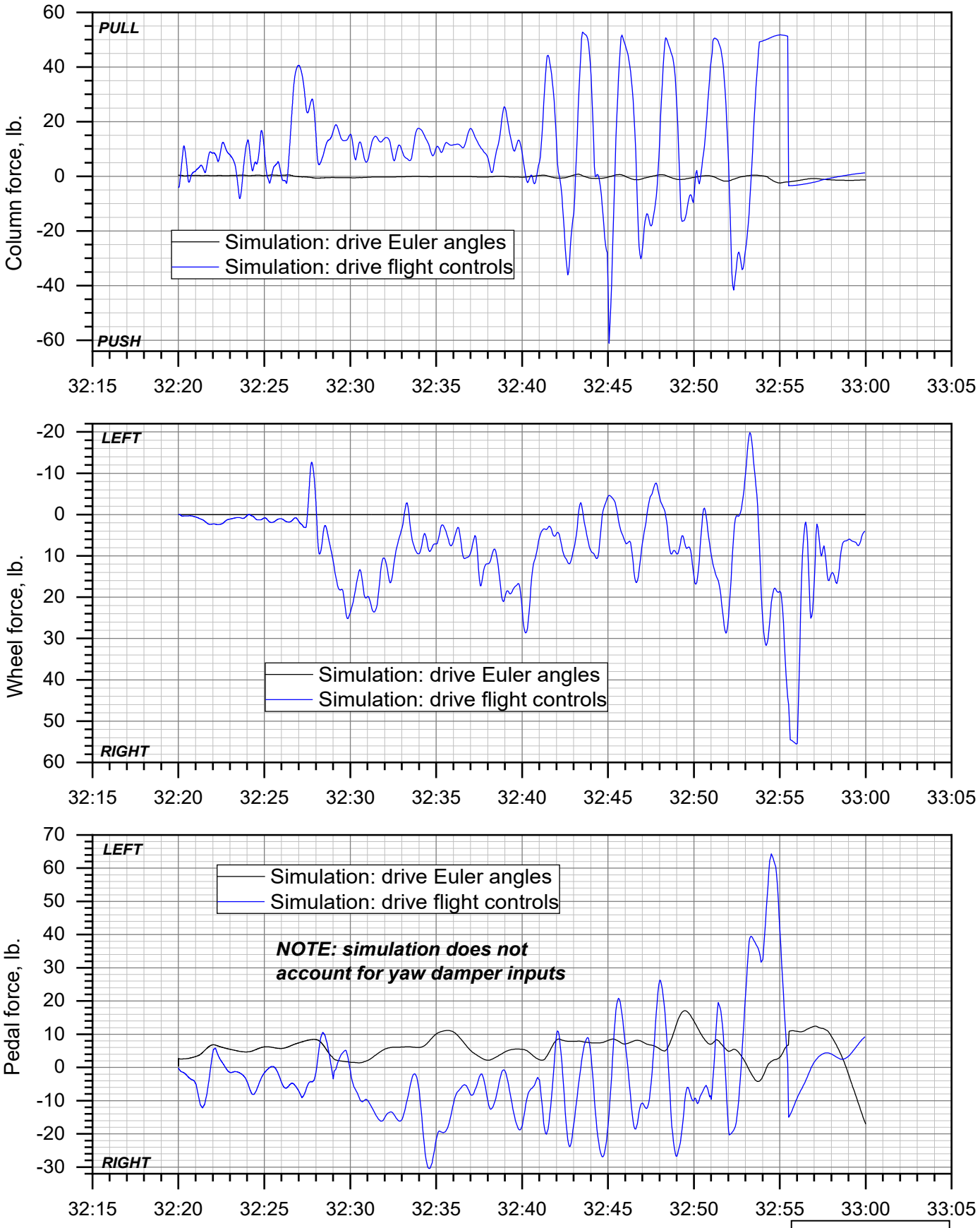

Figure 16.

CEN20FA022: Pilatus PC-12/47E, N56KJ, Chamberlain, SD, 11/20/2019

Accident takeoff simulator match: control surfaces vs. time

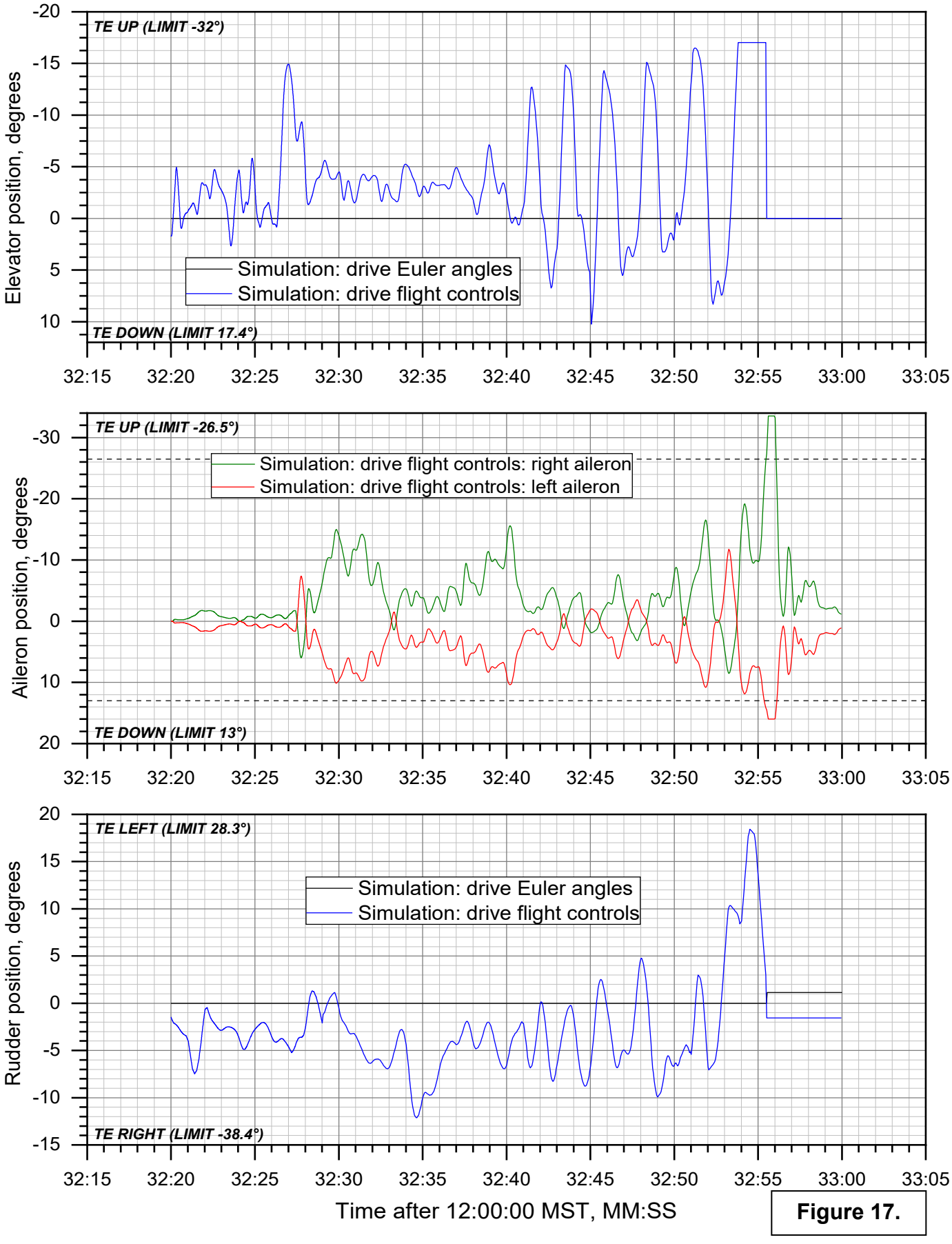

Figure 17.

CEN20FA022: Pilatus PC-12/47E, N56KJ, Chamberlain, SD, 11/20/2019

Accident takeoff simulator match: configuration & power

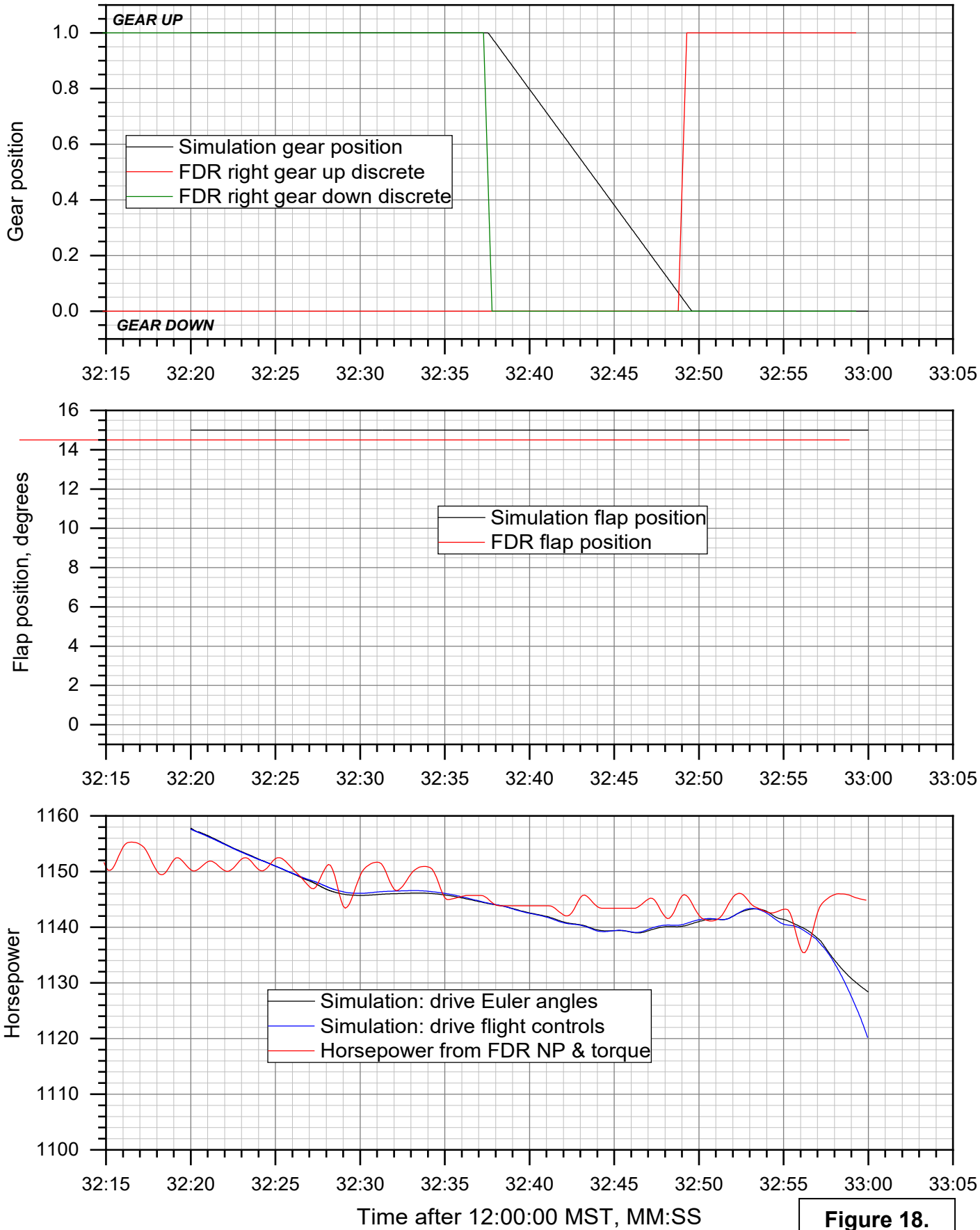

Figure 18.

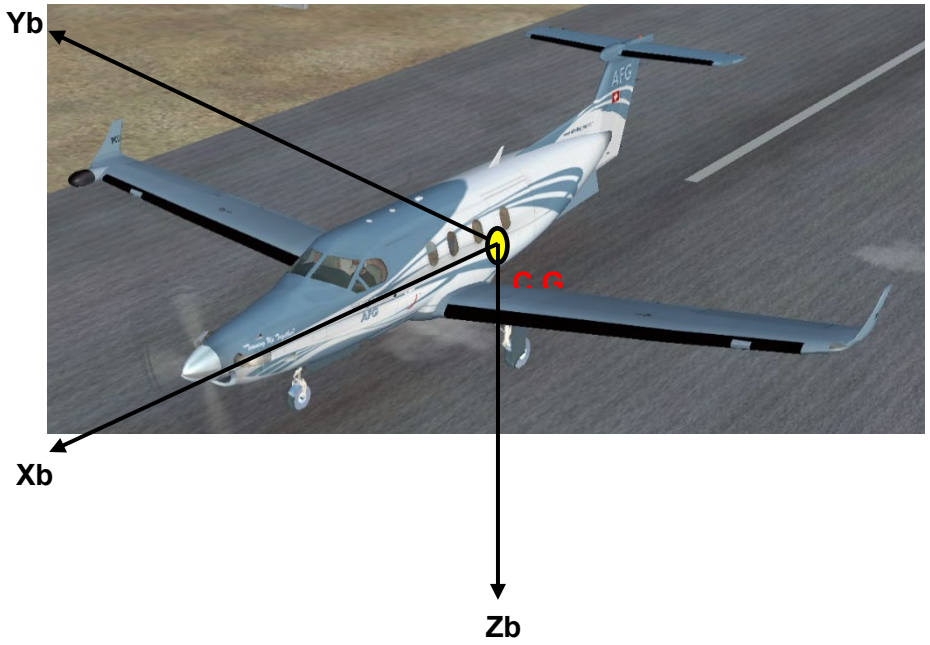

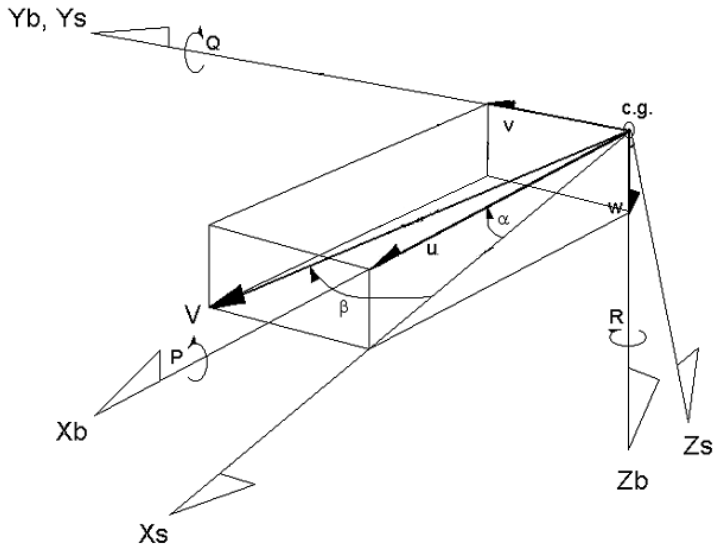

C.G. = center of gravity

{Xb, Yb, Zb} = body axis system

{Xs, Ys, Zs} = stability axis system

V = velocity vector

α = angle of attack

β = sideslip angle

P = body axis roll rate

Q = body axis pitch rate

R = body axis yaw rate

u = component of V along Xb

v = component of V along Yb

w = component of V along Zb

Figure 19. Airplane body axis system, body-axis components of linear and angular velocities, and definitions of α and β.

CEN20FA022: Pilatus PC-12/47E, N56KJ, Chamberlain, SD, 11/20/2019

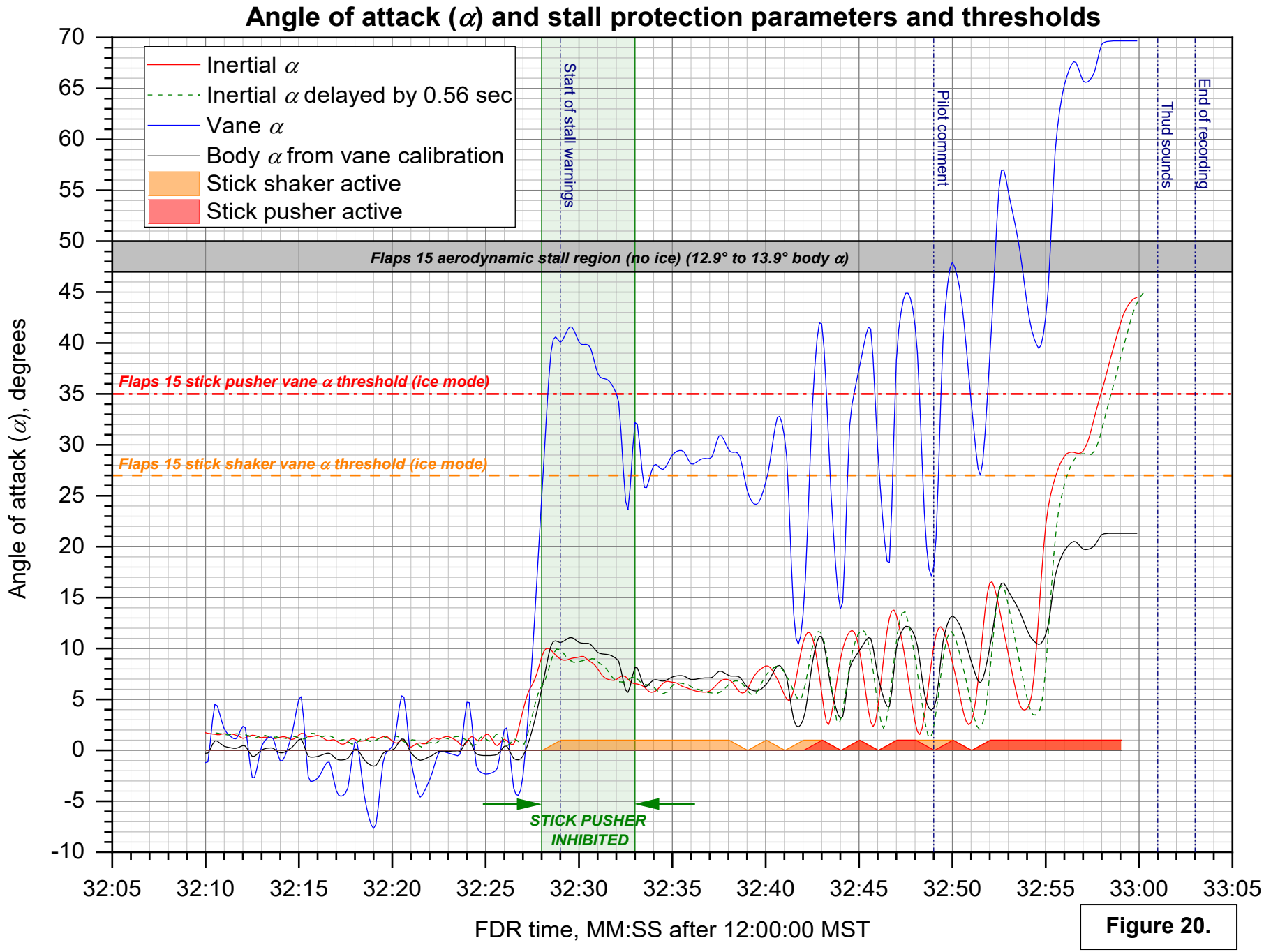

Figure 20.

CEN20FA022: Pilatus PC-12/47E, N56KJ, Chamberlain, SD, 11/20/2019

Takeoff from IDA simulator match: plan view of flight path

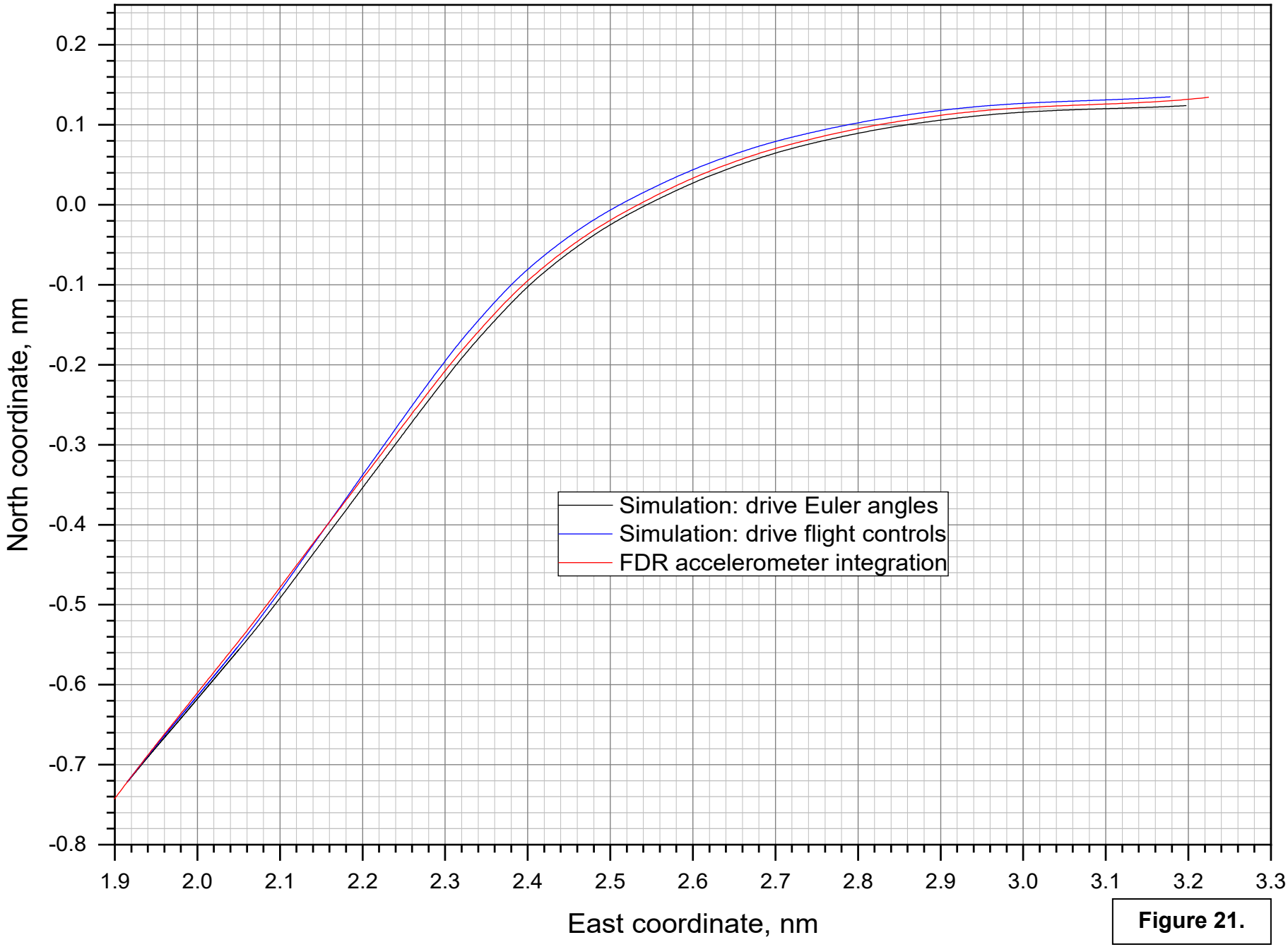

Figure 21.

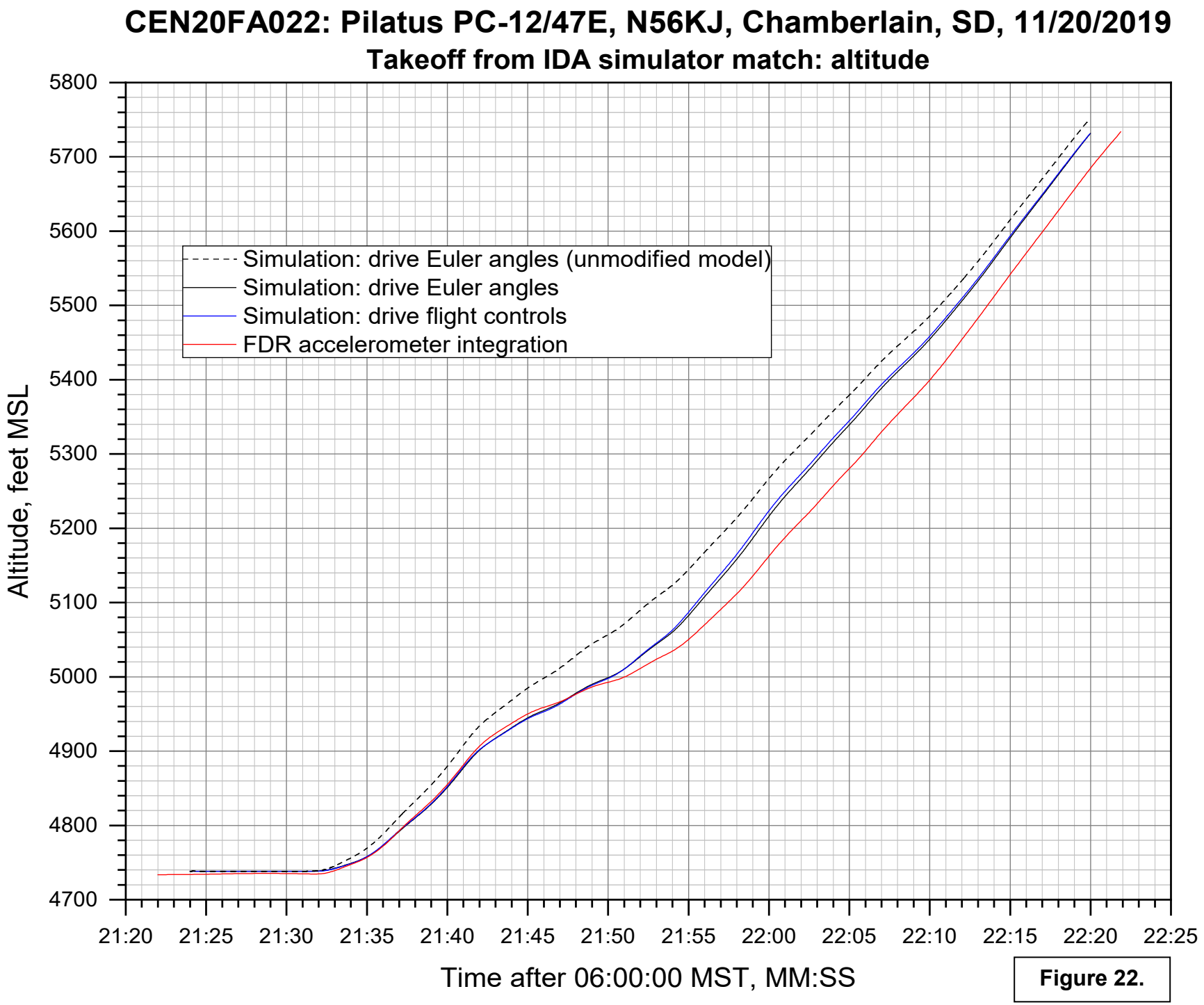
CEN20FA022: Pilatus PC-12/47E, N56KJ, Chamberlain, SD, 11/20/2019
Takeoff from IDA simulator match: altitude
Simulation: drive Euler angles (unmodified model)
Simulation: drive Euler angles
Simulation: drive flight controls
FDR accelerometer integration
Altitude, feet MSL
5800
5700
5600
5500
5400
5300
5200
5100
5000
4900
4800
4700
21:20
21:25
21:30
21:35
21:40
21:45
21:50
21:55
22:00
22:05
22:10
22:15
22:20
22:25
Time after 06:00:00 MST, MM:SS

Figure 22.

CEN20FA022: Pilatus PC-12/47E, N56KJ, Chamberlain, SD, 11/20/2019

Takeoff from IDA simulator match: north and east coordinates vs. time

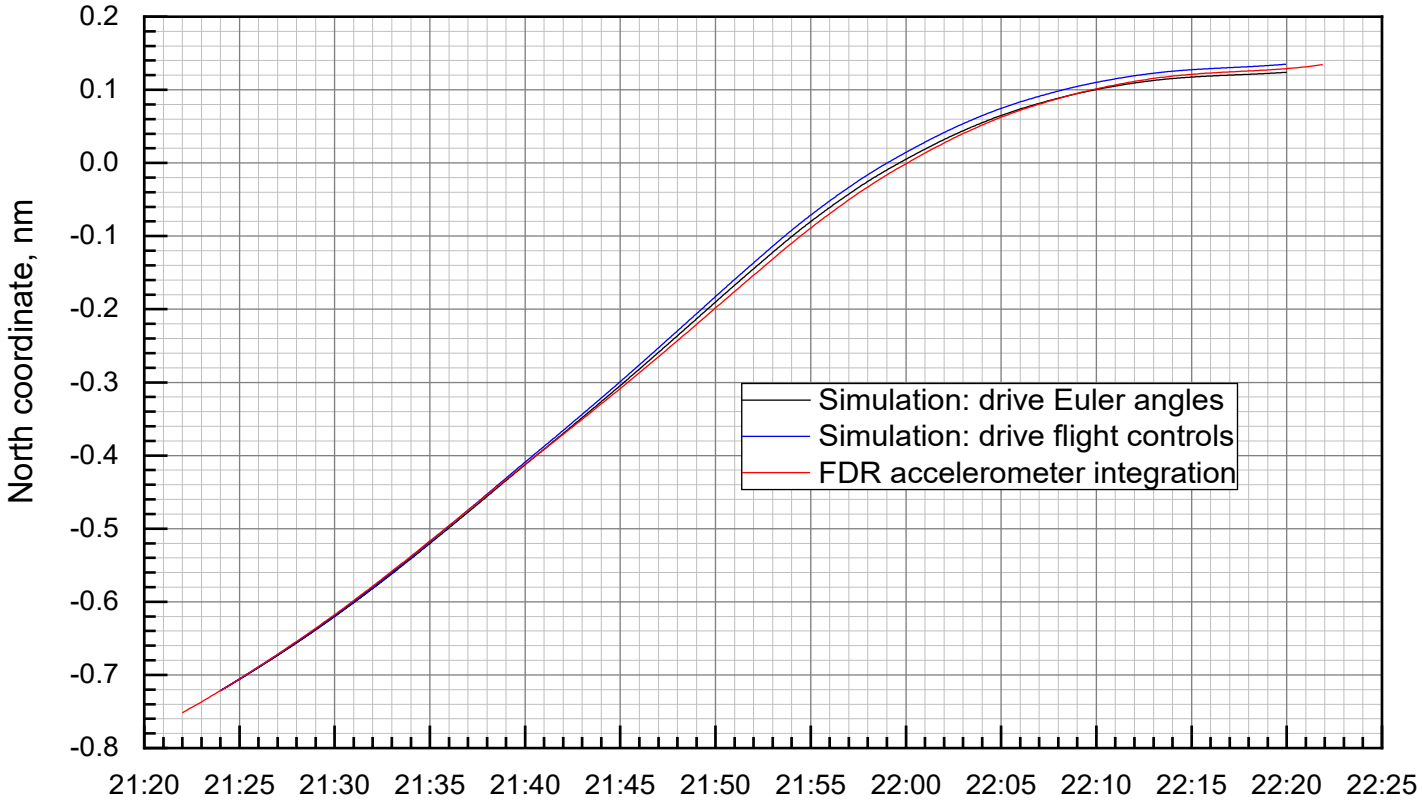

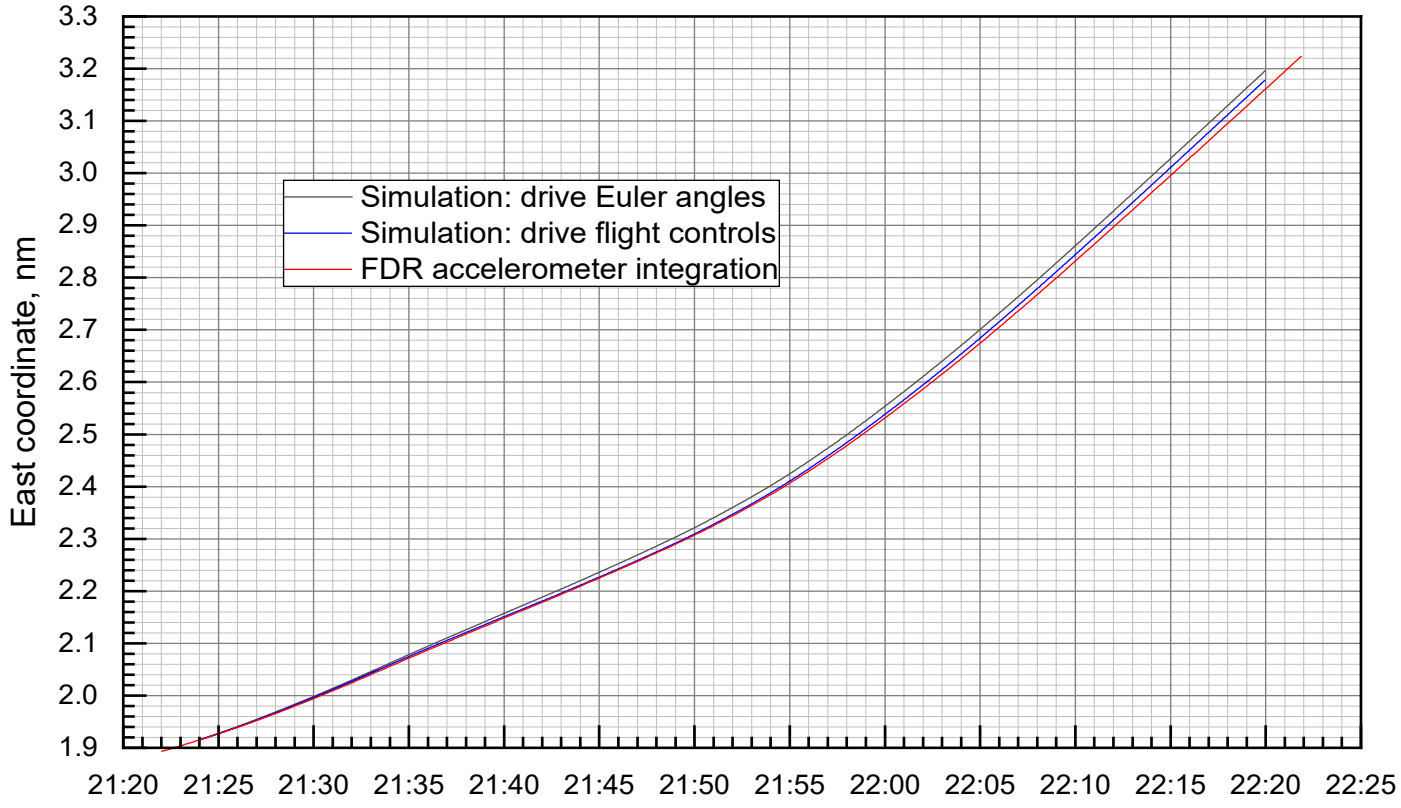

Figure 23.

CEN20FA022: Pilatus PC-12/47E, N56KJ, Chamberlain, SD, 11/20/2019

Takeoff from IDA simulator match: speeds vs. time

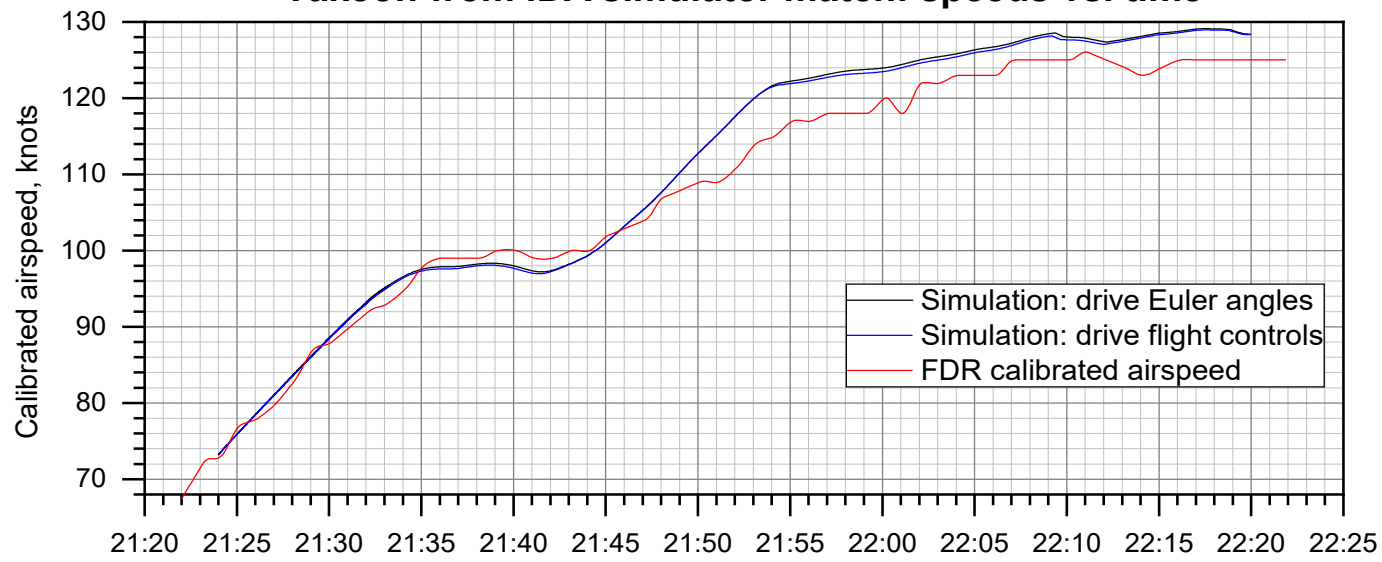

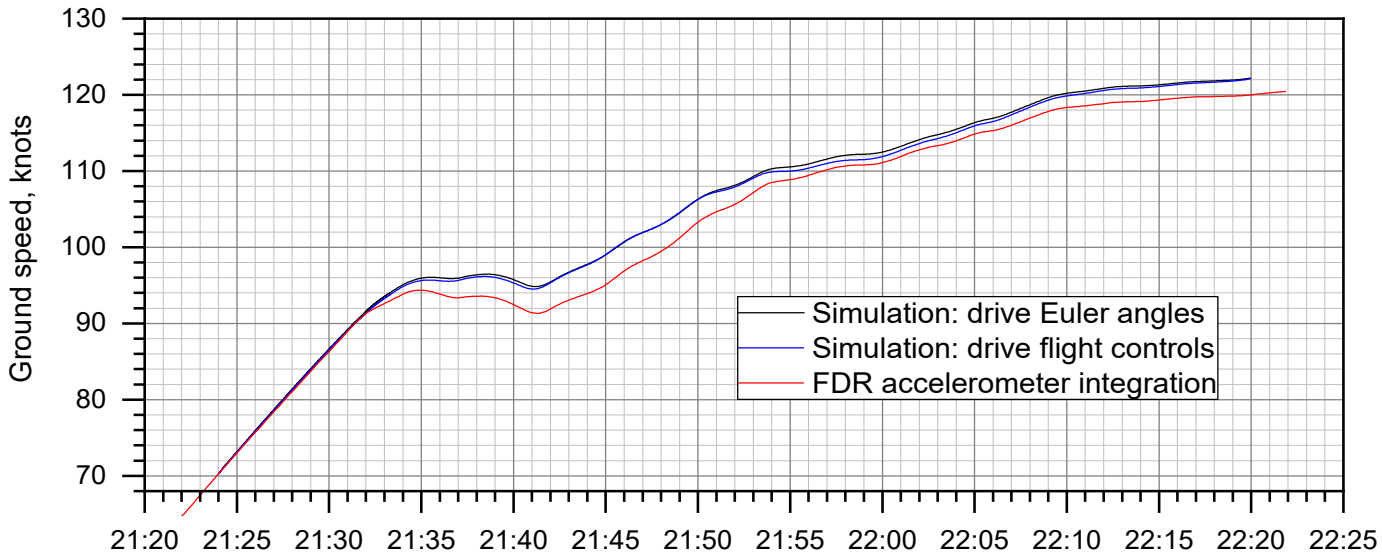

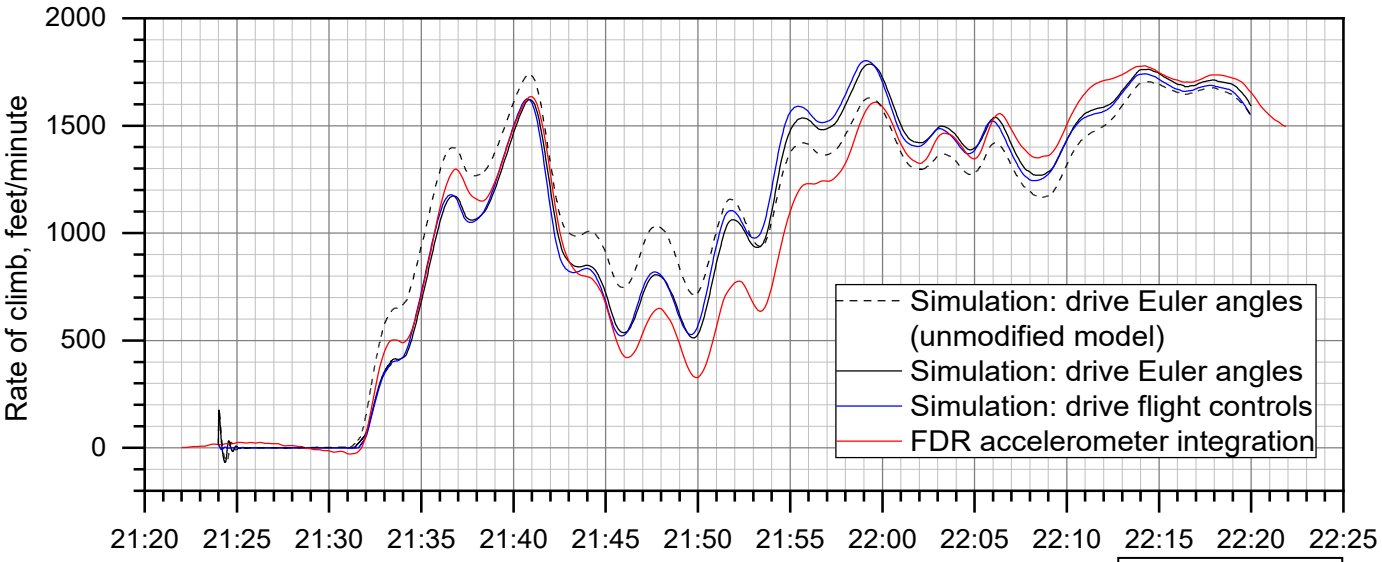

Figure 24.

CEN20FA022: Pilatus PC-12/47E, N56KJ, Chamberlain, SD, 11/20/2019

Takeoff from IDA simulator match: longitudinal flight angles vs. time

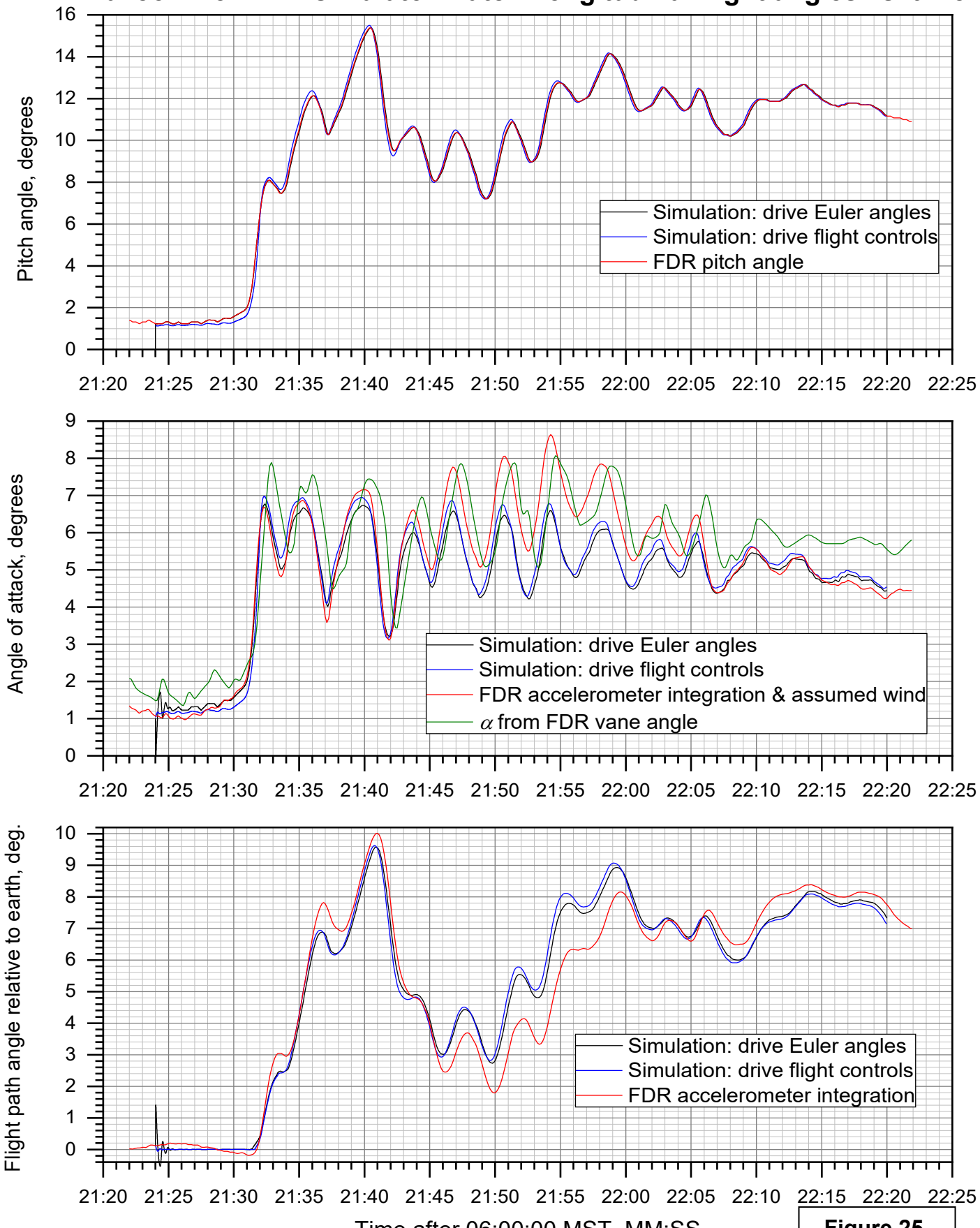

Figure 25.

CEN20FA022: Pilatus PC-12/47E, N56KJ, Chamberlain, SD, 11/20/2019

Takeoff from IDA simulator match: lateral flight angles vs. time

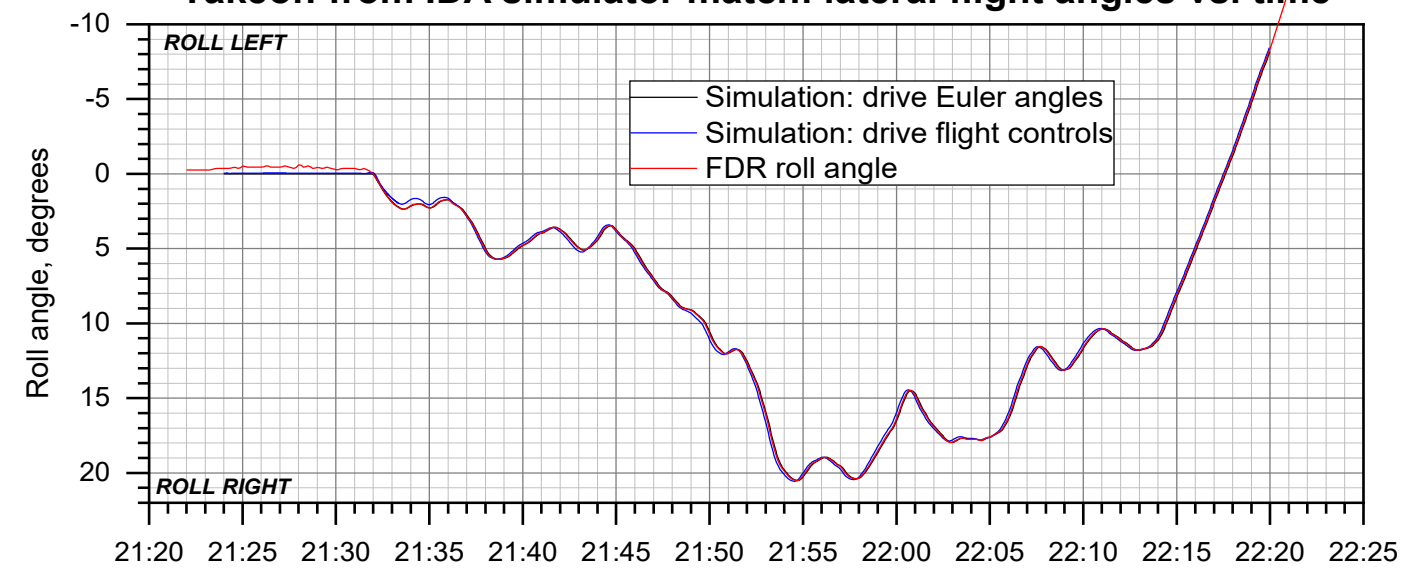

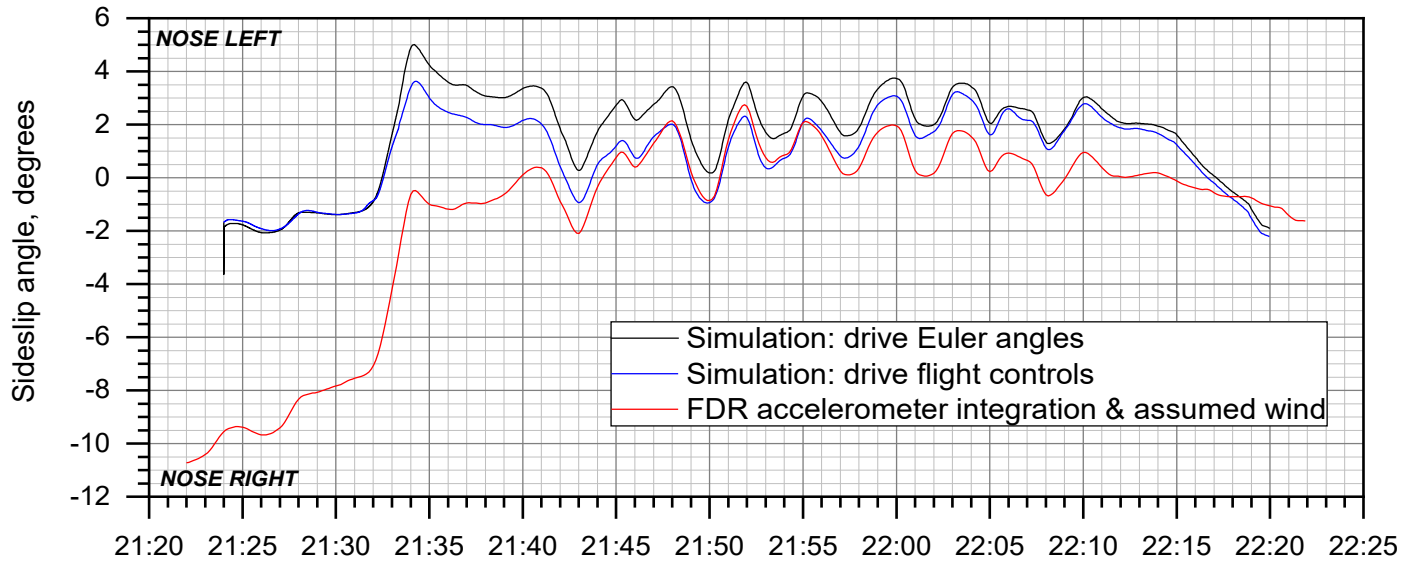

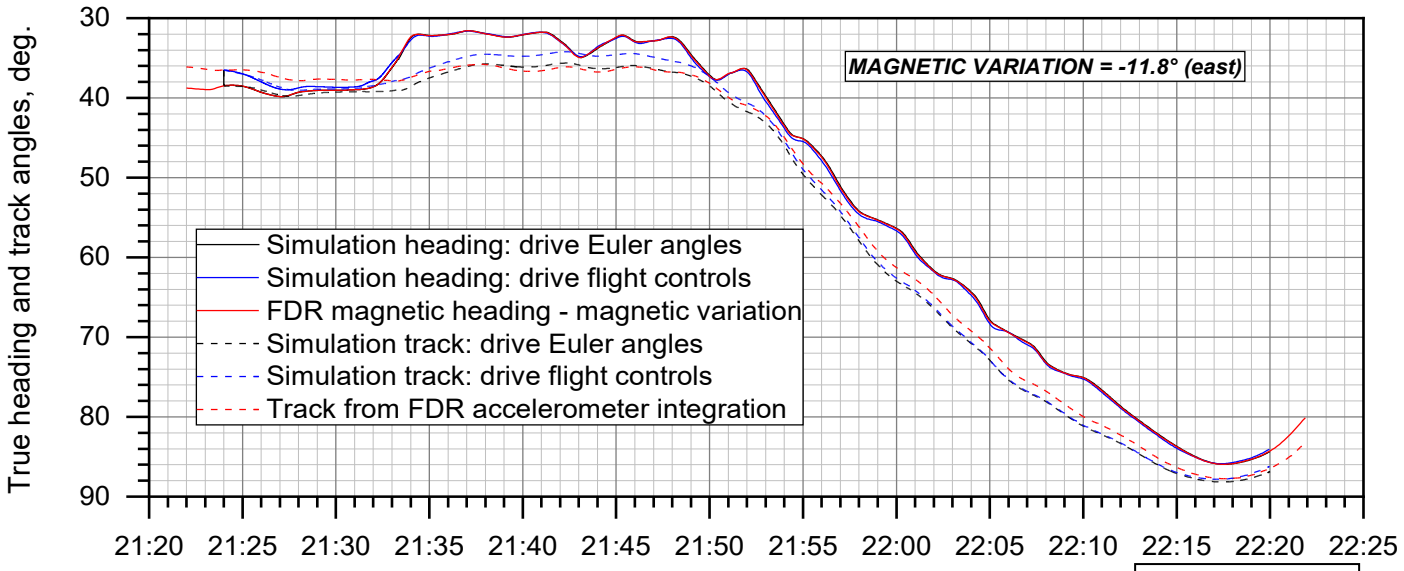

Figure 26.

CEN20FA022: Pilatus PC-12/47E, N56KJ, Chamberlain, SD, 11/20/2019

Takeoff from IDA simulator match: load factors vs. time

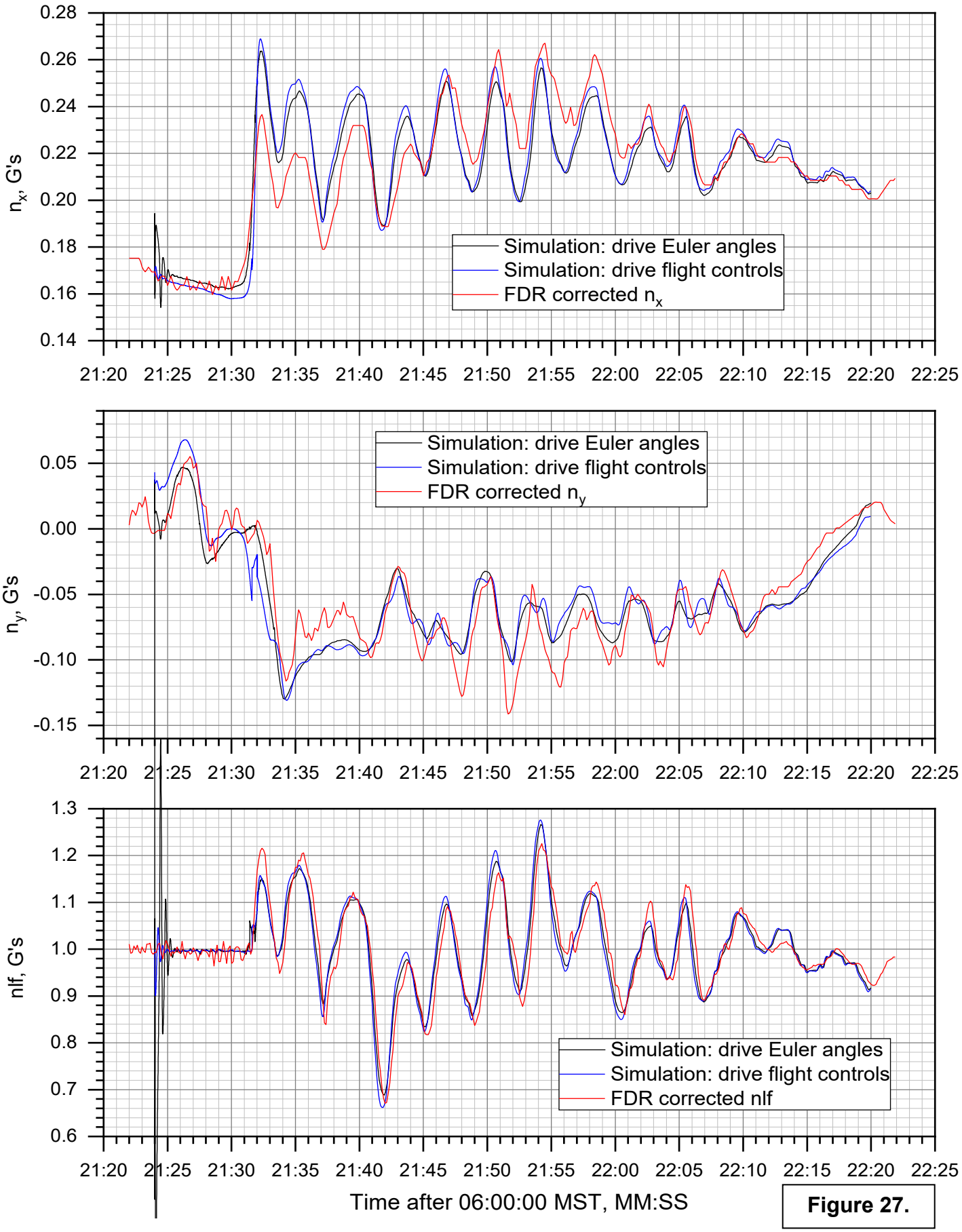

Figure 27.

CEN20FA022: Pilatus PC-12/47E, N56KJ, Chamberlain, SD, 11/20/2019

Takeoff from IDA simulator match: configuration & power

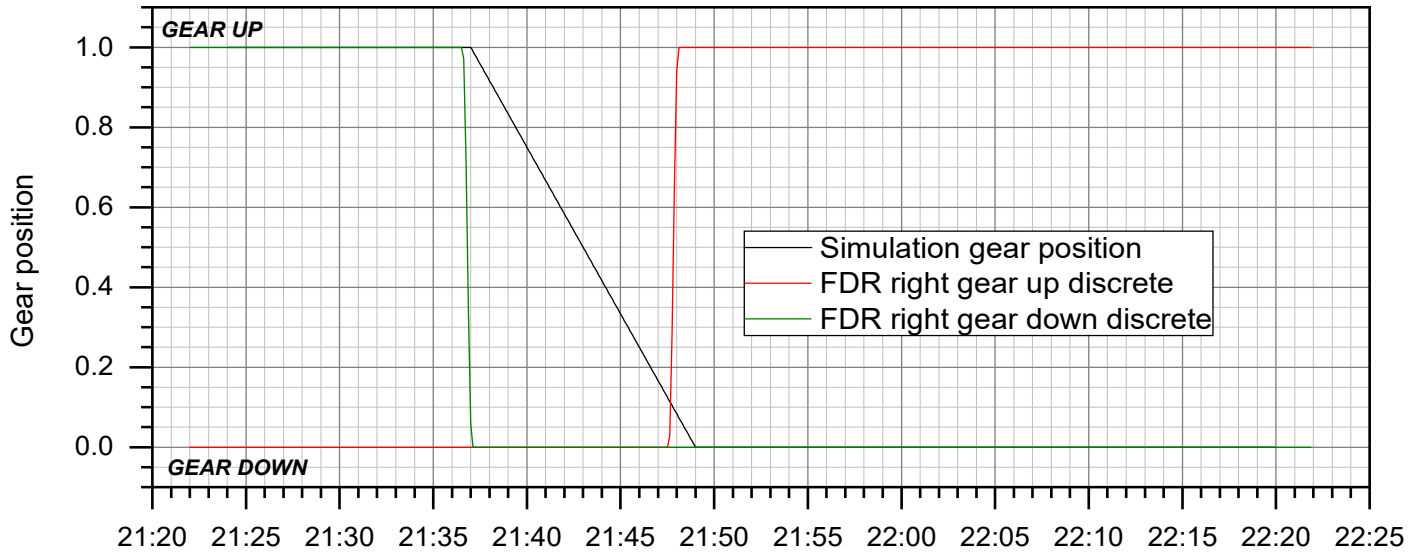

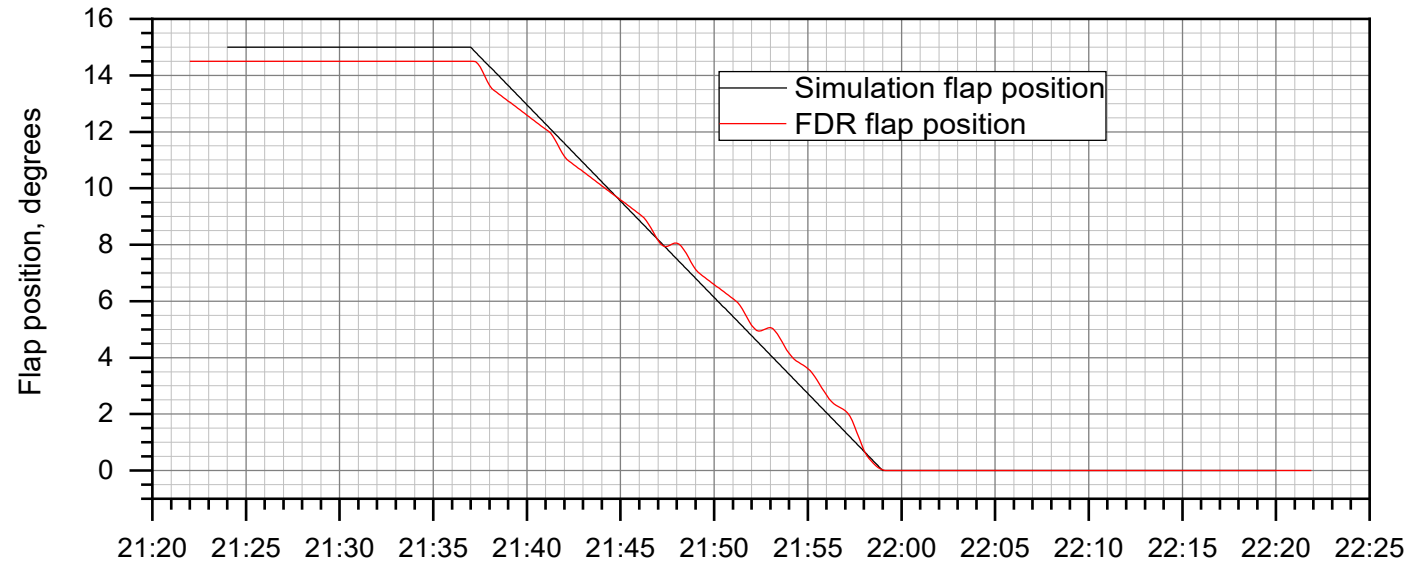

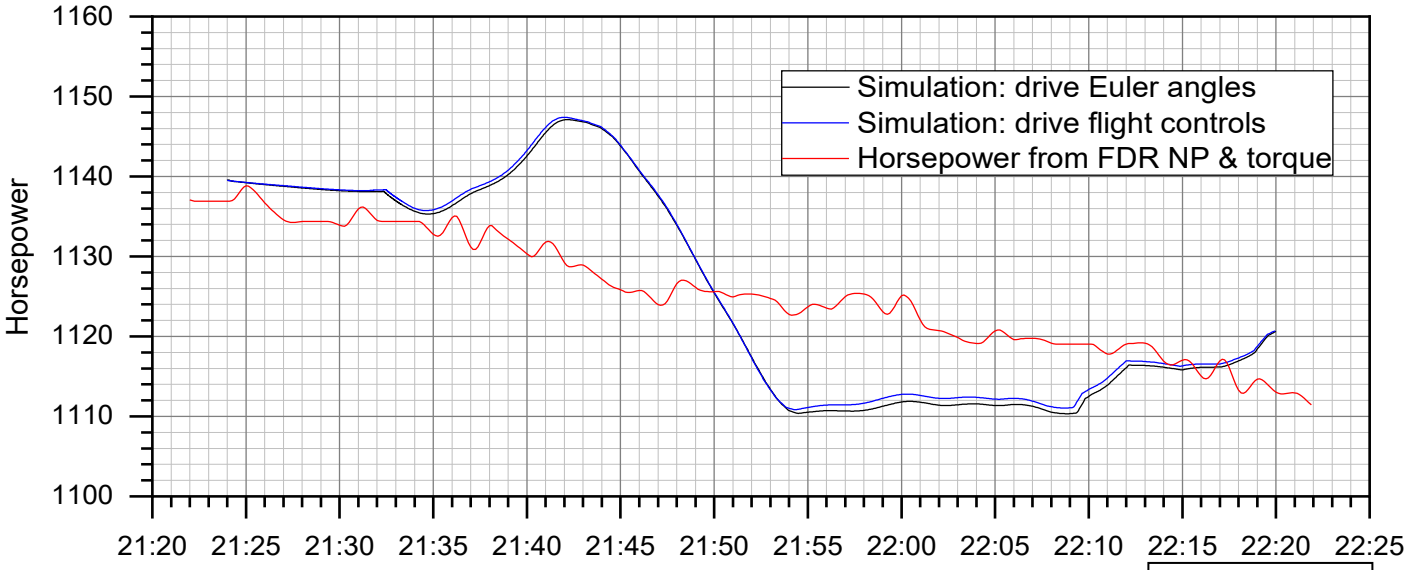

Figure 28.

CEN20FA022: Pilatus PC-12/47E, N56KJ, Chamberlain, SD, 11/20/2019

Takeoff from IDA simulator match: flight controls vs. time

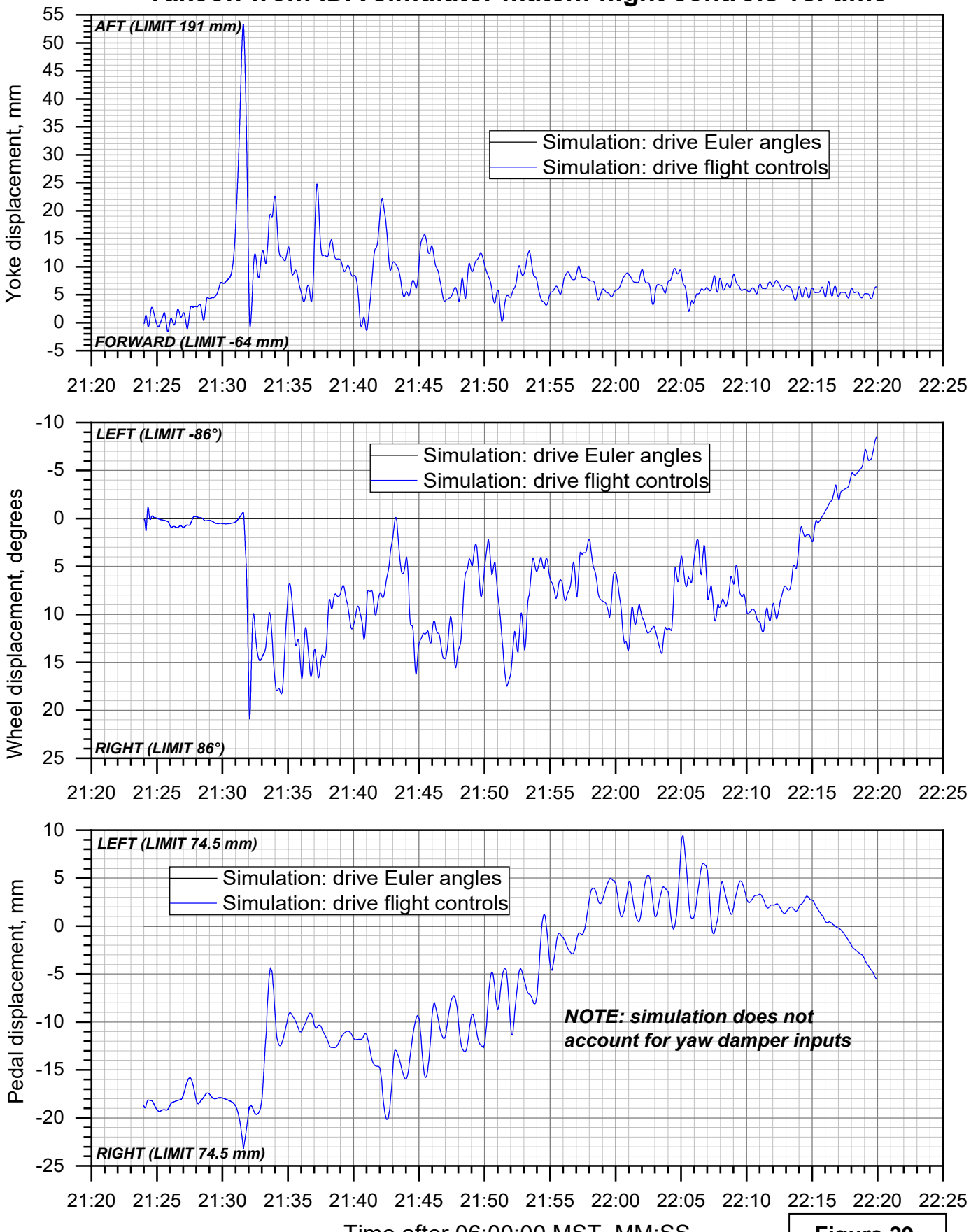

Figure 29.

CEN20FA022: Pilatus PC-12/47E, N56KJ, Chamberlain, SD, 11/20/2019

Takeoff from IDA simulator match: control forces vs. time

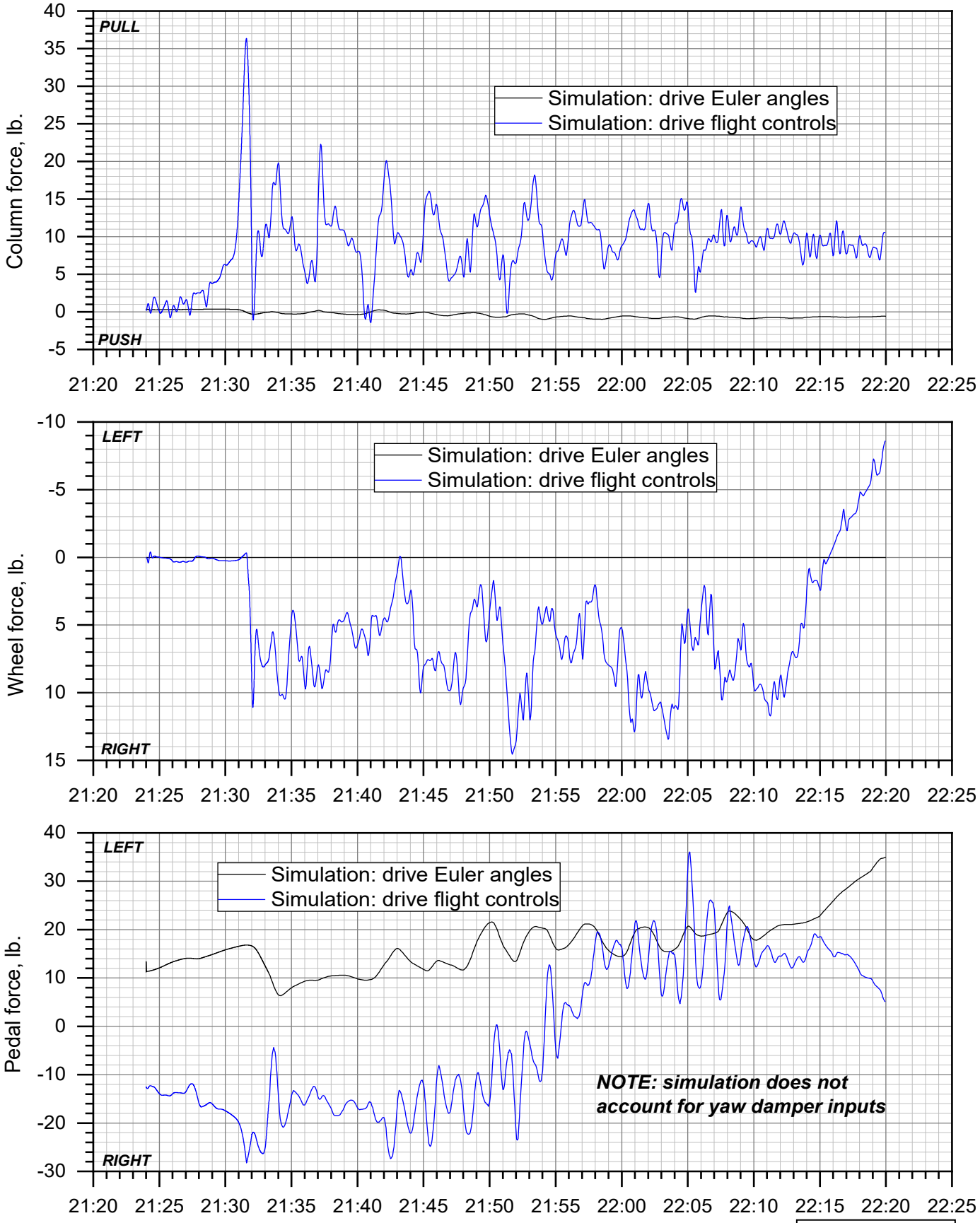

Figure 30.

CEN20FA022: Pilatus PC-12/47E, N56KJ, Chamberlain, SD, 11/20/2019

Takeoff from IDA simulator match: control surfaces vs. time

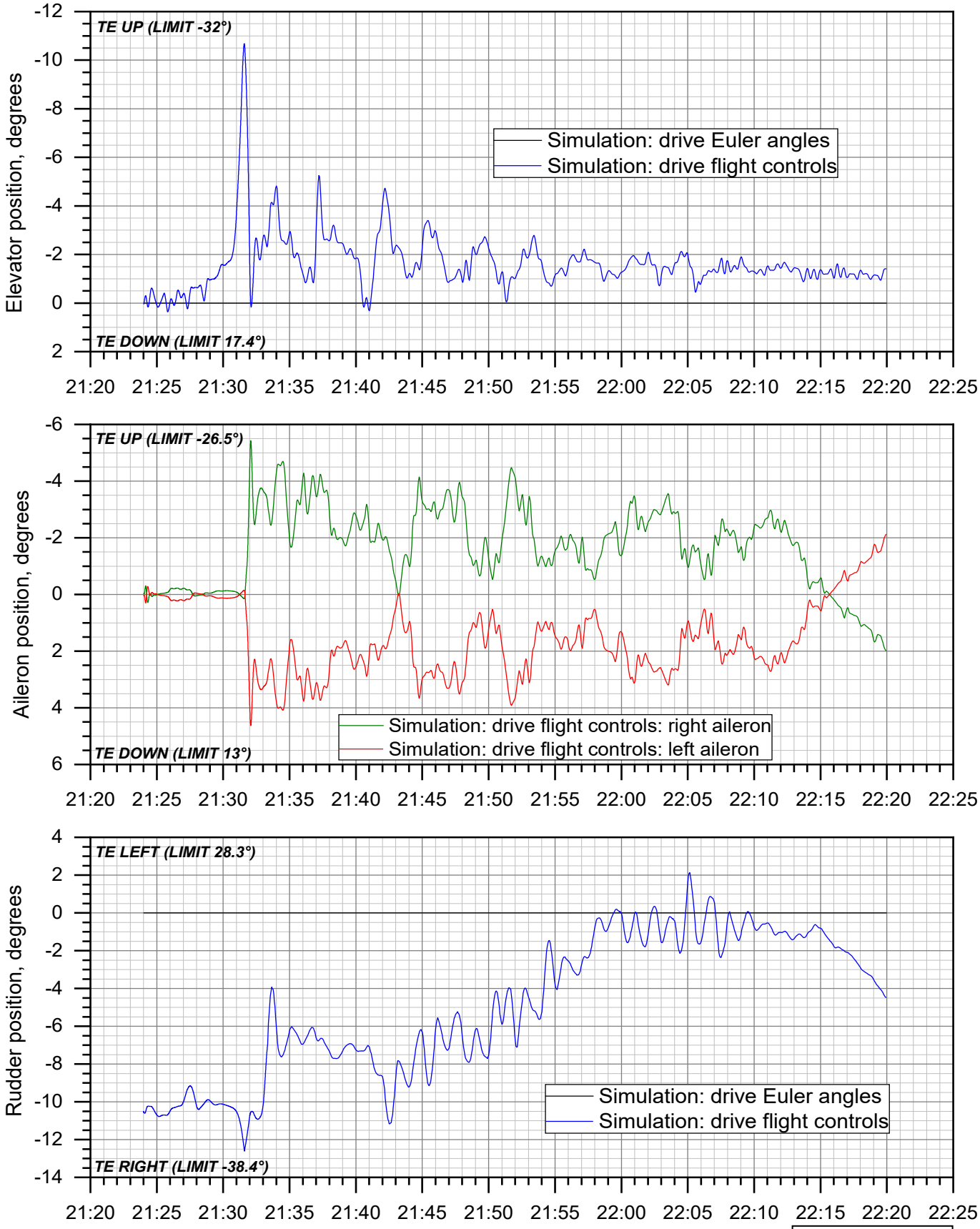

Figure 31.

CEN20FA022: Pilatus PC-12/47E, N56KJ, Chamberlain, SD, 11/20/2019

Takeoff pitch angle comparisons: accident pilot & second pilot, multiple flights

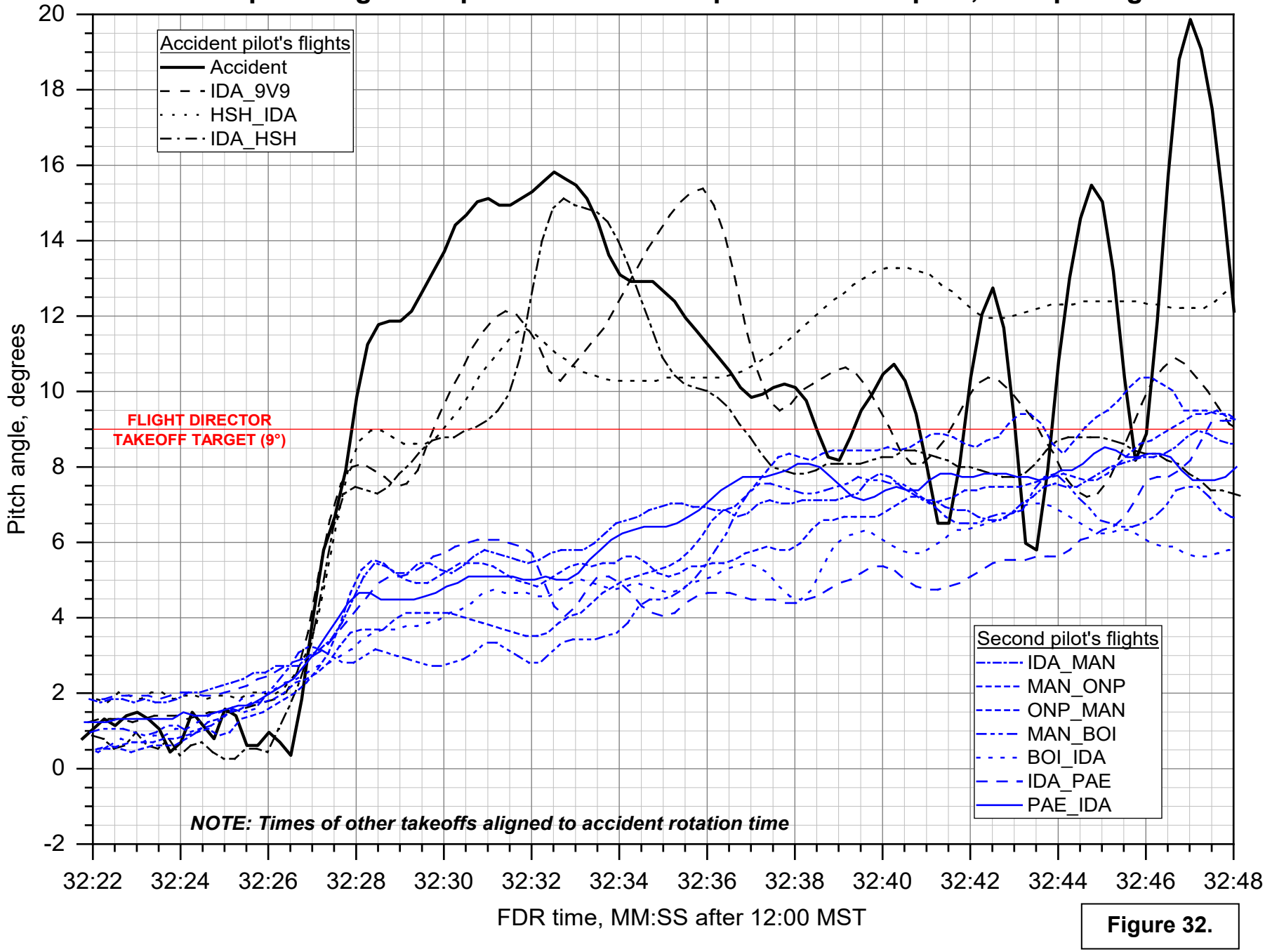

Figure 32.

CEN20FA022: Pilatus PC-12/47E, N56KJ, Chamberlain, SD, 11/20/2019

SimCom FTD model: Static longitudinal stability at mid & accident CG

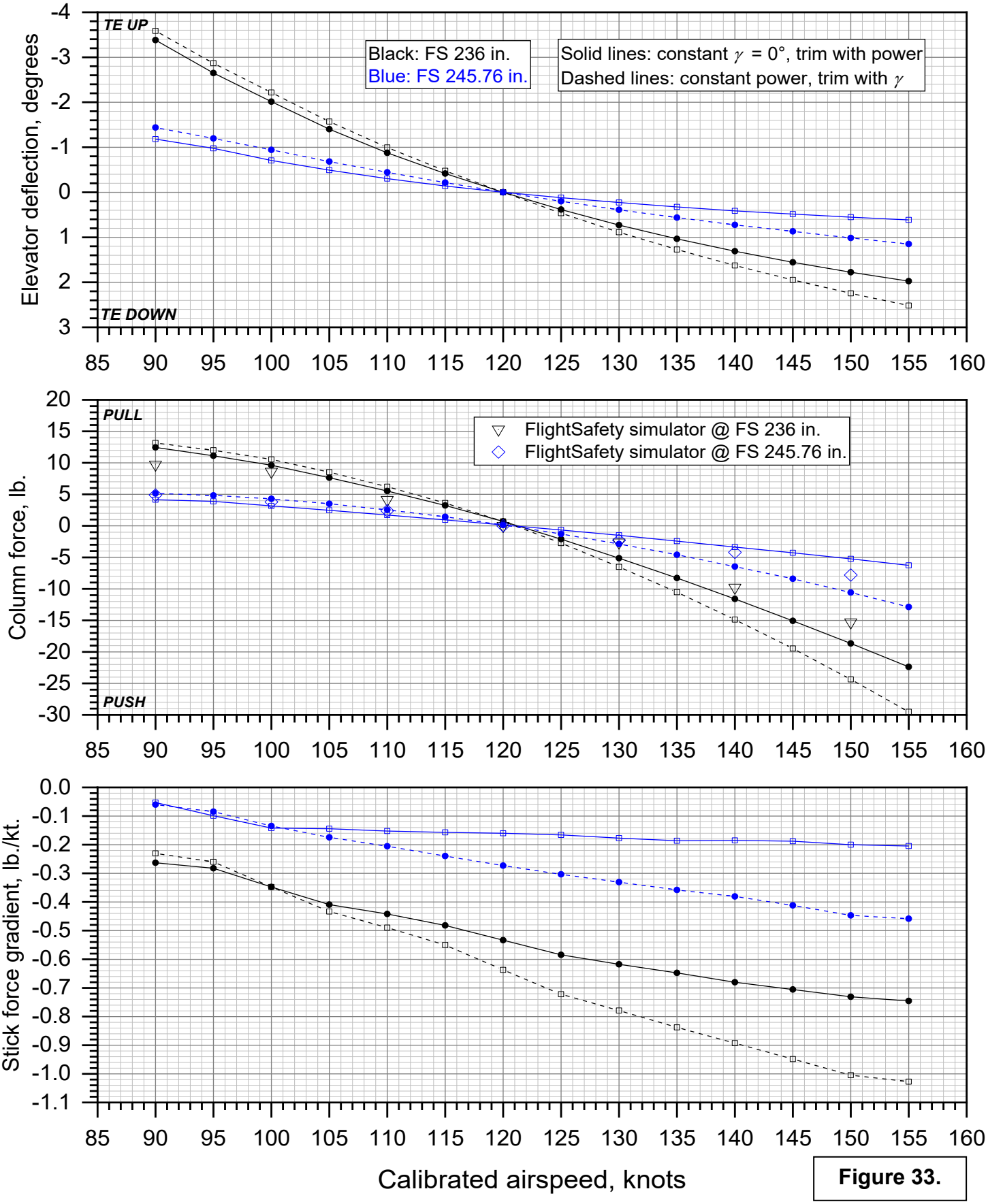

Figure 33.

CEN20FA022: Pilatus PC-12/47E, N56KJ, Chamberlain, SD, 11/20/2019

SimCom FTD model: Manuever stability at mid & accident CG

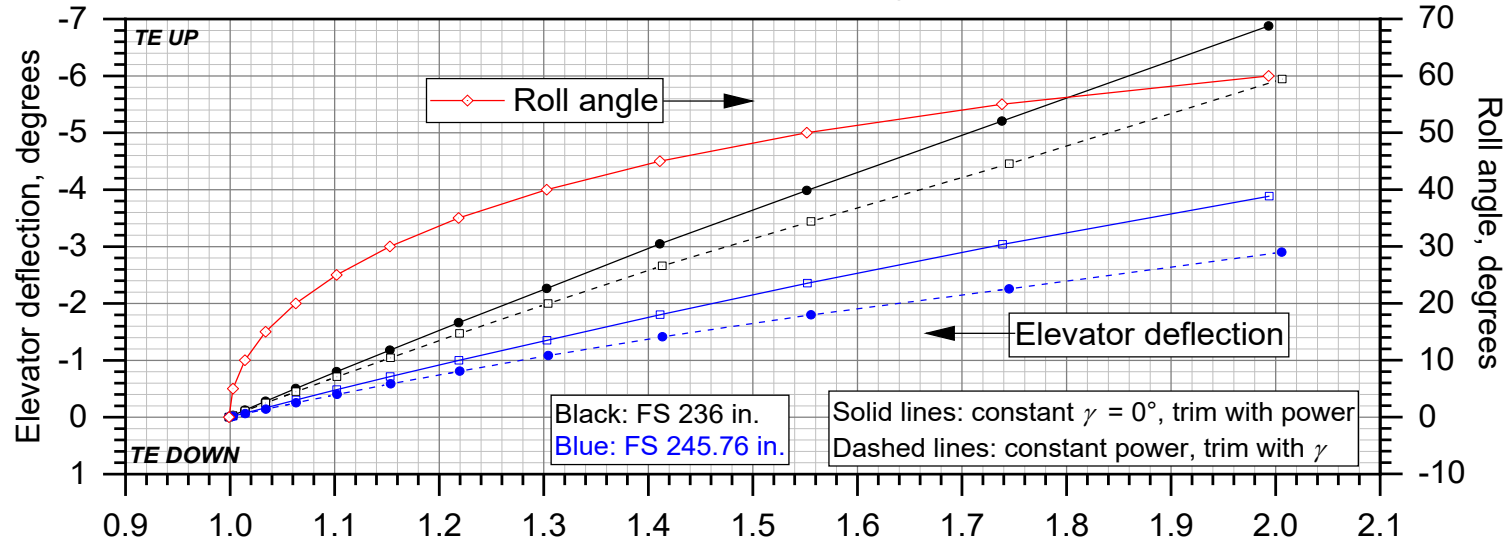

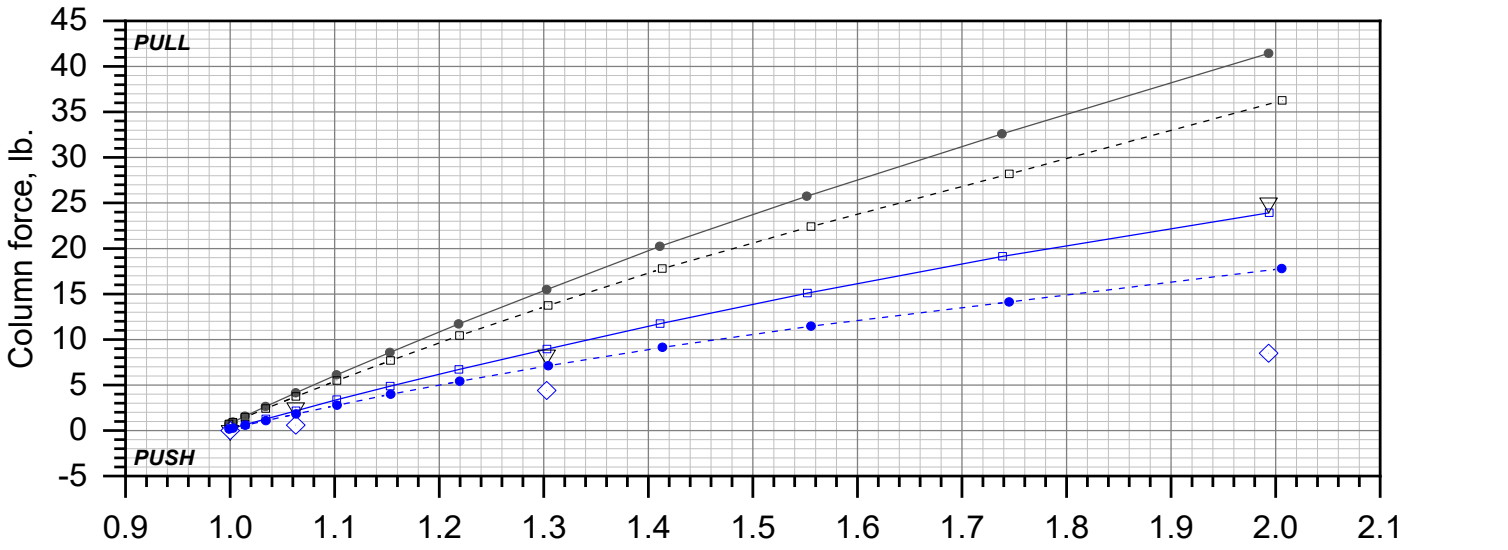

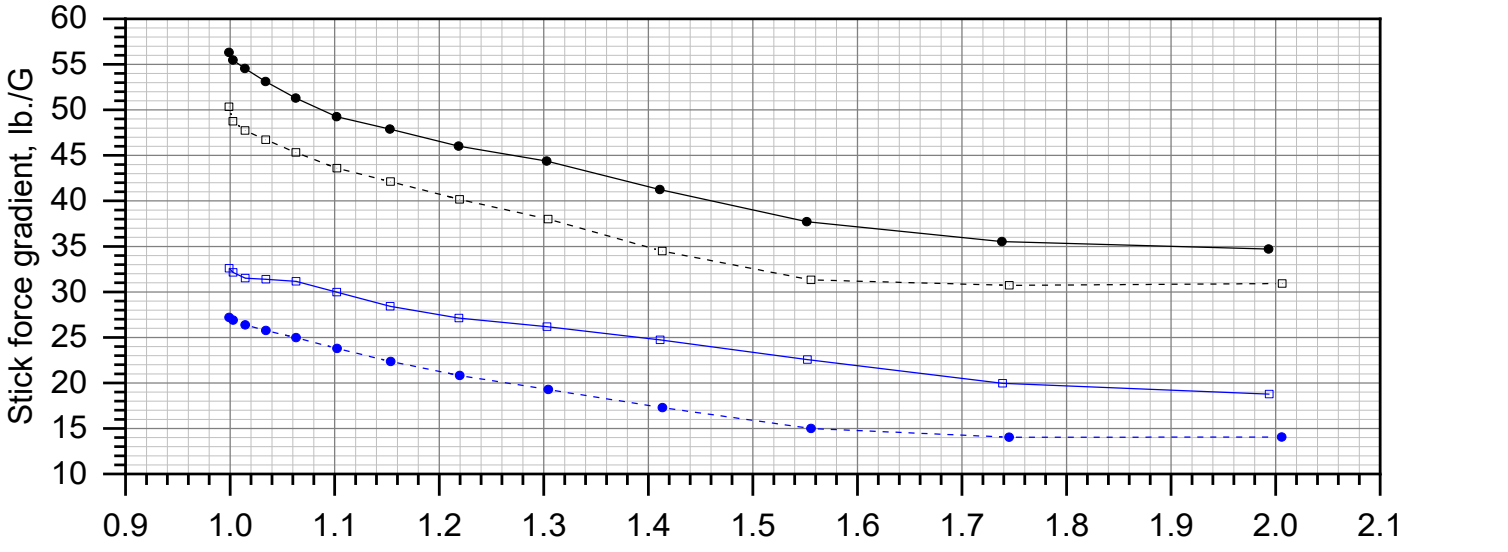

Figure 34.

APPENDIX A

Chamberlain Municipal Airport (K9V9) information

9V9 Chamberlain Municipal Airport
Chamberlain, South Dakota, USA

GOING TO CHAMBERLAIN?	Reserve a **Hotel Room**

FAA INFORMATION EFFECTIVE 12 AUGUST 2021

Loc | Ops | Rwys | IFR | FBO | Links
Com | Nav | Svcs | Stats | Notes

Location

FAA Identifier: 9V9
Lat/Long: 43-45-58.0935N 099-19-16.4251W
43-45.968225N 099-19.273752W
43.7661371,-99.3212292
(estimated)
Elevation: 1696.3 ft. / 517 m (estimated)
Variation: 05E (2020)
From city: 3 miles S of CHAMBERLAIN, SD
Time zone: UTC -5 (UTC -6 during Standard Time)
Zip code: 57325

Airport Operations

Airport use: Open to the public
Activation date: 05/1981
Control tower: no
ARTCC: MINNEAPOLIS CENTER
FSS: HURON FLIGHT SERVICE STATION
NOTAMs facility: 9V9 (NOTAM-D service available)
Attendance: CONTINUOUS
Wind indicator: lighted
Segmented circle: yes
Lights: MIRL RY 13/31 PRESET ON LOW INTST, TO INCR INTST & ACTVT PAPI RYS 13 & 31 - CTAF.
Beacon: white-green (lighted land airport)
Operates sunset to sunrise.

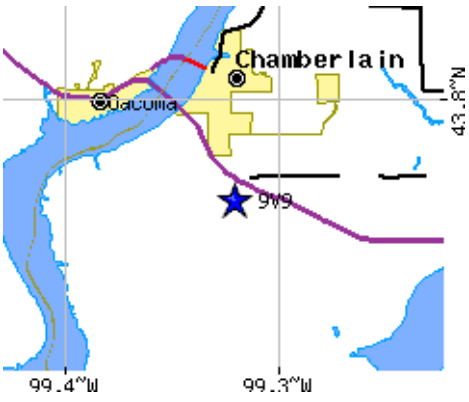

Road maps at: MapQuest Bing Google

Airport Communications

CTAF/UNICOM: 122.8
WX AWOS-3P: 118.025 (605-234-1437)

- APCH/DEP SVC PRVDD BY MINNEAPOLIS ARTCC ON FREQS 125.1/269.1 (PIERRE RCAG).

Airport Services

Fuel available: 100LL JET-A
100LL:FUEL AVBL 24 HRS WITH CREDIT CARD.
Parking: hangars and tiedowns
Airframe service: MINOR
Powerplant service: MINOR

Runway Information

Runway 13/31

Dimensions: 4299 x 75 ft. / 1310 x 23 m
Surface: asphalt, in fair condition
Weight bearing capacity: Single wheel: 12.5
Runway edge lights: medium intensity

	RUNWAY 13	RUNWAY 31
Latitude:	43-46.217163N	43-45.667647N
Longitude:	099-19.584610W	099-18.969678W
Elevation:	1696.3 ft.	1678.1 ft.
Traffic pattern:	left	left
Runway heading:	136 magnetic, 141 true	316 magnetic, 321 true
Markings:	nonprecision, in fair condition	nonprecision, in fair condition
Visual slope indicator:	2-light PAPI on left (3.00 degrees glide path)	2-light PAPI on left (3.00 degrees glide path)
Runway end identifier lights:	no	no
Touchdown point:	yes, no lights	yes, no lights
Obstructions:	64 ft. tree, 1539 ft. from runway, 415 ft. left of centerline, 20:1 slope to clear	none

Runway 18/36

Dimensions: 3403 x 150 ft. / 1037 x 46 m
Surface: turf, in good condition
Runway edge markings: A-FRAME MARKINGS - BLACK & YELLOW.

	RUNWAY 18	RUNWAY 36
Latitude:	43-46.278752N	43-45.722935N
Longitude:	099-19.221735W	099-19.317198W
Elevation:	1696.0 ft.	1680.0 ft.
Traffic pattern:	left	left
Runway heading:	182 magnetic, 187 true	002 magnetic, 007 true
Touchdown point:	yes, no lights	yes, no lights
Obstructions:	46 ft. pole, 1000 ft. from runway, 21:1 slope to clear	none

Aerial photo

WARNING: Photo may not be current or correct

Photo by Steve Hamilton
Photo taken 23-Apr-2006

Do you have a better or more recent aerial photo of Chamberlain Municipal Airport that you would like to share? If so, please **send us your photo**.

Sectional chart

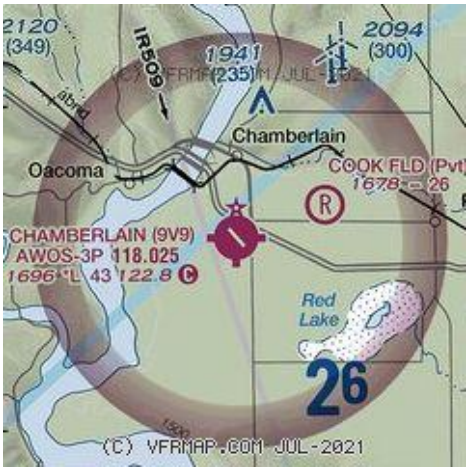

Airport distance calculator

Flying to Chamberlain Municipal Airport? Find the distance to fly.

From to 9V9
CALCULATE DISTANCE

Sunrise and sunset

Times for 25-Aug-2021

	Local (UTC-5)	Zulu (UTC)
Morning civil twilight	06:24	11:24
Sunrise	06:54	11:54
Sunset	20:25	01:25
Evening civil twilight	20:55	01:55

Current date and time

Zulu (UTC) 25-Aug-2021 17:29:27
Local (UTC-5) 25-Aug-2021 12:29:27

METAR

K9V9 251715Z AUTO 07008G16KT 10SM CLR 22/11 A3018 RMK AO2 T02220108

TAF

NOTAMs

Airport Ownership and Management from official FAA records

Click for the latest **NOTAMs**
NOTAMs are issued by the DoD/FAA and will open in a separate window not controlled by AirNav.

Ownership: Publicly-owned
Owner: CITY OF CHAMBERLAIN
715 N. MAIN ST.
CHAMBERLAIN, SD 57325
Phone (605) 680-9935
Manager: DUSTEN HRABE
101 AIRPORT ROAD
CHAMBERLAIN, SD 57325
Phone 605-680-9935

Airport Operational Statistics

Aircraft based on the field: 17
Single engine airplanes: 17

Aircraft operations: avg 21/day *
87% local general aviation
13% transient general aviation
<1% military
<1% air taxi
* for 12-month period ending 04 September 2019

Additional Remarks

- WATERFOWL ON & INVOF ARPT.
- GCO AVBL ON FREQ 121.725 (4 CLICKS TO MINNEAPOLIS CENTER AND 6 CLIKCS TO FLIGHT SERVICES)
- FOR CD IF UNA VIA GCO CTC MINNEAPOLIS ARTCC AT 651-463-5588.

Instrument Procedures

NOTE: All procedures below are presented as PDF files. If you need a reader for these files, you should download the free Adobe Reader.

NOT FOR NAVIGATION. Please procure official charts for flight.
FAA instrument procedures published for use from 12 August 2021 at 0901Z to 9 September 2021 at 0900Z.

IAPs - Instrument Approach Procedures

RNAV (GPS) RWY 13	download (211KB)
RNAV (GPS) RWY 31	download (217KB)
NOTE: Special Take-Off Minimums/Departure Procedures apply	download (156KB)

Other nearby airports with instrument procedures:

KICR - Winner Regional Airport (32 nm SW)
9D1 - Gregory Municipal Airport - Flynn Field (33 nm S)
4X4 - Wessington Springs Airport (38 nm NE)
9D0 - Highmore Municipal Airport (47 nm N)
KMKA - Miller Municipal Airport (48 nm N)

FBO, Fuel Providers, and Aircraft Ground Support

Business Name	Contact	Services / Description	Fuel Prices	Comments

Automated Fueling Systems, Inc.	605-234-6018 [email] Aviation fuel More info about Automated Fueling Systems, Inc.	Phillips 66 100LL Jet A SS $5.35 $4.20 Updated 03-Aug-2021 SS=Self service UPDATE PRICES	not yet rated 1 read write

Would you like to see your business listed on this page?

If your business provides an interesting product or service to pilots, flight crews, aircraft, or users of the Chamberlain Municipal Airport, you should consider listing it here. To start the listing process, click on the button below

ADD YOUR BUSINESS OR SERVICE

Other Pages about Chamberlain Municipal Airport

ADD A LINK

eNASR

Cycle: Current (2020-01-02) Resource: Airport Query Screen

Airport 9V9

General | Location | Associated FAA Facilities | Contacts | Services and Facilities | Usage, Rules, and Regulations | Pad Rwy | Linear Rwy

Item 2 of 2

Status:	EXISTING	**Rwy ID:**	13/31	**Gross Wt SW:**	12.5	**Gross Wt DW:**		**Gross Wt DTW:**	
Gross Wt DDTW:		**PCN Number:**		**Pavement Type:**		**Subgrade Strength Category:**		**Tire Pressure:**	
Evaluation Method:									

Rwy General

Edge Intensity:	MED	**Length:**	4299	**Length Source:**	3RD PARTY SURVEY	**Length Source Date:**	2009-02-09
Width:	75						

Rwy Surface

Condition:	FAIR	**Surface Type:**	ASPH	**Treatment:**	

Base Rwy End

Rwy End ID: 13

Arresting Systems

System Code	

Apch Lights:		**Centerline:**		**Marking Cond:**	FAIR	**Marking Type:**	NPI
REIL:		**RVR:**		**RVV:**		**TDZ:**	
Thr Crossing Hgt:	40	**VGSI:**	P2L	**Visual Glide Angle:**	3.0		

Obstruction

Clearance Slope:	20	**Close In:**		**Cntrln Offset**		**Ctlg Obstn:**	TREE	**Displaced Thr Len:**	
				Offset:	415				
				Direction:	L				
Dist From Rwy End:	1539	**FAR 77 Category:**	A(NP)	**Hgt Above Rwy End:**	64	**Marked Lighted:**		**Slope to Displaced Thr:**	

Displaced Threshold

Elevation

Elevation ft:
Source:
Source Date:
Datum:

Position

Latitude:
Longitude:
Source:
Source Date:

Runway End

Elevation

Elevation ft: 1696.3
Source: 3RD PARTY SURVEY
Source Date: 2009-09-09
Datum: NGVD29

Position

Latitude: 43-46-13.0298N
Longitude: 99-19-35.0766W
Source: 3RD PARTY SURVEY
Source Date: 2009-09-09

Touchdown Zone

Elevation ft:	1696.3	**Source:**	3RD PARTY SURVEY
Source Date:	2009-09-09	**Datum:**	NAVD88

Rwy Distances

Aclt Stop Dist Avbl:		**Lndg Dist Avbl:**	
Overrun Len:		**Stopway Len:**	
Tkof Dist Avbl:		**Tkof Run Avbl:**	

LAHSO

LAHSO Lndg	**Hold Short of Intersecting**

Rwy End General

Gradient:	**Grad Drctn:**

Dist:
Rwy:

Hold Short of Other:

Hold Short Point
Latitude:
Longitude:
Source:
Source Date:

Right Traffic: True Heading: 141

Reciprocal Rwy End

Rwy End ID: 31

Arresting Systems
System Code

Apch Lights: Centerline: Marking Cond: FAIR Marking Type: NPI REIL:

RVR: RVV: TDZ: Thr Crossing Hgt: 40 VGSI: P2L

Visual Glide Angle: 3.0

Obstruction

Clearance Slope: 50 Close In:

Cntrln Offset
Offset:
Direction:

Ctlg Obstn: Displaced Thr Len:

Dist From Rwy End: FAR 77 Category: A(NP) Hgt Above Rwy End: Marked Lighted: Slope to Displaced Thr:

Displaced Threshold

Elevation
Elevation ft:
Source:
Source Date:
Datum:

Position
Latitude:
Longitude:
Source:
Source Date:

Runway End

Elevation
Elevation ft: 1678.1
Source: 3RD PARTY SURVEY
Source Date: 2009-09-09
Datum: NGVD29

Position
Latitude: 43-45-40.0588N
Longitude: 99-18-58.1807W
Source: 3RD PARTY SURVEY
Source Date: 2009-09-09

Touchdown Zone

Elevation ft: 1687.4 Source: 3RD PARTY SURVEY
Source Date: 2009-09-09 Datum: NAVD88

Rwy Distances

Aclt Stop Dist Avbl: Lndg Dist Avbl:
Overrun Len: Stopway Len:
Tkof Dist Avbl: Tkof Run Avbl:

LAHSO

LAHSO Lndg Dist:
Hold Short of Intersecting Rwy:

Hold Short of Other:

Hold Short Point
Latitude:
Longitude:
Source:
Source Date:

Rwy End General

Gradient: Grad Drctn:
Right Traffic: True Heading: 321

APPENDIX B

Piloted simulation test plan & run log

CEN20FA022 Simulation Test Plan:

CG position effect on longitudinal handling qualities of the Pilatus PC-12 during takeoff

I. Test Overview and Objective

The objective of this piloted simulator test for is to evaluate the effect of the center of gravity (CG) position of the airplane on its longitudinal handling qualities. Specifically, several takeoffs will be performed, starting with the CG in a mid-position and moving the CG further aft during each successive takeoff, ending at the accident CG. For each takeoff, a record will be kept of both the subjective pilot assessment of the workload required to maintain a predetermined climb airspeed and associated pitch attitude while performing other normal tasks, and of objective measures of the pitch attitudes, rates of climb, and speeds achieved, and of the flight control inputs required. If time allows, measures of stick force per knot and per G will also be taken.

This evaluation may help investigators understand the reasons for the pitch oscillations recorded on the accident airplane's LDR during the accident takeoff and the previous takeoff (for which the airplane was likely loaded in a similar manner to the accident flight). This information may also help evaluate the accident pilot's workload and susceptibility to spatial disorientation during the accident takeoff.

II. Simulation Device:

- FlightSafety International Pilatus PC-12 NG (PC-12/47E) Level D full flight simulator

III. Configuration:

- Weight: 10,557 lb. (per "Wt&Bal Calc -- N56KJ (RevA_30Jan).xlsx")
- Flaps: 15
- Propeller Deice ON & Inertial Separator OPEN (STICK PUSHER ICE MODE active)
- Propeller Deice OFF & Inertial Separator CLOSED (STICK PUSHER ICE MODE inactive – scenarios 1c and 5c only)
- CG: varies (see Scenario Table below)
- Trim settings: accident trim settings, as determined from examination of trim actuators in wreckage and illustrated in this image:

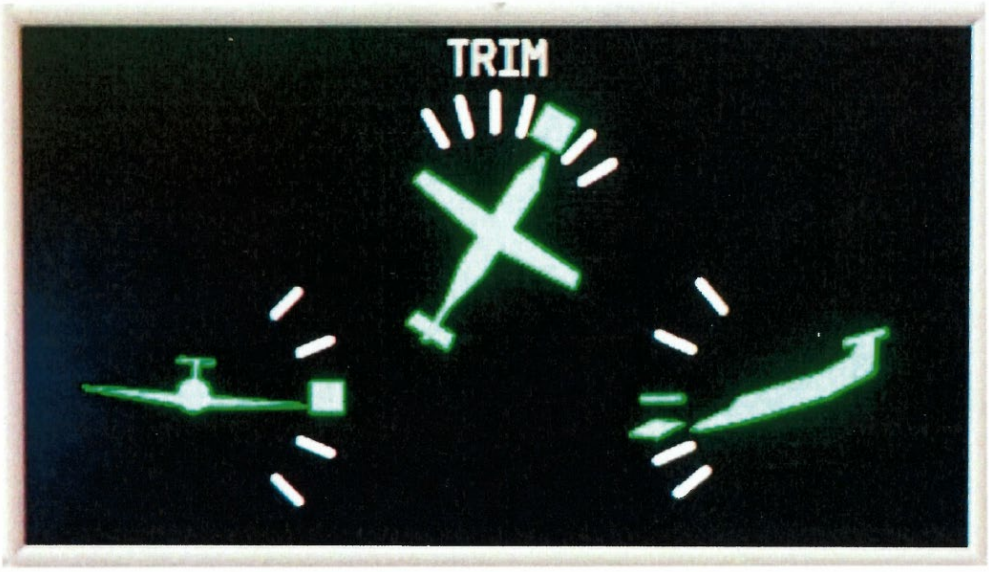

Scenario #	CG position (arm, inches)	ICE MODE	Notes
1a: flaps 15 to 0 1b: flaps held at 15 1c: flaps 15 to 0	236	On On Off	Mid-CG
2a: flaps 15 to 0 2b: flaps held at 15	238	On On	Between mid-CG and aft limit
3a: flaps 15 to 0 3b: flaps held at 15	240.2	On On	Aft limit
4a: flaps 15 to 0 4b: flaps held at 15	244.26	On On	Accident, aisle passengers forward, per Ref. 1[1]
5a: flaps 15 to 0 5b: flaps held at 15 5c: flaps 15 to 0	245.76	On On Off	Accident, aisle passengers aft, per Ref. 1
6a: flaps 15 to 0 6b: flaps held at 15	249	On On	Extreme aft CG (optional)

IV. Conditions:

- Location: Chamberlain Municipal Airport, Chamberlain, SD (9V9), runway 31
- Elevation: 1,678 ft. MSL
- Altimeter Setting: 29.30” Hg
- Temperature: 1° C
- Winds: 015° @ 7 kt.
- Sky condition: 500 ft. overcast
- Visibility: 0.5 nm in light snow

V. Test Procedure: takeoffs

1. Verify configuration:
    a. Flaps 15
    b. Gear down
    c. Weight and CG per desired scenario #
    d. Ice protection systems ON & STICK PUSHER ICE MODE active:
        i. Propeller Deice ON
        ii. Inertial Separator OPEN
        iii. Windshield Deice ON
        iv. Probes Deice ON
        v. V_R = 92 KIAS
        vi. V_{50ft} = 113 KIAS.
        vii. V_{CLIMB} = 135 KIAS
    e. Ice protection systems OFF & STICK PUSHER ICE MODE inactive (Scenarios 1c & 5c only):
        i. Propeller Deice OFF
        ii. Inertial Separator CLOSED
        iii. Windshield Deice OFF
        iv. Probes Deice OFF
        v. V_R = 82 KIAS
        vi. V_{50ft} = 105 KIAS

[1] Reference 1: Wt&Bal Calc -- N56KJ (RevA_30Jan).xlsx

vii. V_{CLIMB} = 130 KIAS

2. Record run data:
    a. Run #
    b. Time
    c. Scenario # (CG position)
    d. Data file number (if applicable)
3. Trim aircraft at rest at departure end of runway.
4. Confirm data & video recording devices ready.
5. Perform takeoff:
    a. Advance throttle to takeoff power
    b. Rotate at V_R
    c. Target V_{50ft}
6. Upon confirming positive rate of climb: select gear UP
7. Upon accelerating through V_{50ft}: select flaps UP (“a” and “c” scenarios only)
8. Set pitch attitude for V_{CLIMB}
9. Climbing through 400 ft. AGL (2,100 ft. MSL):
    a. Set climb power
    b. Switch radio from tower to departure frequency (simulated ATC prompt)
    c. Start climbing, standard-rate left turn to 220° (90° heading change) and climb to 1000’ AGL (2,700 ft. MSL) while maintaining 135 KIAS.
    d. End of run climbing through 1000’ AGL (2,700 ft. MSL).
10. For one scenario with ice protection ON and one scenario with ice protection OFF, raise the nose until stick shaker and then stick pusher are activated, to demonstrate and experience these systems.

VI. Test Procedure: longitudinal and maneuver stability (if time allows)

1. Trim airplane at flaps 15, gear up, and 120 knots / 2,500 ft. MSL., load per Scenario 1.
2. Turn off simulator position integrators to keep altitude and position constant (if able).
3. Without changing trim, use column to reduce and stabilize speed in 10 knot increments. Measure column force using a digital scale at the following speeds: 110, 100, and 90 knots. (See section VII-4 below for use of digital scale.)
4. Return to 120 knot trim speed. Without changing trim, use column to increase and stabilize speed in 10 knot increments. Measure column force at the following speeds: 130, 140, 150 knots.
5. Return to 120 knot trim speed. Increase bank angle in 20 degree increments. Use column to maintain 120 knots. Measure column force at the following bank angles: 20°, 40°, and 60°.
6. Repeat items 3-5 with airplane loading per Scenario 5 (aft CG).

Data Recording

1. Pilot assessment of difficulty /ease of task:
    a. General statements / comments
    b. Cooper-Harper rating, if applicable / useful (see Section VII)
2. Time-history data (if data recording capability is available):
    a. See list of parameters for recording in Section VIII.
3. Video recording (if permitted / available):
    a. Recording video and audio with an iPhone is acceptable.
    b. iPhone operator should state run number and time at the start of each run.
    c. Prior to advancing throttles, sweep camera over cockpit to record as many switches etc. (including Deice switches) as possible.
    d. During takeoff, keep camera steady and focused on pilot's instrument panel.
    e. If possible, include position of yoke in video frame.
    f. If necessary, two recordings with different iPhones can be taken: one of instruments, the second focused on pilot inputs at the yoke.
4. Column force measurements (for longitudinal and maneuver stability tests)
    a. Loop a cord around the control yoke (column).
    b. Use a digital scale with a hook to pull on the cord attached to the yoke and measure the required force.

VII. Cooper-Harper Rating Scale

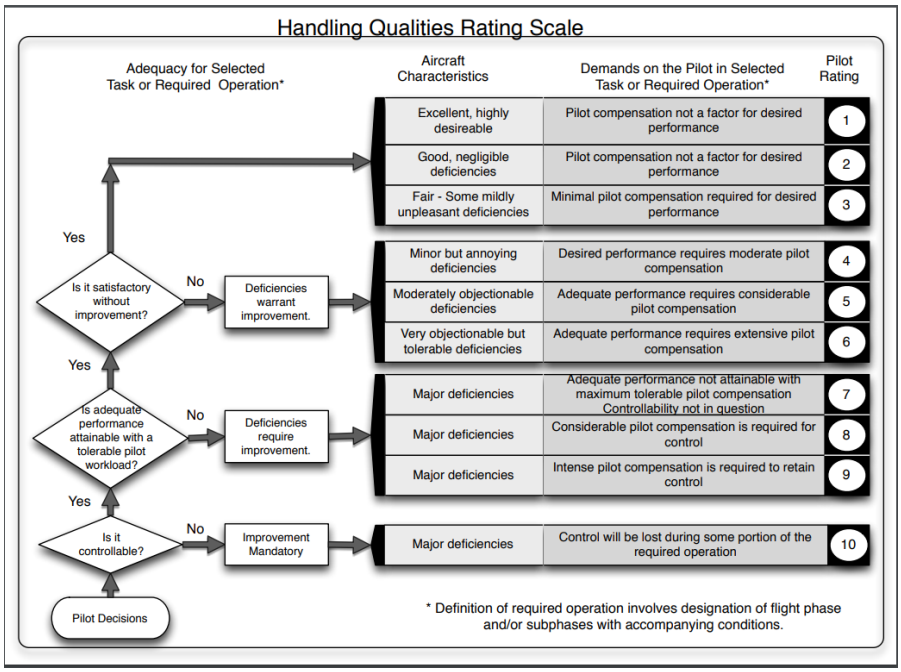

VIII. List of parameters for recording

NOTE: per conversation with FlightSafety, recorded digital data will only be available for viewing on FlightSafety's premises using the "*Debrief*" software. Recorded digital data cannot be output to a file outside of the *Debrief* system. Consequently, the list below is provided for general interest only, and to serve as a guide for future simulator exercises in new cases.

Case Identification

Date
Time
Case Number

Time

Elapsed Time (seconds)

Aircraft Configuration

Weight (lb.)
x CG position (% MAC from reference point; define ref. point (e.g., wing leading edge)).
y CG position
z CG position
Ixx (slugs*ft^2)
Iyy (slugs*ft^2)
Izz (slugs*ft^2)
Ixz (slugs*ft^2)
Flap position
Gear position

Aircraft Position

Pressure Altitude (ft.)
Radar Altitude (ft.)
North distance from reference (ft.) (Reference can be any fixed point, e.g. a runway threshold, etc.)
East distance from reference (ft.)
Latitude / longitude of reference point

Aircraft Orientation

Yaw angle (deg.) (Aircraft true heading)
Pitch angle (deg.)
Roll angle (deg.)

Aircraft Motion -Relative to Earth

Groundspeed (kts.)
Track Angle (deg.)
Rate of Climb (ft/min)
Flight path angle (deg.)

Aircraft Motion - Relative to Air

Calibrated Airspeed (kts.)
True Airspeed (kts.)
Dynamic Pressure (PSF)
Angle of Attack (deg.)
Angle of Sideslip (deg.)

Aircraft Motion - Angular Rates

P (deg/s) (body axis roll rate)
Q (deg/s) (body axis pitch rate)
R (deg/s) (body axis yaw rate)

Aircraft Motion - Accelerations

nx (g's) (load factor along body x axis)
ny (g's) (load factor along body y axis)
nlf (g's) normal load factor (load factor along body -z axis)

Pilot Control Positions

Column position (deg.)
Control wheel position (deg.)
Rudder pedal position (deg.)
Throttle lever position (deg.)

Pilot Control Forces

Column force (lb.)
Wheel force (lb.)
Rudder force (lb.)

Control Surface Positions

Stabilizer position (deg.)
Elevator position (deg.) (each elevator)
Aileron position (deg.) (each aileron)
Rudder position (deg.) (each rudder)

Engine Parameters

Torque (% or ft*lb or psi)
N_P (rpm)
Net thrust (lb.)
Shaft horsepower (HP)

Environment

Ambient static pressure (PSF)
Ambient static temperature (deg. F)
Vertical wind (kts.)
Wind speed (kts.)
Wind direction (deg. true)

Ice Protection

Propeller Deice switch position
Inertial Separator position
Probes Deice switch position
Windshield Deice switch position

RUN LOG: CEN20FA022 PC-12 simulator tests at FlightSafety Dallas, May 18-19, 2021

DATE: May 18, 2021 **Page 1 of 1**

Run #	Scenario #	Time	Pilot	Tim's iPhone file	John's iPhone file	Notes
1	1b	11:26	Paul London	Tim's phone	n/a	Flaps @ 15
2	1a	11:30				Heading bug, FD bars
3	1a	11:35				Bad run brakes locked
4	1a	11:37				Good run
5	1b	11:41				
6	1a*	11:46				Straight out climb following FD bars
7	1a*	11:49				Rotate @ 88 KIAS
8	4a*	11:55				243" CG, rotate @ 88 kt.
9	4a*	12:00				Same w/ simulated ice load, 88 KIAS rotation
10	4a*	12:04				Rotate @ 92 KIAS, no ice load
11	1c	12:08				ICE mode off, straight out climb w/ FD, rotate 82 KIAS
12	4c*	12:11				Same, CG 243"
13	4c*	12:16				"Heavy ice"
14	1c	12:51	Tim S.	n/a	John's iPhone	Rotate 82 KIAS
15	4c	12:59				Rotate 82 KIAS, CG 243"
16	4c	13:01				Repeat
17	3c	13:05				240.2" CG
18	1a	13:09				
19	4c	13:11				"Definitely less stable"
20	4c	13:14				Left to 220° - unstable on runway
21	4c	13:15				Repeat
22	3c	13:20				CG 240.2"
23	1c	13:26	John O'C	Tim's phone	n/a	Normal takeoff
24	1c	13:30				
25	1c	13:32				
26	3a	13:36				CG 240.2"
27	3a	13:39				
28	4c	13:42				
29	4c	13:44				
30	4a	13:46				Ice protection on
30b						Called "Run 31" on recording

RUN LOG: CEN20FA022 PC-12 simulator tests at FlightSafety Dallas, May 18-19, 2021

DATE: May 19, 2021 **Page 1 of 1**

Run #	Scenario #	Time	Pilot	Tim's iPhone file	John's iPhone file	Notes
31	1c	12:00	Tim S.	n/a	John's iPhone	VR 82 KIAS
32	1a	12:05				VR 92 KIAS
33	5a	12:07				No accel; directional control
34	5a	12:09				Repeat; push forward during TO roll; says "Run 35" on recording (error)
35	5a	12:12				Hold brakes during power up
36	5b	12:15				VR 88 KIAS; fast rotation; late rotation?
37	5b	12:17				VR 88 KIAS
38	5b	12:21				VR 88 KIAS, slow rotation
39	1c	12:27	Paul London	n/a	John's iPhone	VR 82 KIAS, late rotation
40	1a	12:30				VR 92 KIAS
41	5b	12:33				Directional control problems
42	5b	12:35				Stab trim?
43	5b	12:37				
44	5b	12:40				VR 88 KIAS
45	-		-			Normal climb to 5000' w/ autopilot
46	1c	12:52	John O'C	Tim's iPhone		
47	-	13:23	n/a	n/a		W=10450 CG 234"
48	-	13:25	n/a	n/a		W = 10450 CG = 240.2"
49	5a	13:27		n/a		

Participants:

Tim Sorensen: NTSB IIC
John O'Callaghan: NTSB Aircraft Performance Specialist
Paul London: FAA PC-12 Test Pilot

Column Force tests (test plan section VI)

Configuration:

Weight = 10,557 lb.
CG = see table
Flaps = 15
Gear = up
Altitude = 2,500 ft. MSL
Atmosphere = per test plan section IV
Simulation position integrators **OFF**

Stick force per knot tests (roll angle = 0°)

Airpeed (KCAS)	Column force, lb. (CG @ 236")		Column force, lb. (CG @ 245.76")	
	Screen value	Scale value	Screen value	Scale value
90		9.75		4.9
100		8.60		3.8
110		4.13		2.4
120 (trim speed)		0		0
130		2.63		2.3
140		9.8		4.2
150		15.3		7.8

Stick force per G tests (airspeed = 120 KCAS)

Roll angle	Normal load factor (G's)	Column force, lb. (CG @ 236")		Column force, lb. (CG @ 245.76")	
		Screen value	Scale value	Screen value	Scale value
0°			0		0
20°			2.5		0.6
40°			8.3		4.4
60°			25		8.5